Technical Letter Report to the U.S. Nuclear Regulatory Commission JCN Q-4151, Task Order No. 10

Technical Evaluation Report with No Open Items for the Levy County, Florida, COL Review

By Eric L. Geist (USGS, Menlo Park), Patrick J. Lynett (Texas A&M University), Jason Chaytor (USGS, Woods Hole), David C. Twichell (USGS, Woods Hole), and Uri S. ten Brink (USGS, Woods Hole)

Administrative Report, 2011

U.S. Department of the Interior
U.S. Geological Survey

Table of Contents

2.4.6 Probable Maximum Tsunami Hazards

2.4.6.1 Introduction

The probable maximum tsunami hazards are addressed to ensure that any potential tsunami hazards to the structure, system, or components (SSCs) important to safety are considered in plant design. The specific areas of review are as follows: (1) historical tsunami data, including paleotsunami mappings and interpretations, regional records and eyewitness reports, and more recently available tide gauge and real-time bottom pressure gauge data, (2) probable maximum tsunami (PMT) that may pose hazards to the site, (3) tsunami wave propagation models and model parameters used to simulate the tsunami wave propagation from the source towards the site, (4) extent and duration of wave runup during the inundation phase of the PMT event, (5) static and dynamic force metrics, including the inundation and drawdown depths, current speed, acceleration, inertial component, and momentum flux that quantify the forces on any safety-related SSCs that may be exposed to the tsunami waves, (6) debris and water-borne projectiles that accompany tsunami currents and may impact safety-related SSCs, (7) effects of sediment erosion and deposition caused by tsunami waves that may result in blockage or loss of function of safety-related SSCs, (8) potential effects of seismic and non-seismic information on the postulated design bases and how they relate to tsunami in the vicinity of the site and the site region, (9) any additional information requirements prescribed within the "Contents of Application" sections of the applicable subparts to 10 CFR Part 52.

2.4.6.2 Summary of Application

2.4.6.2.1 Probable Maximum Tsunami

Section 2.4.6.1 of the applicant's FSAR contains only the general definition of the Probable Maximum Tsunami (PMT). Although there is no summary of the PMT assessment included in this section, most of the information is contained in other sections of the FSAR, such as 2.4.6.5.3.

2.4.6.2.2 Historical Tsunami Record

The applicant reviewed two primary sources of information to establish the historical record of tsunamis affecting the Caribbean region and the U.S. Gulf Coast: (a) the NOAA/NGDC Historical Tsunami Database (internet), and (b) a Caribbean tsunami catalog published by Lander et al. (2002) in the journal *Science of Tsunami Hazards*. Various other web sites were used as ancillary sources of information.

From these sources of information, the applicant determines that there were three historical cases of tsunamis and seismic seiche that occurred in the Gulf of Mexico: (1) the 1918 Mona Passage (northwest of Puerto Rico) seismogenic tsunami; (2) the 1922 Vieques, Puerto Rico seismogenic tsunamis; and (3) a seismic seiche caused by the 1964 Gulf of Alaska earthquake.

2.4.6.2.3 Source Generator Characteristics

The applicant identified possible tsunami sources that may affect the Levy County site from three general regions: (1) far-field sources outside of the Gulf of Mexico and Caribbean Sea, (2) earthquakes along the Caribbean plate boundary, and (3) earthquakes and landslides inside the Gulf of Mexico. Far-field source scenarios considered include the 1964 Gulf of Alaska seismic seiche, the 1755 Lisbon seismogenic tsunami, and far-field landslide sources in the Atlantic Ocean. Caribbean sources include earthquakes along the North Panama deformation belt, the northern South America convergence zone, the northern Caribbean subduction zone, and the Cayman transform fault system. Gulf of Mexico tsunami sources considered include intra-plate earthquakes and landslides. All of the aforementioned information was obtained by the applicant primarily from published journal articles and web sites. Some of the description of tsunami-source generator characteristics can also be found in Section 2.4.6.4 of the FSAR.

2.4.6.2.4 Tsunami Analysis

The applicant's original tsunami analysis consists of using past studies to ascertain the tsunami propagation characteristics from the three source regions discussed in Section 2.4.6.3. Offshore amplitude estimates were used to determine whether a tsunami could potentially impact the Levy County Nuclear Plant site. Different types of tsunami analyses were used to estimate tsunami water levels from each of the three regions. Some of the description of tsunami analysis can also be found in Section 2.4.6.5 of the FSAR. In response to RAI 2.4.6-17 and in the corresponding update to FSAR Section 2.4.6, the applicant uses numerical methods to simulate tsunami generation, propagation, and runup.

For tsunami sources located in the Caribbean region, the applicant primarily relies on previously published tsunami analyses of open-ocean propagation by Knight (2006) (FSAR reference 2.4.6-225) and the USGS Administrative Report (2007) describing tsunami sources affecting U.S. Atlantic and Gulf Coasts (FSAR reference 2.4.6-214).

For tsunami sources located in the Gulf of Mexico region, the applicant considers both earthquake and landslide sources. The applicant suggests that there is "little likelihood that a seismic event in the Gulf of Mexico would produce a tsunami" (FSAR, pg. 2.4-52). However, the applicant includes tsunami analysis for the offshore of Veracruz, Mexico scenario (Knight, 2006) that the applicant links to intra-plate seismic activity. For the

East Breaks landslide source, the applicant uses an attenuation function derived for Caribbean region tsunamis and a Monte Carlo analysis to estimate a maximum offshore wave height.

For tsunami sources located in the far-field, the applicant focuses on seismogenic sources only, indicating that "Far-field landslides (e.g., the Canary Islands) and volcanoes (e.g., the Lesser Antilles) …are unlikely to produce tsunamis that will be destructive to the Gulf Coast." (FSAR pg. 2.4-59). The applicant uses previously published analyses of the 1755 Lisbon seismogenic tsunami (Mader, 2001; FSAR Reference 2.4.6-213) to estimate tsunami amplitudes in the Gulf of Mexico.

2.4.6.2.5 Tsunami Water Levels

Using the various methods of tsunami analysis, primarily from previously published studies, the applicant estimates maximum tsunami levels for far-field sources, sources in the Caribbean region and sources inside the Gulf of Mexico. The applicant concludes that the maximum likely tsunami runup is less than the nominal plant grade and, therefore, will not impact safety-related facilities at the Levy County Nuclear Plant site.

2.4.6.2.6 Hydrography and Harbor or Breakwater Influences on Tsunami

The applicant indicates that routing of the controlling tsunami, including breaking wave formation and resonance effects, is expected to by minor and limited to the shorelines. In addition, the applicant indicates that hydrography and harbor or breakwater influences are not expected to be severe enough to impact safety-related structures.

2.4.6.2.7 Effects on Safety-related Facilities

The applicant indicates that the effects of the PMT are not expected to be severe enough to impact the operation of safety-related structures. The applicant further indicates that measures to protect the site against the effects of tsunami are not included in the design criteria.

2.4.6.3 Regulatory Basis

The applicable regulatory requirements for identifying probable maximum tsunami hazards are:

1. 10 CFR Part 100, as it relates to identifying and evaluating hydrological features of the site. The requirement to consider physical site characteristics in site evaluations is specified in 10 CFR 100.20(c).

2. 10 CFR 100.23(d) sets forth the criteria to determine the siting factors for plant design bases with respect to seismically induced floods and water waves at the site.

3. 10 CFR 52.79(a)(1)(iii), as it relates to identifying hydrologic site characteristics with appropriate consideration of the most severe of the natural phenomena that have been historically reported for the site and surrounding areas and with sufficient margin for the limited accuracy, quantity, and period of time in which the historical data have been accumulated.

The related acceptance criteria are summarized from SRP Section 2.4.6:

1. Historical Tsunami Data: The application should provide a complete description of historical tsunami data near the proposed plant site.

2. Probable Maximum Tsunami: The application should provide an assessment of the PMT for the proposed site.

3. Tsunami Propagation Models: The application should provide a description of the tsunami wave propagation models used in the applicant's SAR.

4. Wave Runup, Inundation, and Drawdown: The application should provide the extents and durations of inundation and drawdown near the proposed site.

5. Hydrostatic and Hydrodynamic Forces. The application should provide a set of metrics that describes the hydrostatic and hydrodynamic forces caused by the PMT on the safety-related SSCs.

6. Debris and Water-Borne Projectiles. The application should provide an assessment of the debris and water-borne projectiles that may accompany PMT currents.

7. Effects of Sediment Erosion and Deposition. The application should provide an assessment of the effects of sediment erosion and deposition near the proposed locations of safety-related SSCs.

8. Consideration of Other Site-Related Evaluation Criteria. The application should provide an evaluation of the potential effects of site-related proximity, seismic, and non-seismic information as they affect tsunamis near the plant site and site regions.

In addition, the hydrologic characteristics should be consistent with appropriate sections from: Regulatory Guide 1.27, "Ultimate Heat Sink for Nuclear Power Plants," Regulatory Guide 1.29, "Seismic Design Classification," Regulatory Guide 1.59, "Flood Design Basis for Nuclear Power Plants," as supplemented by best current practices, and Regulatory Guide 1.102, "Flood Protection for Nuclear Power Plants."

2.4.6.4 Technical Evaluation

2.4.6.4.1 Probable Maximum Tsunami

Because the applicant did not include a summary of the PMT assessment in Section 2.4.6.1 of the FSAR, information from other sections of the FSAR was used to determine which sources were considered and what the applicant determined were the water levels associated with each source. Three tsunami source regions were considered by the applicant to determine the PMT: (1) far-field sources outside the Gulf of Mexico and Caribbean region, (2) seismogenic sources along the Caribbean plate boundary, and (3) earthquake and landslide tsunami sources in the Gulf of Mexico. For the far-field sources, the applicant appears to consider that the maximum wave height would be from an event similar to the 1755 Lisbon seismogenic tsunami (<1 m wave heights in the Gulf of Mexico). For Caribbean sources, the worst-case scenario is determined by the applicant to be a seismogenic tsunami offshore Venezuela (in the Caribbean Sea), with a maximum wave height of 0.65 m offshore of the site (FSAR, pg. 2.4-58). For Gulf of Mexico tsunami sources, the applicant considered the East Breaks slump in the northwest Gulf of Mexico as the worst-case scenario, with a maximum wave height of 1.68 m offshore of the site (FSAR, pg. 2.4-53). As indicated by the applicant in the original FSAR, the controlling source of the PMT appears to be the East Breaks landslide. This was later revised to be the Mississippi Canyon landslide in response to the RAI's (e.g., RAI 2.4.6-01).

Request for Additional Information (RAI) 2.4.6-01: Section C.I.2.4.6.1 of Regulatory Guide 1.206 (RG 1.206) provides specific guidance with respect to determination of the PMT. This includes a discussion of the most reasonably severe geo-seismic activity possible and corresponding tsunami analysis.
Provide a summary of the PMT assessment for the Levy County site, including the controlling source for the PMT and corresponding tsunami water level determination.

Resolution of RAI 2.4.6-01 and issuance of Open Items: The applicant refers to the responses of RAI 2.4.6-08 and 2.4.6-10, suggesting that the Mississippi Canyon slide is the controlling source for the PMT. The PMT runup indicated in the response to RAI 2.4.6-01 does not agree with either the uncorrected or corrected PMT runup values indicated in the applicant's responses to RAI 2.4.6-06 (Tables 1 and 2), RAI 2.4.6-08 (Table 3), and RAI 2.4.6-10 (Table 1). Supplemental RAI 2.4.6-11 issued.

Supplemental RAI 2.4.6-11: To meet the requirements of GDC 2, 10 CFR 52.17, and 10 CFR Part 100, the applicant must provide an assessment of the Probable Maximum Tsunami (PMT) for the proposed site. Section C.I.2.4.6.1 of Regulatory Guide 1.206 (RG 1.206) provides specific guidance with respect to determination of the PMT. This includes a discussion of the most reasonably severe geo-seismic activity possible and corresponding tsunami analysis.

The PMT runup indicated in the response to RAI 2.4.6-01 does not agree with either the uncorrected or corrected PMT runup values indicated in the applicant's responses to RAI 2.4.6-06 (Tables 1 and 2), RAI 2.4.6-08 (Table 3), and RAI 2.4.6-10 (Table 1). Clarify the PMT runup value in Section 2.4.6.1 of the FSAR or justify why this clarification is not needed.

Resolution of RAI 2.4.6-11 and issuance of Open Items: The applicant has corrected the PMT runup values indicated in the Supplemental RAI (letter ML1009102991). RAI Status (2.4.6-01 and Supplemental 2.4.6-11): Closed.

Request for Additional Information (RAI) 2.4.6-02: Section C.I.2.4.6.1 of Regulatory Guide 1.206 (RG 1.206) provides specific guidance with respect to determination of the PMT. This includes a discussion of the generation of tsunami-like waves from hill-slope failures and the stability of the coastal area.
Provide a discussion in the updated FSAR of the hill-slope failures near the Levy County site with reference to the findings in Section 2.5 of the FSAR.

Resolution of RAI 2.4.6-02 and issuance of Open Items: The applicant indicates in their response to RAI 2.4.6-02 that no permanent slopes or hill slopes are present near the site or within the coastal areas near the site. RAI Status: Closed.

Results of Contractor's Independent Confirmatory Analysis

We have conducted an independent confirmatory analysis to determine the PMT at the Levy County site that is described in detail in the sections that follow. In summary, numerical hydrodynamic modeling of three different types of tsunami sources has been performed to determine their impact on the Levy County site. The three source types are (1) distant earthquake sources, (2) a regional earthquake source in the Gulf of Mexico, and (3) regional submarine landslide sources in the Gulf of Mexico. Most of the analysis is focused on source type (3) for determination of the PMT. For all conditions, the most conservative source parameters were employed, even when arguably unphysical, to provide an absolute upper limit on the possible tsunami effects at the Levy County site.

There are very significant differences between how the PMT is determined in our confirmatory analysis and how it is determined by the applicant. The applicant did not use any of the standard methods of tsunami propagation and inundation modeling. In response to RAI 2.4.6-08, the applicant describes a procedure in which an estimated source amplitude is multiplied by three factors: (1) propagation loss, (2) shoaling correction, and (3) "beaching" amplification. Each of the multiplicative factors is determined from analytic expressions—variations in water depth along the propagation path between the source and the site were not explicitly accounted for. Results of their analysis indicate that the PMT is from a Mississippi Canyon landslide source, with a maximum runup of 21.4 m (Response to RAI 02.04.06-8). Including sea-level rise, sea-level anomaly, and high tide, their PMT maximum water level is 22.5 m (NAVD88) (Response to RAI 02.04.06-10), substantially above the plant grade elevation of 15.5 m (NAVD88).

In the independent confirmatory analysis, using conservative source parameters and neglecting the radial spreading of wave energy, one horizontal dimension (1HD) simulations indicate that the Mississippi Canyon source clearly has the greatest potential to bring a large wave to the Levy County site, with water elevations near the site in excess of +30 m. 2HD simulations of this source and the WORST CASE Florida Slope landslide source that include radial spreading predict a maximum wave elevation of 7 m offshore of the site (30 m water depth). However, as the Mississippi Canyon wave is longer in period and has a longer train of large waves, it is designated as the PMT for the Levy County site. Highly refined nearshore simulations show that this source results in a maximum onshore water level of +3 m. Because of non-linear effects during wave propagation, an antecedent sea level that includes 10% exeedance high tide, sea level anomaly, and sea-level rise cannot simply be added to the +3 m maximum water level. A separate 2HD simulation that includes the non-linear propagation effects and a +1.2 m (NAVD88) antecedent sea level results in a maximum water level of +6.1 m. Thus, results from the confirmatory analysis indicate that the PMT does not reach the Levy County site plant grade elevation.

2.4.6.4.2 Historical Tsunami Record

The applicant reviews tsunami catalogs for the Caribbean and the Gulf of Mexico regions and determines that there were three events that affected the Gulf coast: two seismogenic tsunamis and one seismic seiche. The sources of information primarily include the NOAA/NGDC Historical Tsunami Database (internet) and the published report of Lander et al. (2002).

The first seismogenic tsunami considered by the applicant was triggered by the 1918 Mona Passage earthquake, located northwest of Puerto Rico. Maximum runup from the tsunami was reported to be 6 m local to the source. In the Gulf of Mexico, the tsunami was recorded at the Galveston tide gauge station, but the maximum amplitude of the wave was not indicated by the applicant.

The second seismogenic tsunami was caused by an earthquake near Vieques Island in 1922. In the Gulf of Mexico, a maximum amplitude of 0.6 m was recorded at the Galveston tide gauge station, with a dominant period of 45-minutes.

A seiche was observed in the Gulf of Mexico in 1964 that was set up by seismic waves emanating from the 1964 Gulf of Alaska earthquake. The applicant did not indicate the maximum amplitude of the seiche in the Gulf of Mexico.

Request for Additional Information (RAI) 2.4.6-03: Section C.I.2.4.6.2 of Regulatory Guide 1.206 (RG 1.206) provides specific guidance with respect to the historical tsunami record, including paleo-tsunami evidence.

Provide a clarification in the updated FSAR of the meaning of the descriptor "impact" as used on pg. 2.4-45 of the FSAR: "…historically no Caribbean tsunami has *impacted* the United States Gulf Coast."

Resolution of RAI 2.4.6-03 and issuance of Open Items: Applicant explains in their response to RAI 2.4.6-03 that the descriptor "impact" means "no tsunami are known to have originated in the Caribbean Sea and generated a runup exceeding 1.0 m at any location along the United States Gulf Coast." However, FSAR has not been updated. RAI Status: Closed.

Request for Additional Information (RAI) 2.4.6-04 Section C.I.2.4.6.2 of Regulatory Guide 1.206 (RG 1.206) provides specific guidance with respect to the historical tsunami record, including paleo-tsunami evidence.
Provide a clarification in the updated FSAR whether any of the Maximum Water Height measurements listed in Table 2.4.6-202 are located in the Gulf of Mexico.

Resolution of RAI 2.4.6-04 and issuance of Open Items: Applicant indicates that none of the locations of Maximum Water Height measurements are located in the Gulf of Mexico. It should be noted that the Maximum Water Height measurements are typically located near the source—not necessarily in the Caribbean as the applicant indicates in their response to RAI 2.4.6-04. RAI Status: Closed.

Request for Additional Information (RAI) 2.4.6-05: Section C.I.2.4.6.2 of Regulatory Guide 1.206 (RG 1.206) provides specific guidance with respect to the historical tsunami record, including paleo-tsunami evidence.
Provide a clarification in the updated FSAR about whether there is any geologic evidence of tsunami deposits at the Levy County site or at nearby regions. Additionally, indicate whether there are geologically conducive locations for the deposition and preservation of tsunami deposits in the vicinity of the Levy County site. If such paleo-tsunami evidence exists, indicate how they are distinguished from storm wash-over deposits.

Resolution of RAI 2.4.6-05 and issuance of Open Items: The applicant indicates that site-specific borings lead them to conclude that there is no geologic evidence of paleo-tsunami or tsunami-like deposits in the vicinity of the Levy County site. The applicant needs to provide additional details of the sedimentological analysis used to arrive at this conclusion, including the thickness of sand layers that the methods used were capable of detecting, and cross references to applicable parts of FSAR Section 2.5. Supplemental RAI 2.4.6-12 issued.

Supplemetal RAI 2.4.6-12: To meet the requirements of GDC 2, 10 CFR 52.17, and 10 CFR Part 100, the applicant must provide an assessment of the Probable Maximum Tsunami (PMT) for the proposed Levy County site. Section C.I.2.4.6.2 of Regulatory Guide 1.206 (RG 1.206) provides specific guidance with respect to the historical tsunami record, including paleo-tsunami evidence. The applicant indicates that site-specific borings lead them to conclude that there is no geologic evidence of paleo-tsunami or tsunami-like deposits in the vicinity of the Levy County site. Provide additional details

of the sedimentological analysis used to arrive at this conclusion, including the thickness of sand layers that the methods used were capable of detecting, and cross references to applicable parts of FSAR Section 2.5.

Resolution of RAI 2.4.6-12 and issuance of Open Items: The applicant provided cross-references to FSAR Section 2.5.1.2.5.2.1 that presents the Quaternary stratigraphy and Section 2.4.4.2.1.1 through 2.5.4.2.1.1 indicating soil sampling conducted near the site. The investigations did not identify any sands with characteristics diagnostic of past tsunami deposits. (Letter ML1009102991) RAI Status (2.4.6-05 and Supplemental 2.4.6-12): Closed.

Results of Contractor's Independent Confirmatory Analysis

Historic Tsunami Record

Primary references of historical observations and measurements of tsunami and seismic seiche waves occurring along the Gulf Coast were examined. The applicant has summarized the essential historical record of tsunamis in the region.

Paleo-Tsunami Record

The closest locations of interpreted paleotsunami deposits to the Levy County site are in southern Alabama, as shown in Figure 2.4.6.4.2-1. The deposits are thought to be part of a regional tsunami event in the Gulf of Mexico at or near the time of the Cretaceous-Tertiary (K-T) boundary.

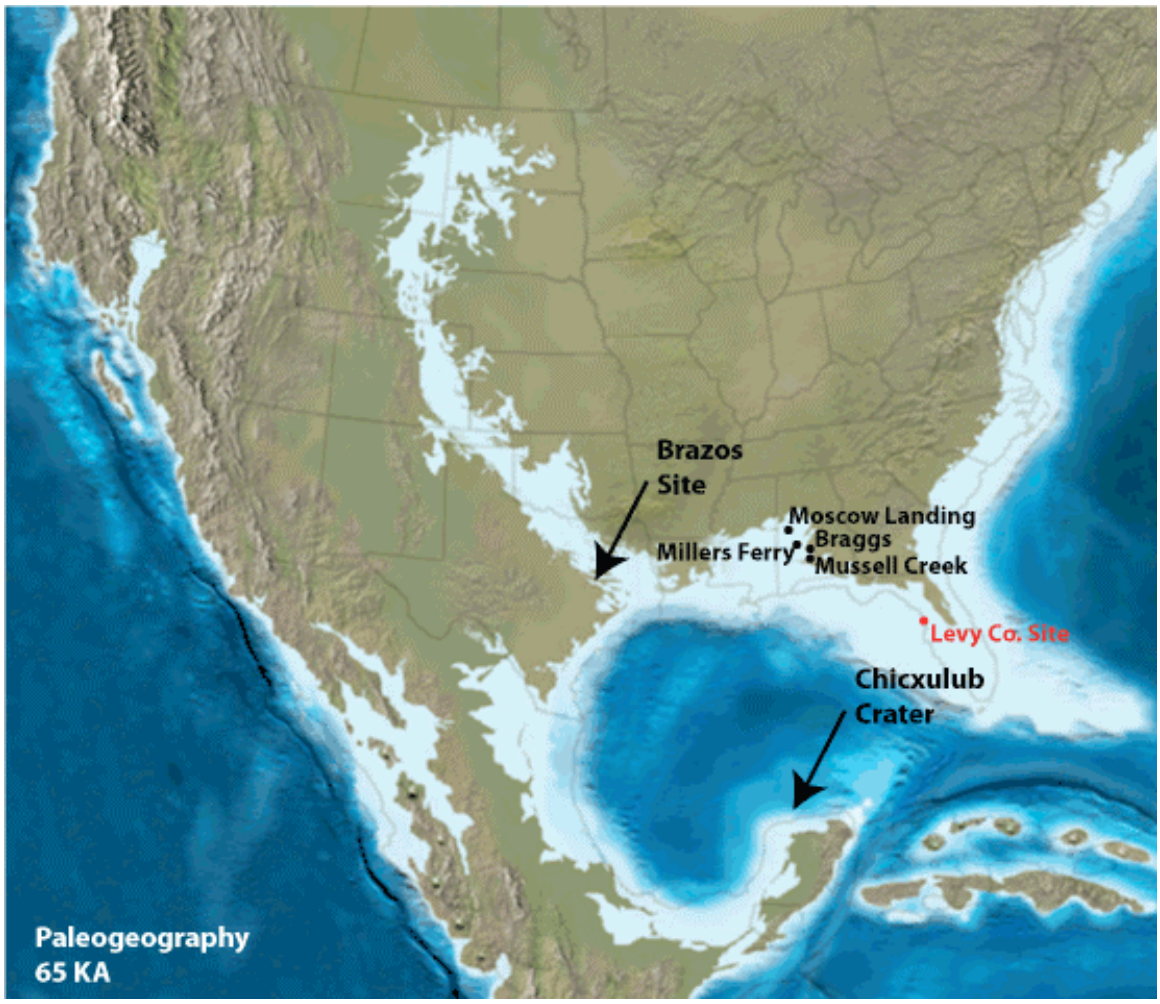

Figure 2.4.6.4.2-1: Paleogeography (Blakey, 2005) at the time when a regional tsunami deposit was emplaced (approx. 65 Ka). Locations of southern Alabama deposit sites, the Brazos site (Texas), and Chicxulub impact crater are also shown.

The common interpretation of this deposit, owing to its date and the existence of impact ejecta at the Brazos site and elsewhere, is that it was emplaced by a tsunami generated from the Chicxulub asteroid impact. However, the tsunami deposit was discovered by Bourgeois et al. (1988) prior to the discovery of the Chicxulub impact crater (Hildebrand et al., 1991). An important alternate hypothesis related to possible tsunamigenic sources in the Gulf of Mexico is provided by Bourgeois et al. (1988):

> "If the tsunami were produced by a major submarine landslide, it should not occur precisely at the K-T boundary unless the landslide were caused by an earthquake related to boundary events, which is a possibility"
> (pg. 569).

Bourgeois et al. (1988) suggested that a tsunami wave 50-100 m high was necessary to explain this deposit. It is not conceivable that the wave that created these deposits was generated by any landslide source that would be of relevance to the present-day PMT determination. As we demonstrate in our independent analysis, any landslide wave

generated at the present-day continental shelf break would not be able to maintain a large wave height across such a long propagation distance over very shallow water. The depth-limiting dissipation effect, in which large amplitude waves are dissipated much faster than small amplitude waves during long propagation over shallow depth, would necessarily reduce any landslide-generated wave located at the shelf break to a minimal event at the shoreline. It is possible that this deposit was generated by a paleo-landslide source, but this landslide event would have been local to the Brazos site. It is considerably more likely that a wave of the estimated height would be caused by a relatively nearby large impact event. Waves emanating from such a source would have the needed extreme wave heights and long periods to be able to propagate significant wave energy this far inland.

During the last 20 years, the Brazos deposit has been extensively sampled from outcrops and subsurface cores at sites near the banks of the Brazos River. Recently, studies have both corroborated and disputed whether the Brazos deposit was emplaced by a tsunami, whether it occurred exactly at the geologic boundary between the Cretaceous and Tertiary periods (i.e., at the K-T boundary), and whether the trigger was the Chicxulub impact (e.g., Smit et al., 1996; Gale, 2006; Schulte et al., 2006; Keller et al., 2007). Conflicting interpretations of the deposits at the southern Alabama locations shown in Figure 2.4.6.4.2-1 are described in earlier studies (Mancini et al., 1989; Liu and Olsson, 1992; Savrda, 1993; Keller and Stinnesbeck, 1996). The exact age and hydrologic process that formed the regional tsunami deposits remain controversial. However, in light of these studies over the last 20 years, the lead author of the original study identifying the deposit maintains that it was emplaced by a tsunami (J. Bourgeois, pers. comm., 2009).

Conclusion

Primary references of historical observations and measurements of tsunami and seismic seiche waves occurring along the Gulf Coast were examined. Our assessment of the historical record is consistent with that of the applicant's.

The applicant did not provide evidence that an adequate investigation was conducted for tsunami deposits at or near the proposed site. Additionally, the applicant does not consider the existence of a possible paleotsunami (Bourgeois et al., 1988) that occurred along the ancient Gulf Coast shoreline, including locations in southern Alabama. The common interpretation of this deposit is that it was emplaced by a tsunami generated by the Chixulub impact or by landslide or earthquake activity associated with the impact. Although arguments have been presented against this interpretation, this deposit, along with the historical record, should be considered as possible evidence of tsunami occurrence along the Gulf Coast. It is unlikely, however, that the flow speeds and wave heights inferred from the deposit are relevant to determination of the present-day PMT.

2.4.6.4.3 Source Generator Characteristics

The applicant identifies possible tsunami sources from three general regions: (1) far-field sources outside of the Gulf of Mexico and Caribbean Sea, (2) the Caribbean plate boundary, and (3) inside the Gulf of Mexico.

Far-field source scenarios initially considered include the 1964 Gulf of Alaska seismic seiche, the 1755 Lisbon seismogenic tsunami, and far-field landslide sources in the Atlantic Ocean. The applicant considers only the 1755 Lisbon seismogenic tsunami in determining water levels from a far-field source.

Caribbean sources include earthquakes along the boundary of the Caribbean plate. Specific earthquake and tectonic segments considered by the applicant include the North Panama Deformation Belt, the northern South America convergence zone, the northern Caribbean subduction zone, and the Cayman transform fault system.

Gulf of Mexico tsunami sources considered include intra-plate earthquakes and landslides. For intra-plate earthquakes, the applicant mentions the occurrence of the Mw=5.8 September 10, 2006 Gulf of Mexico earthquake, but does not include a seismogenic source in this region of the Gulf of Mexico in their tsunami analysis. The applicant does include the results from a scenario by Knight (2006) offshore Veracruz, Mexico, that the applicant links to present-day seismic activity. For landslides in the Gulf of Mexico, the applicant primarily considers the East Breaks landslide offshore Texas, but not other possible landslide sources in the Gulf of Mexico. All of the aforementioned information was obtained by the applicant from published journal articles and web sites.

Request for Additional Information (RAI) 2.4.6-06: Section C.I.2.4.6.3 of Regulatory Guide 1.206 (RG 1.206) provides specific guidance with respect to the source characteristics needed to determine the PMT. These characteristics include detailed geo-seismic descriptions of the controlling local tsunami generators, including location, source dimensions, and maximum displacement.
Provide a discussion in the updated FSAR of submarine landslides in the Gulf of Mexico, other than East Breaks, as potential tsunami generators, including the Mississippi Canyon landslide, and landslides along the Florida Escarpment and along the slope above the Florida Escarpment. Clarify text in the FSAR indicating whether the East Breaks landslide is considered as the PMT source, in relation to discussion of the north Venezuela seismogenic tsunami as having “the most severe impacts for the Gulf Coast” (pg. 2.4-58).

Resolution of RAI 2.4.6-06 and issuance of Open Items:
1. In their response to RAI 2.4.6-06, the applicant is inconsistent in their characterization of the Mississippi Canyon and Florida Escarpment tsunami sources. On pages 9-10 of their response, the applicant appears to discount the tsunami potential based on the date of the last landslides in those regions. In the rest of their response, the applicant indicates that these sources are used for PMT determination (and, in fact, the Mississippi Canyon slide is the applicant’s controlling PMT source). The applicant needs to clarify whether

the Mississippi Canyon and Florida Escarpment are considered to be significant potential sources for PMT determination.
2. The applicant indicates identical source parameters for "Florida Escarpment" and "Slope above the Florida Escarpment" in Table 1 of their response to RAI 2.4.6-06. However, the water depth in these two regions is different. The applicant needs to explain this apparent discrepancy, or justify why the entries in Table 1 are correct.
Supplemental RAI 2.4.6-13 issued.

Supplemental RAI 2.4.6-13: To meet the requirements of GDC 2, 10 CFR 52.17, and 10 CFR Part 100, the applicant must provide an assessment of the Probable Maximum Tsunami (PMT) for the proposed site. Section C.I.2.4.6.3 of Regulatory Guide 1.206 (RG 1.206) provides specific guidance with respect to the source characteristics needed to determine the PMT. These characteristics include detailed geo-seismic descriptions of the controlling local tsunami generators, including location, source dimensions, and maximum displacement.
1. The applicant is inconsistent in their characterization of the Mississippi Canyon and Florida Escarpment tsunami sources. The applicant appears to discount the tsunami potential based on the date of the last landslides in those regions. In the rest of their response, they indicate that these sources are used for PMT determination (and, in fact, the Mississippi Canyon is the applicant's controlling PMT source). Clarify that the Mississippi Canyon and Florida Escarpment are considered to be significant potential sources for PMT determination.
2. The applicant indicates identical source parameters for "Florida Escarpment" and "Slope above the Florida Escarpment" in Table 1 of their response to RAI 2.4.6-06. However, the water depth in these two regions is different. Explain this apparent discrepancy, or justify why the entries in Table 1 are correct.

Resolution of RAI 2.4.6-13 and issuance of Open Items: For item 1, the applicant clarifies that the Mississippi Canyon and Florida Escarpment landslides are considered as potential PMT sources. For item 2, the applicant revised the water depth in the Florida Escarpment and Slope above the Florida Escarpment region. (Letter ML1009102991)
RAI Status (2.4.6-06 and Supplemental 2.4.6-13): Closed.

Request for Additional Information (RAI) 2.4.6-07: Section C.I.2.4.6.3 of Regulatory Guide 1.206 (RG 1.206) provides specific guidance with respect to the source characteristics needed to determine the PMT. These characteristics include detailed geo-seismic descriptions of the controlling distant tsunami generators, including location, source dimensions, fault orientation, and maximum displacement.
Provide clarification in the updated FSAR regarding seismologic characterization of the region offshore Veracruz, Mexico, relative to the generation of tsunamis.

Resolution of RAI 2.4.6-07 and issuance of Open Items: The applicant's explanation in response to RAI 2.4.6-07 provides additional details of the source parameters considered, although we are not aware of 15-20 earthquakes > M7 that occurred near Veracruz, Mexico. The applicant needs to clarify the location of "15-20 earthquakes of magnitude 7 or greater…near Veracruz" indicated in the applicant's response to RAI 2.4.6-07, in

terms of tsunami potential for the Gulf of Mexico versus the Pacific Ocean. The applicant should also provide the information source for this statement. Supplemental RAI 2.4.6-14 issued.

Supplemental RAI 2.4.6-14: To meet the requirements of GDC 2, 10 CFR 52.17, and 10 CFR Part 100, the applicant must provide an assessment of the Probable Maximum Tsunami (PMT) for the proposed Levy County site. Section C.I.2.4.6.3 of Regulatory Guide 1.206 (RG 1.206) provides specific guidance with respect to the source characteristics needed to determine the PMT. These characteristics include detailed geo-seismic descriptions of the controlling distant tsunami generators, including location, source dimensions, fault orientation, and maximum displacement. Clarify the location of "15-20 earthquakes of magnitude 7 or greater…near Veracruz" indicated in the applicant's response to RAI 2.4.6-07, in terms of tsunami potential for the Gulf of Mexico versus the Pacific Ocean. Provide the information source for this statement.

Resolution of RAI 2.4.6-14 and issuance of Open Items: The applicant clarified the location of the magnitude 7 earthquakes, indicating that they originated at depths greater than 70 km. The applicant removed the statement in the revised FSAR that several of the earthquakes near Veracruz originated within 35 km of sea level. (Letter ML1009102991) RAI Status (2.4.6-07 and Supplemental 2.4.6-14): Closed.

Results of Contractor's Independent Confirmatory Analysis

In this section, tsunami sources used for the independent confirmatory analysis are described in terms of their identification, characteristic, and tsunami generation parameters. Potential tsunamigenic sources are discussed below, including parameters associated with the maximum submarine landslides in the Gulf of Mexico. At the end of this section, we briefly discuss seismic seiches.

Potential tsunami sources that are likely to determine the PMT at the Levy County site are submarine landslides in the Gulf of Mexico. Subaerial landslides, volcanogenic sources, near-field intra-plate earthquakes and inter-plate earthquakes along Caribbean plate boundary faults are unlikely to be the causative tsunami generator for the PMT at the Levy County site as discussed below.

Subaerial Landslides

With regard to subaerial landslides, there are no major coastal cliffs near the site that would produce tsunami-like waves that exceed the amplitude of those generated by other sources.

Volcanogenic Sources

According to the Global Volcanism Program of the Smithsonian Institution (http://www.volcano.si.edu/), there are three general regions of volcanic activity that have

the potential to generate localized wave activity in the Gulf of Mexico and Caribbean Sea: (1) two Mexican volcanoes near the Gulf of Mexico coastline, (2) two volcanoes in the western Caribbean, and (3) volcanic activity along the Lesser Antilles island arc. Two Mexican volcanoes, (Cerro el Abra/Los Atlixos and San Martin) associated with the eastern Trans-Mexican Volcanic Belt, are located near the Gulf of Mexico coastline (Figure 2.4.6.4.3-1). Basaltic flows associated with Los Atlixcos have reached as far as the coast. Capra et al. (2002) provide an inventory of major debris avalanches associated with the Trans-Mexican Volcanic Belt. In that study, there does not appear to be any major catastrophic failures that would reach the Gulf of Mexico coast.

In the eastern Caribbean, Utila Island, located offshore of Honduras, is composed of primarily pyroclastic cones and rises only 74 m above sea level. However, any flank failures are unlikely to generate significant wave activity in the Gulf of Mexico, owing to the size of the failures and obstructed propagation paths around the Yucatan Peninsula. Also in the eastern Caribbean, Volcán Azul on the coast of Nicaragua is composed of three small cinder cones, but these are unlikely to generate significant failures.

There are many active volcanoes along the Lesser Antilles island arc, some of which have historically caused local tsunamis (Pelinovsky et al., 2004). Because of their distance to the Levy County site and the obstructed propagation path created by the islands of the Greater Antilles, however, tsunami amplitudes from these volcanoes are unlikely to be significant at the site (e.g., Smith and Shepherd, 1995). Similarly, tsunamis generated by volcanic processes in the eastern Atlantic Ocean (e.g., Canary Islands sector collapse) would be greatly attenuated because of the propagation distance (approx. 8,000 km) and scattering caused by obstructions through the Caribbean. In summary, catastrophic failures associated with volcanoes along the eastern coasts of Mexico and Central American are either too far inland or too small in size to generate significant wave activity in the Gulf of Mexico near the Levy County site. Based on existing evidence, volcanoes along the Lesser Antilles or in the eastern Atlantic Ocean are too far away and/or unfavorably situated to generate significant wave activity in the Gulf of Mexico.

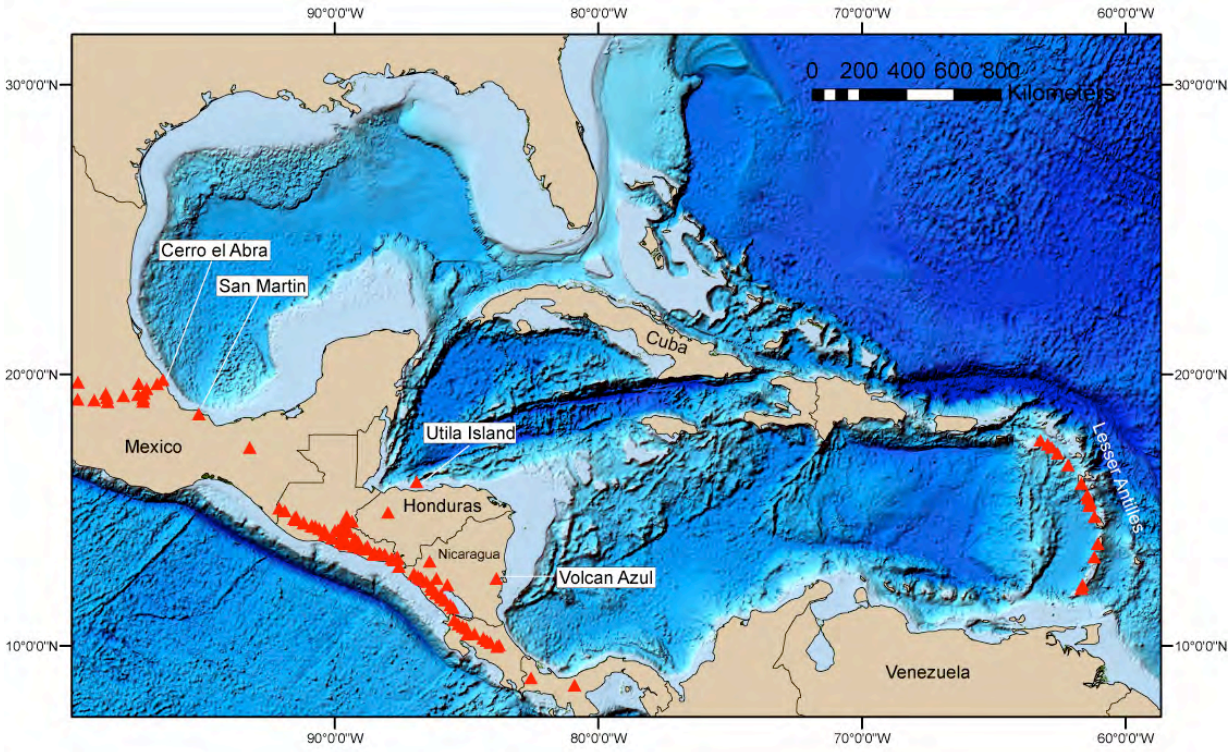

Figure 2.4.6.4.3-1: Location of volcanoes near the Gulf of Mexico and Caribbean Sea.

Intra-Plate Earthquakes

Because there are no tectonic plate boundaries in the Gulf of Mexico region, earthquakes *local* to the Levy County site occur in an intra-plate tectonic environment, limiting the maximum magnitude these earthquakes can attain. According to the documentation for the 2008 update of the United States National Seismic Hazard Maps (Petersen et al., 2008), the maximum magnitude (M_{max}) for the Florida Gulf coast is estimated to be approximately M_{max}=7.5. See Wheeler (2009) and Mueller (2010) for further details. Because the maximum slip, and consequently the maximum sea floor displacement, associated with an earthquake scales with its magnitude, the initial tsunami wave amplitude associated with an intra-plate earthquake would therefore be less than that used for local, submarine landslides under the conservative hot-start conditions as described in Section 2.4.6.4.5. Empirical evidence from global earthquakes indicates that the maximum local tsunami runup from M_w=7.5 earthquakes is approximately 6 m (Geist, 2002). This maximum is related to an earthquake along an island arc (Kuril Islands) without a broad continental shelf that may attenuate the tsunami during propagation.

Inter-Plate Earthquakes

In the far-field, offshore tsunami amplitudes from Caribbean inter-plate earthquakes are estimated in Chapter 8 of ten Brink et al. (2008) using the linear-long wave equations. The description of major plate boundary faults and specific source parameters are described in that study. The tsunami propagation model presented in ten Brink et al. (2008) has been refined during our confirmatory analysis for two of the principal sources

(the northern South America Convergent Zone and the northern Caribbean Subduction Zone) using the COMCOT tsunami model discussed in Sections 2.4.6.4.4 and 2.4.6.4.5. Tsunami amplitudes at the Florida Gulf coast from these seismogenic sources generally are small (i.e., < 1 m) compared to tsunami amplitudes determined for submarine landslides in establishing the PMT. Tsunami amplitudes from earthquakes along the Azores-Gibraltar oceanic convergence boundary also are likely to be small (i.e., < 1 m) in the Gulf of Mexico (Mader, 2001; Barkan et al., 2009). For the remainder of this section, we focus on submarine landslide sources as the principal generator for the PMT at the Levy County site.

Evidence Regarding Potential Tsunamigenic Submarine Landslides in the Gulf of Mexico

Submarine landslides in the Gulf of Mexico are considered a potential tsunami hazard for the Levy County site for several reasons: (1) some dated landslides in the Gulf of Mexico have post-glacial ages (Coleman et al., 1983), suggesting that triggering conditions for these landslides are still present, (2) the size and shallow initiation depth of landslides in the Gulf of Mexico, and (3) analyses of recent seismicity suggest the presence of small-scale energetic landslides in the Gulf of Mexico.

With regard to (1), the Mississippi Canyon landslide is dated 7,500-11,000 years before present (ybp) (Coleman et al., 1983; Chapter 3 in ten Brink et al., 2008) and the East Breaks landslide is dated 15,900 ± 500 ybp (Piper and Behrens, 2003). Both landslides, which are among the largest landslides in the Gulf of Mexico, occurred after the end of the last glacial maximum, during post-glacial transgression. Although landslide activity along the passive margins of North America may be decreasing with time since the last glacial period, the 1929 Grand Banks landslide is a historical example of such an event that produced a destructive tsunami (Fine et al., 2005). In addition, the Mississippi River continues to deposit large quantities of water-saturated sediments on the continental shelf and slope, making them vulnerable to over-pressurization and slope failure.

With regard to (2), several submarine landslide characteristics have been found to be significant in determining tsunami generation potential of the landslide, including headwall depth, landslide volume, initial acceleration of the slide mass, and slide velocity (Ward, 2001; Harbitz et al., 2006). The volume of failed material for several of the landslides in the Gulf of Mexico (see below) and the shallow headwall depths (< 300 m) of the East Breaks and Mississippi Canyon landslides suggest that these landslides had the potential to generate tsunamis.

Finally, with regard to (3), seismograms of an event that occurred on February 10, 2006 (i.e., the Green Canyon event, Figure 2.4.6.4.3-2) offshore of southern Louisiana (Dewey and Dellinger, 2008) suggest that energetic landslides continue to occur in the Gulf of Mexico (Nettles, 2007). Most landslides affected by salt tectonics are small in size (e.g., in comparison to the East Breaks landslide; Chapter 3 of ten Brink et al., 2008) and are unlikely to be tsunamigenic. However, in terms of the failure duration, the 2006 event must have occurred rapidly enough to have generated seismic energy. While source

analyses of this event cannot definitively distinguish between a fault and landslide source and evidence of significant sediment failure has not yet been found (Dellinger and Blum, 2009) this event reveals the potential for present-day slope failure. Shown below is the multibeam bathymetry near the event (Figure 2.4.6.4.3-2) and three seismograms and accompanying spectrograms (P. Whitmore, personal communication). The first seismogram is for a typical earthquake (Figure 2.4.6.4.3-3), showing a sudden onset of the seismic waves (body waves) and significant high frequency energy indicative of fault slip. The second seismogram is for a known subaerial landslide that occurred in SE Alaska (Figure 2.4.6.4.3-4), showing a gradual (emergent) build up of seismic waves, no obvious P-waves, and a deficiency in high-frequency energy. The third seismogram is for the 2006 Gulf of Mexico event (Figure 2.4.6.4.3-5) and shares many of the same characteristics as the SE Alaska landslide (emergent, lack of high-frequency energy).

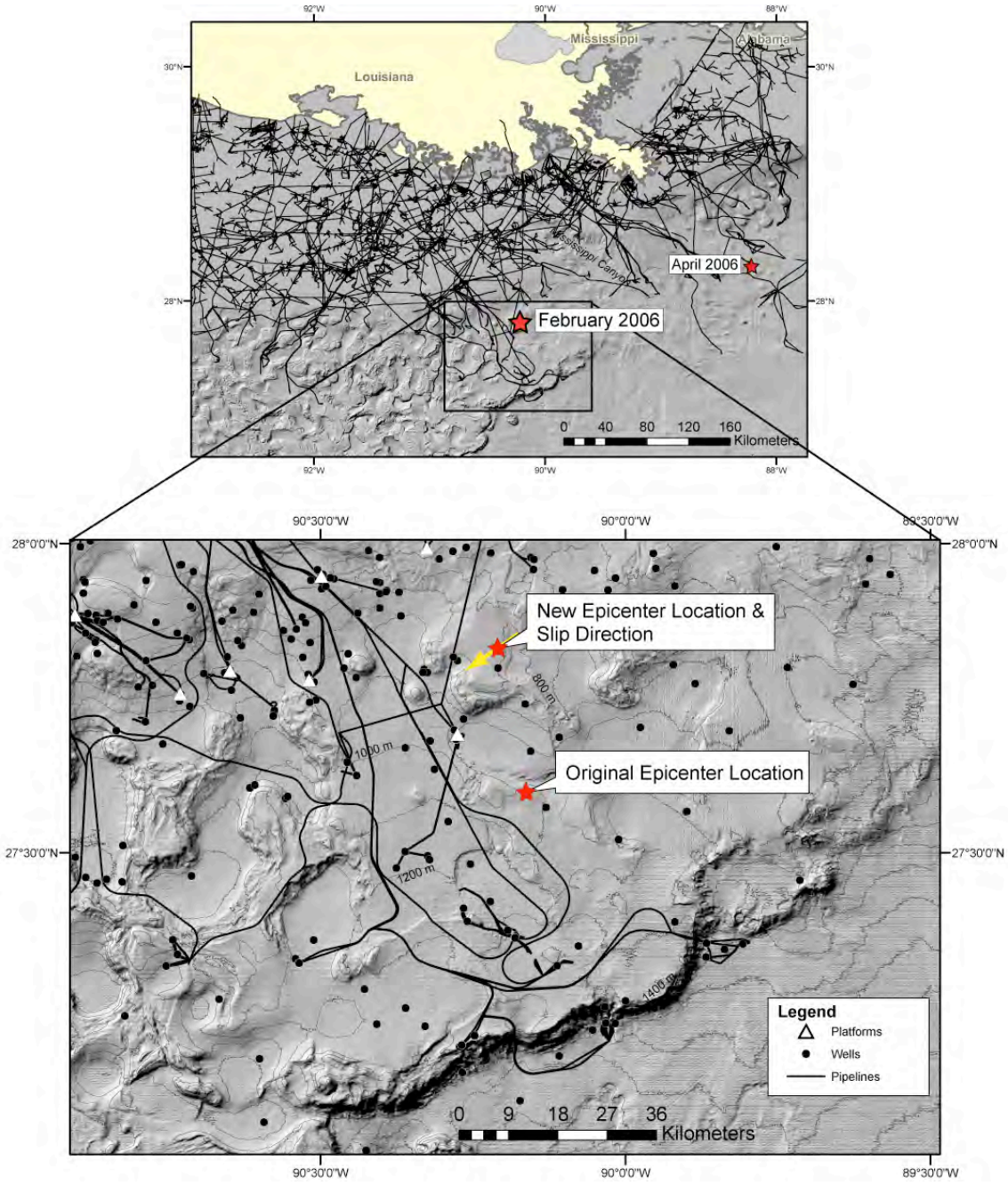

Figure 2.4.6.4.3-2: Multibeam bathymetry showing the area around the February 10, 2006 Green Canyon event in the Gulf of Mexico that was seismically recorded.

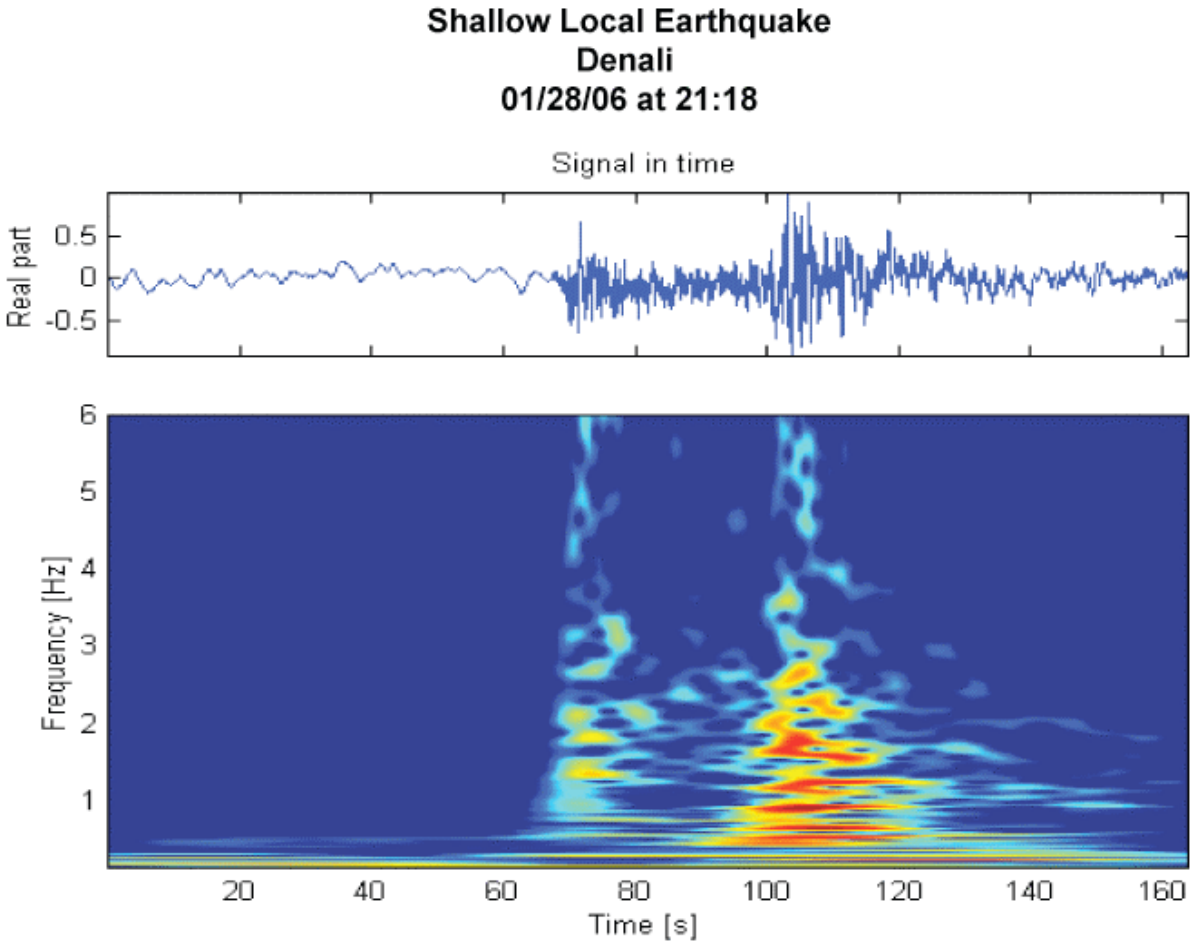

Figure 2.4.6.4.3-3: Seismogram (top) and spectrogram of a typical shallow earthquake (M 3.9 January 27, 2006 Denali earthquake)

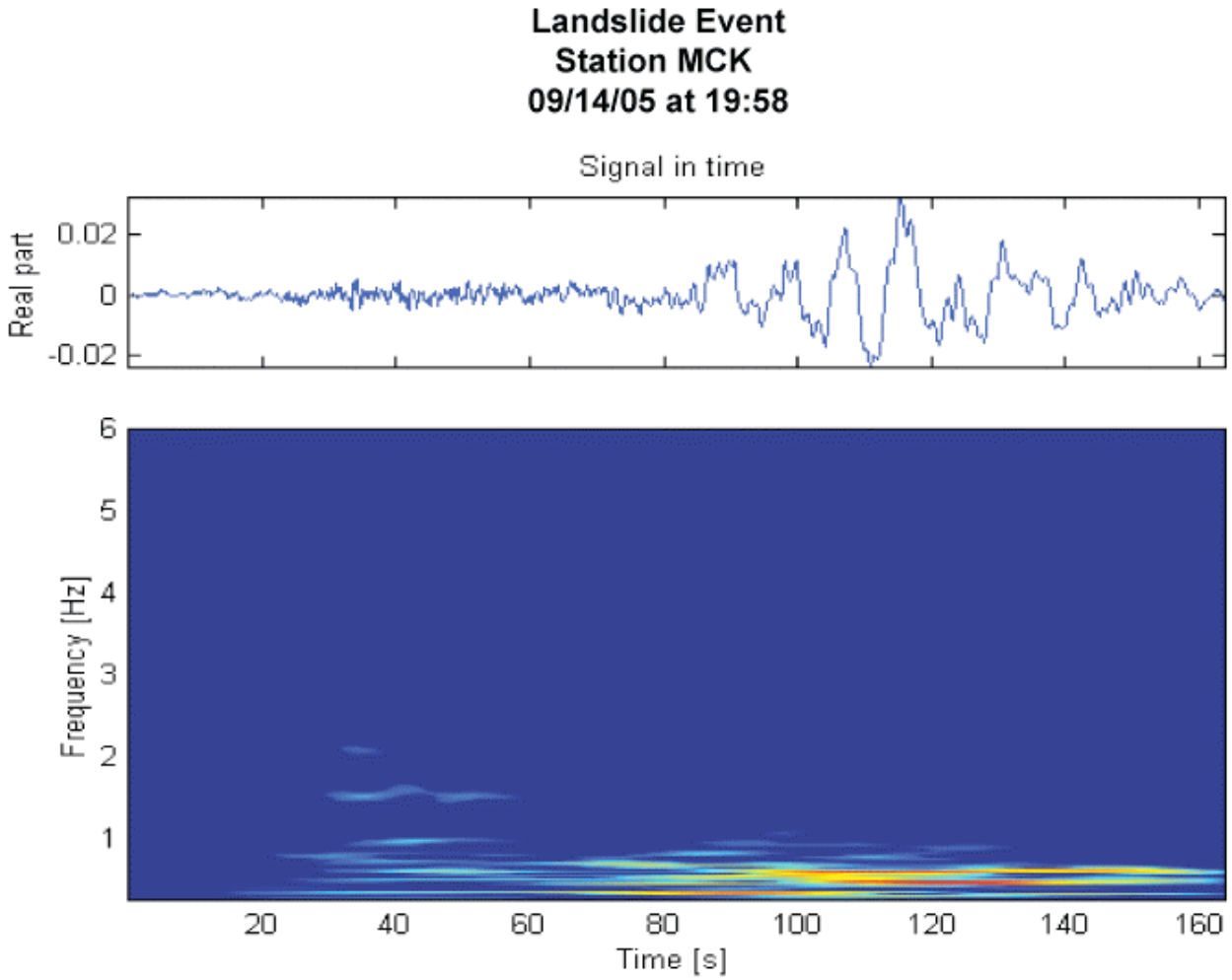

Figure 2.4.6.4.3-4: Seismogram (top) and spectrogram of a known subaerial landslide in SE Alaska. MCK: McKinley Park seismic station.

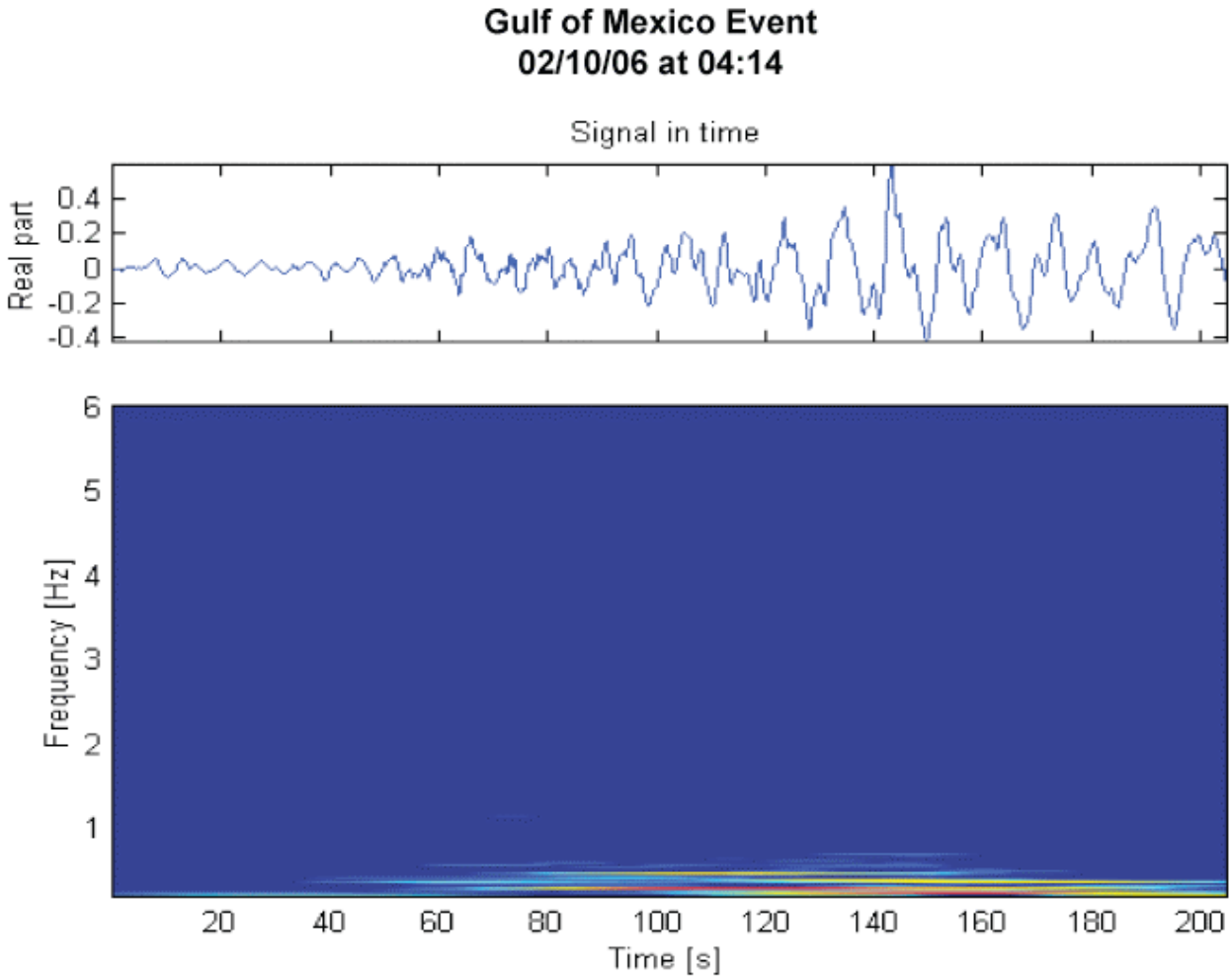

Figure 2.4.6.4.3-5: Seismogram (top) and spectrogram of the February 10, 2006 Gulf of Mexico Green Canyon event (see Fig. 1 for location). Note the similarity with Fig. 2.4.6.4.3-3 (landslide) and the dissimilarity with Fig. 2.4.6.4.3-2 (earthquake).

Maximum Submarine Landslides

We define four provinces in the Gulf of Mexico that are likely to be the origin of submarine landslides that control the determination of the PMT. Three additional provinces defined in Chapter 3 of ten Brink et al. (2008) are not likely to be sites of major tsunamigenic landslides. The four provinces defined for PMT analysis are the Florida Escarpment and Slope region (immediately off the Levy County site), Mississippi Canyon, Northwest Gulf of Mexico, and Campeche Escarpment and Slope. The Northwest Gulf of Mexico is a mixed canyon/fan and salt province consisting of terrigenous and hemipelagic sediment, the Mississippi Canyon is a canyon/fan province consisting of terrigenous and hemipelagic sediment, and the Campeche and Florida margins are carbonate provinces formed from reef structures and characterized by having steep slopes. Above these escarpments a broad, gentle slope comprised of carbonate sediment separates the escarpments from the shelf.

The primary landslide parameters that are used in the tsunami models include the excavation depth and slide width, which can be directly measured from sea floor mapping of the largest observed slide in the four geologic provinces. The other necessary parameter is downslope landslide length, interpreted from the runout distance. The runout distance measured from sea floor mapping is a combination of fast plug flow (low viscosity, non-turbulent), creeping plug flow (high viscosity/viscoplastic, non-turbulent) and turbidity currents (turbulent boundary layer fluid). The latter two likely have little to no tsunami-generating potential. Also, turbidity currents often involve entrainment of material during flow, such that the deposition volume may be greater than the excavation volume. Finally, hydroplaning may increase the runout of submarine landslides. The landslide lengths indicated below are intended to represent the main tsunami-generating phase. The amplitude of the initial negative wave above the excavation region is linked to the maximum excavation depth. The amplitude of the initial positive wave above the deposition region is determined from a conservation of landslide volume. The excavation volume can be well determined using GIS techniques (see below). Setting the deposition volume equal to the excavation volume, the positive amplitude is determined for a given landslide length. For a fixed volume, increasing the landslide length decreases the initial positive amplitude of the landslide tsunami.

Landslide volume calculations are based on measuring the volume of material excavated from the landslide source area using a technique similar to that applied by ten Brink et al. (2006) and Chaytor et al. (2009). Briefly stated, the approach involves using multibeam bathymetry to outline the extent of the excavation area, interpolating a smooth surface through the polygons that define the edges of the slide to provide an estimate of the pre-slide slope surface, and subtracting this surface from the present seafloor surface.

The maximum observed landslide from multibeam surveys is taken as the maximum landslide for a given region. It may be possible that larger landslides could occur in a given region, however this determination of the maximum landslide is consistent with the overall definition of PMT as “the most severe of the natural phenomena that have been historically reported or determined from geological and geophysical data for the site and

surrounding area." In this case, the maximum landslide is taken from geologic observations spanning tens of thousands of years. Moreover, because landslide volumes appear to follow a power-law or log-normal distribution (ten Brink et al., 2006; Chaytor et al., 2009), there may be no mathematical or physical constraints on the definition of the theoretical maximum landslide (other than the dimensions of the entire continental slope). These calculations were only completed for part of the East Breaks landslide, the Mississippi Canyon landslide, and a landslide from the slope above the Florida Escarpment. No calculations were made for failures above the Campeche Escarpment because currently available bathymetric data are inadequate.

East Breaks Landslide
Geologic Setting: River delta that formed at the shelf edge during the early Holocene (Figure 2.4.6.4.3-6)
Post Failure Sedimentation: Landslide source area appears to be partially filled (predominantly failure deposits with some post-failure sedimentation)
Age: 10,000 - 25,000 years (Piper, 1997; Piper and Behrens, 2003)

Maximum Single Event (East Breaks landslide): Maximum and minimum parameters are taken from different interpretations of the digitized failure scar surrounding the excavation region (Chaytor et al., 2009).

Max
- Volume: 21.95 km^3
- Area: 519.52 km^2

Min
- Volume: 20.80 km^3
- Area: 420.98 km^2

Width: ~ 12 km

Length: ~ 50 km

Excavation depth: ~160 m (shelf edge to base of headwall scarp)

Run out distance: 91 km from end of excavation and 130 km from headwall based on GLORIA mapping (Rothwell et al., 1991) (See Figure 2.4.6.4.3-7). Multibeam bathymetry is not available for the entire run-out area.

Trabant et al. (2001) have reported volumes of 50-60 km^3 and a run-out distance of 160 km. Trabant et al. (2001) derived their volume estimate from the size of debris lobes in the deposition region using a 3D seismic reflection dataset that is proprietary. We cannot confirm their result owing to the proprietary nature of the dataset and because we lack the necessary bathymetry coverage that far downslope to identify the extent of the debris lobes. Debris lobes are often the result of multiple events that are difficult to distinguish (Chaytor et al., 2009; Twichell et al., 2009) and may include sediment entrainment during

flow. Our volume estimate above is for the amount excavated at the source (within the landslide scarp) and is more representative of a single failure event.

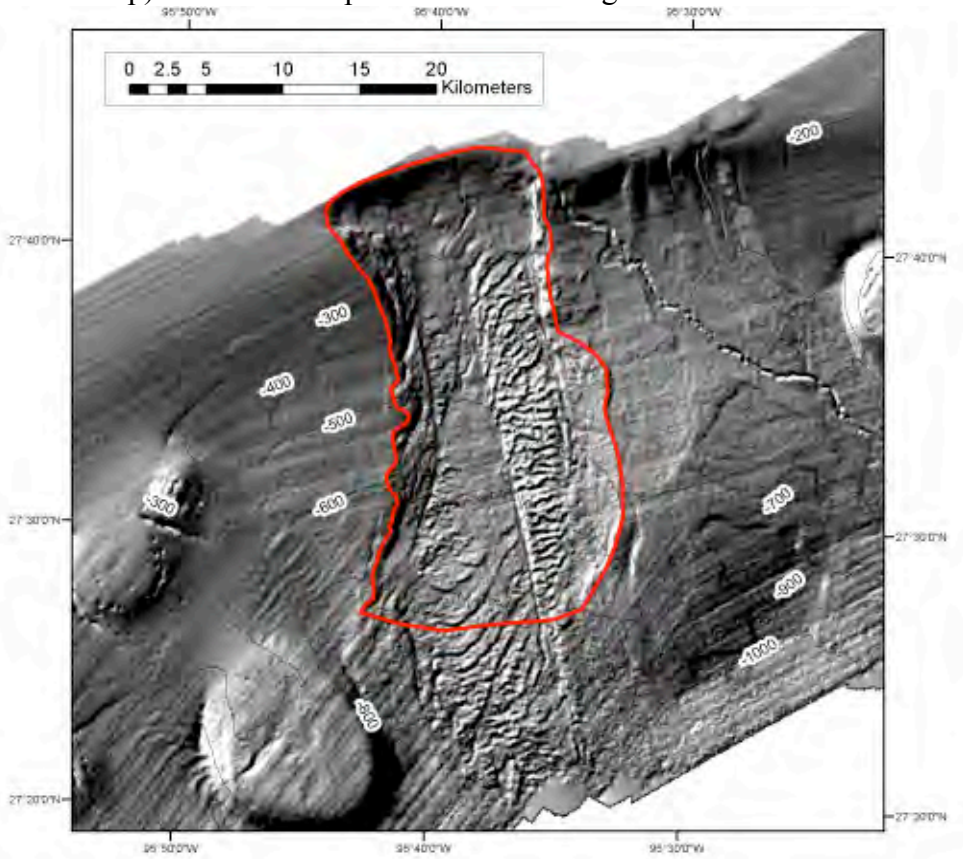

Figure 2.4.6.4.3-6: Outline (red) of excavation area for the East Breaks landslide based on available multibeam bathymetric data.

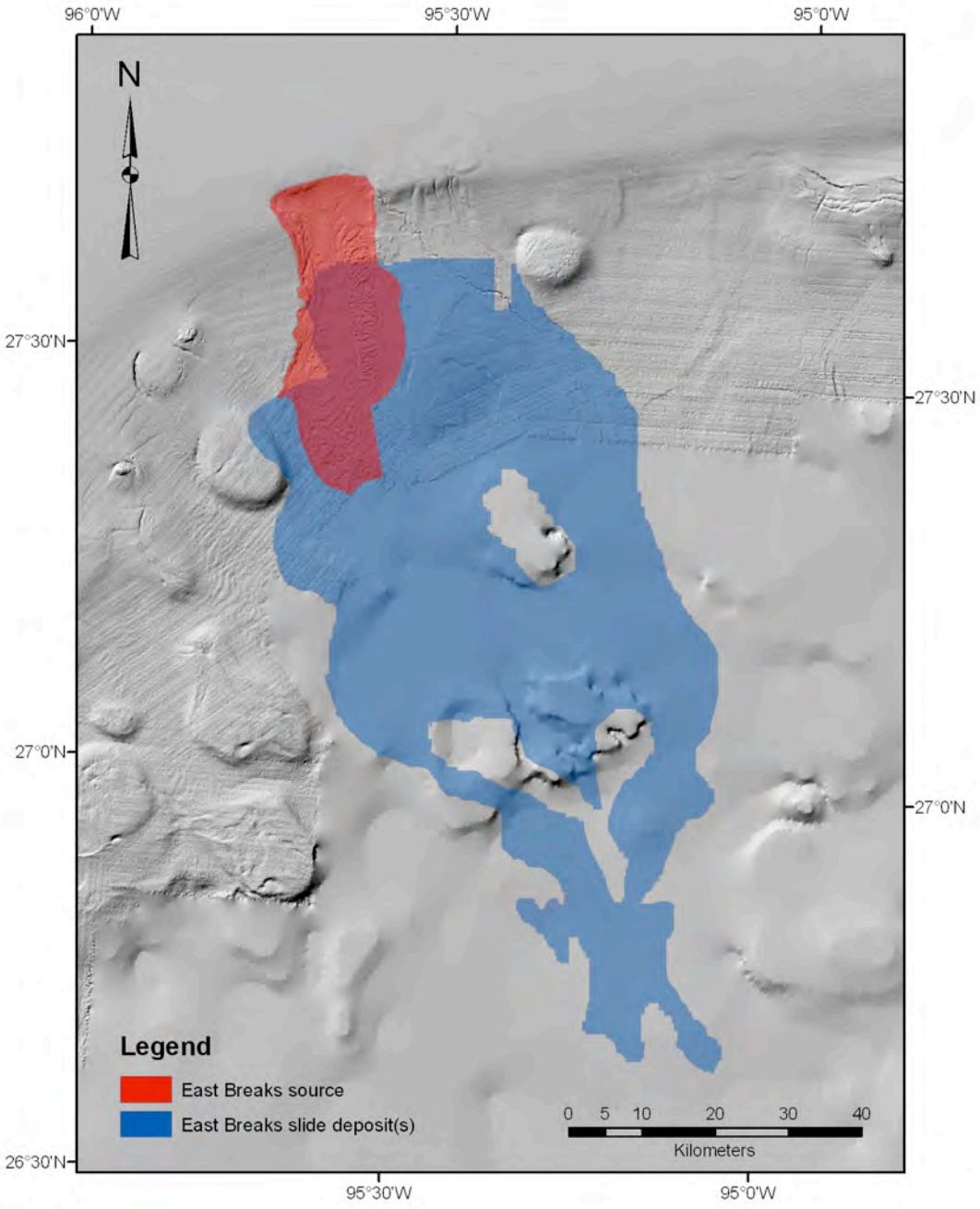

Figure 2.4.6.4.3-7: Comparison of excavation area (red) and depositional area (blue) for the East Breaks landslide. The extent of the landslide deposit was mapped using GLORIA sidescan sonar imagery (Rothwell et al., 1991).

Mississippi Canyon
Geologic Setting: River delta and fan system (Figure 2.4.6.4.3-8).
Post Failure Sedimentation: Canyon appears to be partially filled with failure deposits that are capped by hemipelagic sediments.
Age: 7,500 - 11,000 years (Coleman et al., 1983; Chapter 3 in ten Brink et al., 2007)
Maximum Single Event

- Volume: 425.54 km^3
- Area: 3687.26 km^2
- Excavation depth: ~300 m (in the upper canyon)
- Runout distance: 297 km from toe of excavation area and 442 km from the headwall scarp (see Figure 2.4.6.4.3-9).

Other reported volumes are1,500-2,000 km^3 (Coleman et al., 1983). As with the East Breaks landslide, this estimate is from landslide deposits that most likely represent multiple failure episodes. The volume given above is our best estimate of a maximum single-event volume.

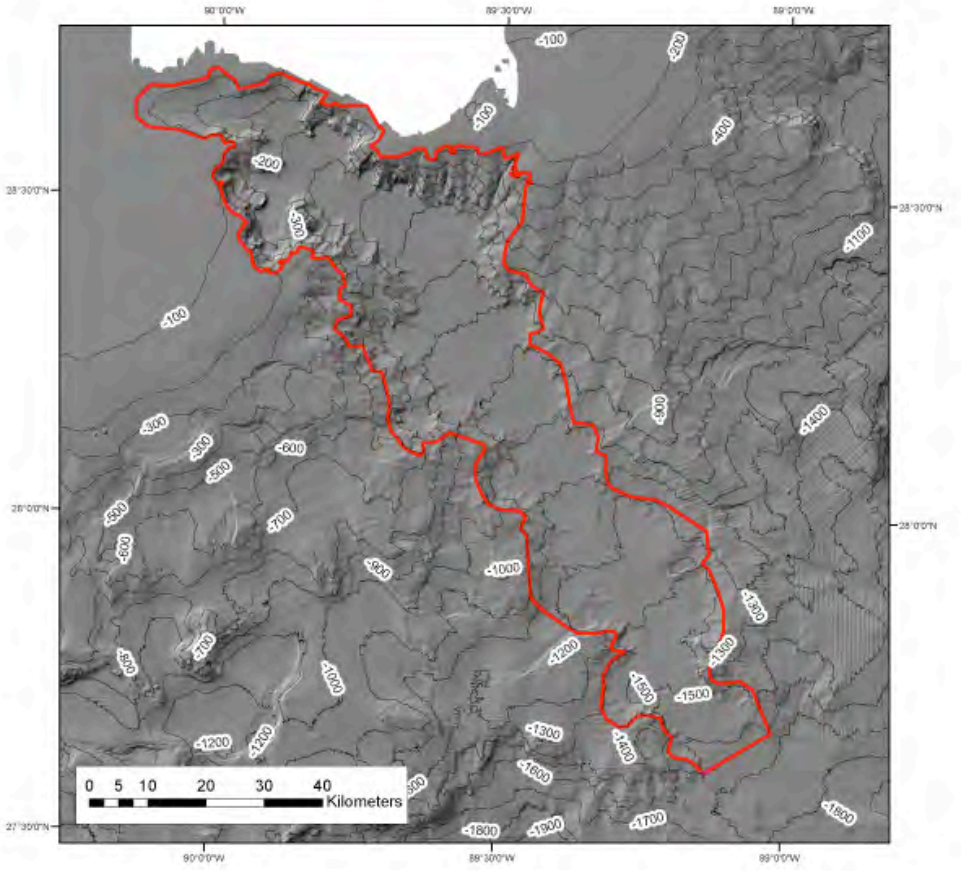

Figure 2.4.6.4.3-8: Outline (red) of excavation area for the Mississippi Canyon landslide based on multibeam bathymetric data and reports by Coleman et al. (1983) and Goodwin and Prior (1989).

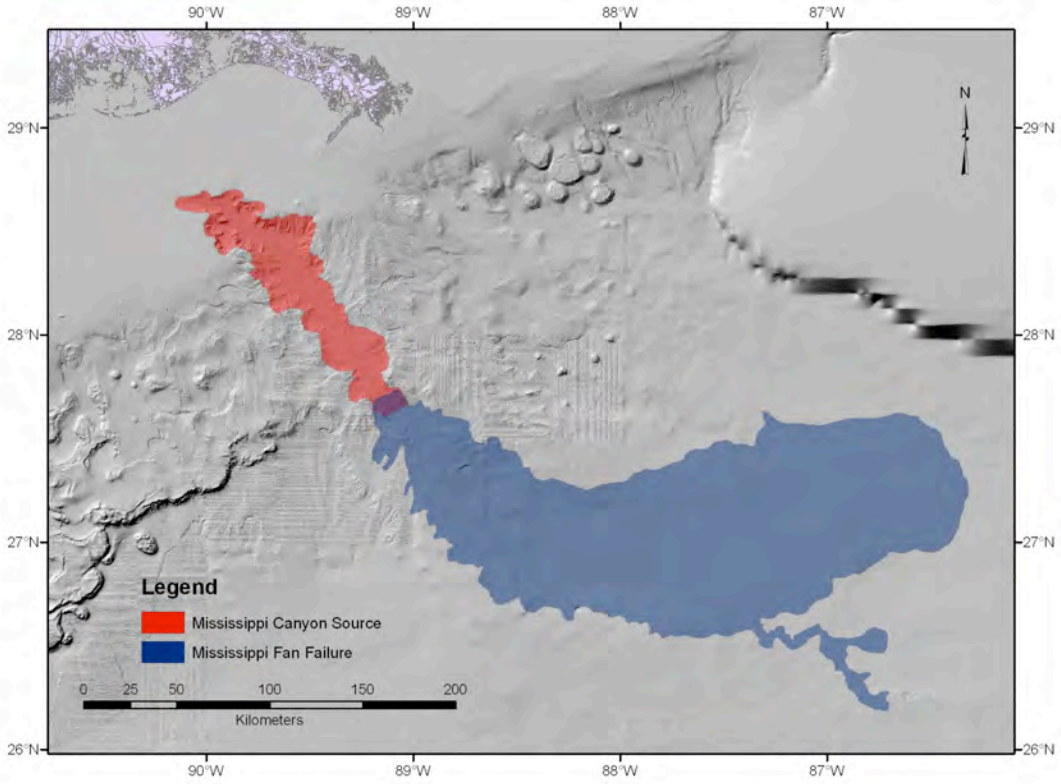

Figure 2.4.6.4.3-9: Comparison of excavation area (red) and depositional area (blue) for the Mississippi Canyon landslide. The extent of the landslide deposit is based on GLORIA sidescan sonar imagery (Twichell et al., 1991).

Florida Escarpment and Slope

Geologic Setting: The slope above the edge of a carbonate platform (Figure 2.4.6.4.3-10).

Post Failure Sedimentation: None visible on multibeam images or on available high-resolution seismic profiles (Twichell et al., 1993).

Age: Early Holocene or older (Doyle and Holmes, 1985). Because the deposits from these carbonate failures accumulate along the base of the Florida escarpment are buried by Mississippi Fan deposits, they are older than the youngest fan deposits dated at about 11,500 years old.

Maximum Single Event

- Volume: 16.2 km^3
- Area: 647.57 km^2
- Excavation depth: ~150 m, but quite variable
- Runout distance: Uncertain. The landslide deposit is at the base of the Florida Escarpment buried under younger Mississippi Fan deposits.

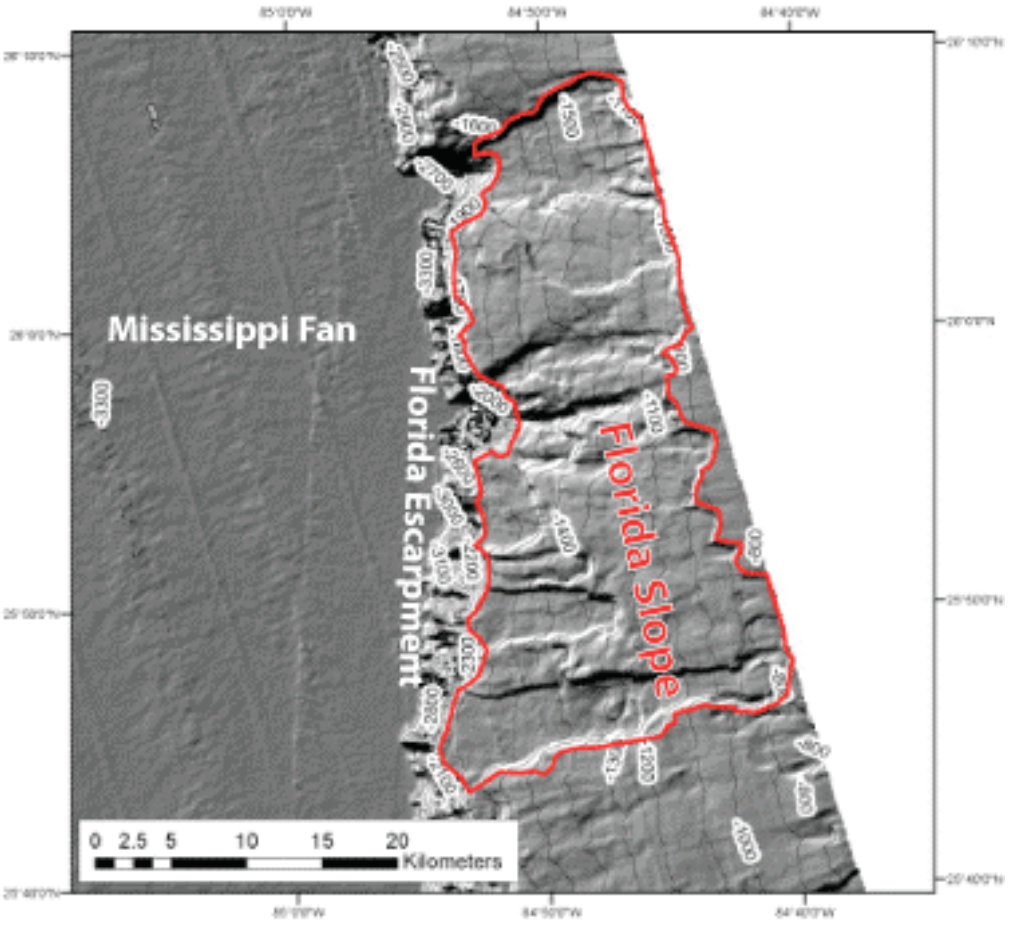

Figure 2.4.6.4.3-10: Outline (red) of excavation area for the maximum landslide above the Florida Escarpment from multibeam bathymetric data.

Campeche Escarpment
Geologic Setting: Carbonate platform

One of the persistent issues during the independent confirmatory analysis is acquiring sufficient geologic information about the Campeche Escarpment with which to estimate the maximum landslide parameters as with the other Gulf of Mexico landslide provinces. Plans to conduct multibeam bathymetry surveys are pending. Presently, there is no published information showing the detailed bathymetry or distribution of landslides on or above the Campeche Escarpment.

Seismic Seiches

Seismic seiches are fundamentally a different type of wave than tsunamis. Rather than being impulsively generated by displacement of the sea floor, seismic seiches occur from resonance of seismic surface waves (continental Rayleigh and Love waves) within enclosed or semi-enclosed bodies of water. The harmonic periods of the oscillation are dependent on the dimensions and geometry of the body of water. In 1964, seiches were set up along the Gulf Coast from seismic surface waves emanating from the M=9.2 Gulf of Alaska earthquake. The efficiency at which the seiches occurred at great distance from the earthquake is explained primarily by amplification of surface wave motion from the thick sedimentary section along the Gulf Coast (McGarr, 1965). Because the propagation path from Alaska to the Gulf Coast is almost completely continental (McGarr, 1965) and because the magnitude of the 1964 earthquake is close to the maximum possible for that subduction zone (e.g., Bird and Kagan, 2004), it is likely that the historical observations of 1964 seiche wave heights are the maximum possible, which are less than the PMT amplitudes from landslide sources.

Conclusions:

In summary, we list the following findings of our independent confirmatory analysis of the tsunami source characteristics below:

- There is sufficient evidence to consider submarine landslides in the Gulf of Mexico as a present-day tsunami hazard for the purpose of defining the PMT at the Levy County Site.
- Four landslide provinces within the Gulf of Mexico are applicable for determining the PMT: Northwest Gulf of Mexico, Mississippi Canyon, slope above the Florida Escarpment, and Campeche Escarpment.
- Parameters for the maximum submarine landslide were determined for each of the provinces, except for the Campeche Escarpment where we are awaiting additional data.
- It is likely that seismic seiche waves resulting from the 1964 Gulf of Alaska earthquake are nearly the highest possible, owing to a predominantly continental ray path for seismic surface waves from Alaska to the Gulf Coast, but are smaller than the PMT amplitudes from submarine landslides in the region.

2.4.6.4.4 Tsunami Analysis

The applicant's tsunami analysis primarily consists of using past studies to ascertain the tsunami propagation characteristics from the three source regions discussed in Section 2.4.6.3 to estimate tsunami amplitudes offshore of the Levy County Nuclear Plant site. Different types of tsunami analyses were used to estimate tsunami water levels for each of the three source regions.

For tsunami sources located in the far-field, the applicant only considers a source with characteristics similar to the 1755 Lisbon tsunami. To determine tsunami amplitudes in the Gulf of Mexico from this far-field earthquake, the applicant cites the results of Mader (2001). The applicant indicates that Mader (2001) uses the non-linear long wave equations and a 10-minute bathymetric grid to calculate tsunami amplitudes.

For tsunami sources located in the Caribbean region, the applicant cites analyses of open-ocean propagation presented by Knight (2006) (FSAR reference 2.4.6-225) and the USGS Administrative Report (2007) describing tsunami sources affecting U.S. Atlantic and Gulf Coasts (FSAR reference 2.4.6-214). The tsunami analysis method used by Knight (2006) is not indicated by the applicant. The Caribbean sources used in the analysis by Knight (2006) include earthquakes along the northern Caribbean subduction zone (i.e., the "Puerto Rico Trench" as termed by Knight, 2006), a source possibly related to the Cayman transform fault system (i.e., the "Swan fault" offshore Cancun, Mexico as termed by Knight, 2006), and the northern South America convergence zone (incorrectly called the "North Panama Deformed Belt" by Knight (2006) and by the applicant). The tsunami analysis method used in the USGS Administrate Report (2007) is a finite-difference approximation to the linear-long wave equations. Tsunami propagation across the continental shelf and tsunami runup were not modeled in the USGS study. The Caribbean sources used in the USGS (2007) analysis, as indicated by the applicant, include earthquakes along the northern Caribbean subduction zone, the Cayman transform fault system, the North Panama Deformation Belt, and the northern South America convergence zone.

For tsunami sources located in the Gulf of Mexico region, the applicant considers both earthquake and landslide sources. Although intra-plate sources in the vicinity of the Mw=5.8 September 10, 2006 Gulf of Mexico earthquake are not further considered for tsunami analysis by the applicant, an offshore Veracruz tsunami scenario from Knight (2006) is considered, which the applicant links to intra-plate seismicity. As with the Caribbean tsunami sources where the applicant cites the work of Knight (2006), the tsunami analysis method used for the Veracruz tsunami scenario is not stated by the applicant. For landslide sources in the Gulf of Mexico, the applicant uses a tsunami attenuation function (FSAR equation 2.4.6-1) derived by Zahibo et al. (2003) (FSAR reference 2.4.6-222) for tsunamis originating in the Caribbean region. The theoretical basis for this attenuation function, and evidence of its applicability for tsunamis in the Gulf of Mexico, is not included in the FSAR. The applicant uses a Monte Carlo analysis to establish the maximum wave height near the Levy County Nuclear Plant from this attenuation function.

Request for Additional Information (RAI) 2.4.6-08: Section C.I.2.4.6.4 of Regulatory Guide 1.206 (RG 1.206) provides specific guidance with respect to tsunami analysis. This includes providing a complete description of the analysis procedure used to calculate tsunami wave height and period at the site, including the theoretical bases of the models, their verification and the conservatism of all input parameters.
Provide theoretical basis, assumptions (e.g., source parameterization), and applicability to the Levy County site for the tsunami attenuation function discussed on pg. 2.4-53 (Equation 2.4.6-1) and make available the details of the Monte Carlo analysis used to estimate the maximum wave height and where the maximum wave height estimate is geographically located. For this and other methods of tsunami analysis indicated in the FSAR, provide the procedure use to calculate tsunami propagation, runup, and inundation (i.e., tsunami water levels) at the Levy County site from offshore tsunami amplitude.

Resolution of RAI 2.4.6-08 and issuance of Open Items: In response to RAI 2.4.6-08, the applicant provides a substantial new effort regarding analysis for tsunami generation, propagation, and runup. However, there are several unresolved issues in the applicant's response: (1) the formulas for source amplitude are poorly documented (they are not contained in Silver et al., 2009); (2) water depths listed in Table 1 seem arbitrary (e.g., 300-800 m for East Breaks); (3) it is unclear how source "diameter" is determined; (4) there are typographic errors in the numbers for the Veracruz and Venezuela source diameters (Table 4); (5) the assumption that "wave amplitude onshore cannot exceed its estimated runup height at shore," is incorrect, but this may be an issue with the terminology; and (6) variable *Co* in equations 17 and 18 is undefined. The applicant needs to provide additional details regarding the method for tsunami analysis in reference to the aforementioned items. Supplemental RAI 2.4.6-15 issued.

Supplemental RAI 2.4.6-15: To meet the requirements of GDC 2, 10 CFR 52.17, and 10 CFR Part 100, the applicant must provide an assessment of the Probable Maximum Tsunami (PMT) for the proposed Levy County site. Section C.I.2.4.6.4 of Regulatory Guide 1.206 (RG 1.206) provides specific guidance with respect to tsunami analysis. This includes providing a complete description of the analysis procedure used to calculate tsunami wave height and period at the site, including the theoretical bases of the models, their verification and the conservatism of all input parameters. Provide additional details regarding the new methodology for tsunami analysis described in response to RAI 2.4.6-08. This discussion should specifically include (1) the basis for source amplitude formulae (they are not contained in Silver et al., 2009); (2) clarify what is meant by "wave amplitude onshore cannot exceed its estimated runup height at shore" (statement is incorrect using standard tsunami terminology); (3) definition of variable Co in equations 17 and 18..

Resolution of RAI 2.4.6-15 and issuance of Open Items: In response to this RAI, the applicant revised their method, clarifying some of the issues (1-3). However, in their revised method, the applicant's maximum "runup" of 22.5 m is not reasonably consistent with a "run-in" distance of 2.07 km that they estimate. In the staff's 2HD analysis using

conservative friction values, an attenuated 3 m runup is associated with an 18 km "run-in" distance. Using similar scaling for the applicant's 22.5 m runup would result in a tsunami that would impact the site. Supplemental RAI 2.4.6-16 issued.

Supplemental RAI 2.4.6-16: In reference to Progress Energy's response to RAI 02.04.06-15 (25 March 2010, NPD-NRC-2010-025, L0696), the PMT runup (21.4 m) given in Table 1 is inconsistent with the accompanying inundation distance. It is noted that runup is defined as the ground elevation at the location of maximum tsunami inundation, which is consistent with the depiction given in Figure ATTACHMENT 02.04.06-15A. As can be found from topographic maps, the ground elevation at a distance of 1.2 miles from the shoreline in the direction of the Site is approximately 1m. The 21 m topographic elevation is well inland of the Site. It would not be expected that two separate equations are needed to find the runup and the inundation distance; calculation of either one, used in conjunction with topographic maps, provides the other value. Please provide clarification on these values (eta and X in Table 1), including which of the two values should be used to define the PMT, and if the variable definitions as given in Figure ATTACHMENT 02.04.06-15A are correct. In Table 1 provided in the response, please provide the geographic location (lat, long) corresponding to the location at the given distance R from the source, as well as the depth at that location, since it is needed to determine the runup elevation. For completeness, please provide a clear presentation of all equations used, discussion of assumptions inherent in these equations and the associated conservatism, and the procedure to calculate the provided values. Please provide all input data sources, calculation packages, and any associated modeling input files.

Resolution of RAI 2.4.6-16 and issuance of Open Items: The applicant has not performed a numerical, site-specific analysis of tsunami water levels. Instead the applicant continues to try to find analytic expressions for tsunami generation, propagation (including shoaling), and runup that are an adequate substitute.

The applicant provided their response to this RAI 2.4.6-016 in three parts (3a, 3b, and 3c). Response 3a concerns the definitions of runup and wave height at the shoreline. This response clarifies their use of these terms. Response 3b describes the location of the different tsunami sources considered, although RAI 2.4.6-016 sought to determine the coordinates of the nearshore location near the site where runup calculations were made (i.e., the "measurement point"). Response 3c presents a revised procedure to determine PMT runup and inundation.

In their revision of FSAR Section 2.4.6.6.3 "Water Levels Due to Worst Case Tsunamigenic Events Using a Simplified Formula-Based Approach", it is unclear where the applicant's source amplitude Equation 2.4.6-3 comes from, as well as values for landslide speed listed in Table 2.4.6-206. For propagation, the applicant relies heavily on a series of papers by Ward and others developed for impact tsunamis sources (not submarine landslides) to estimate the propagation amplitudes. Therefore, there is a disconnect between the landslide source amplitude described in Section 2.4.6.6.3.1 and the propagation equations (really, fitted attenuation curves) for impact tsunamis in

Section 2.4.6.6.3.2. The applicant does not correctly cite where the equations for the propagation attenuation curves come from, their domain of applicability, and assumptions Ward and others made to fit these curves.

The applicant misuses equations for the calculation of nearshore wave amplitude and runup. In section 2.4.6.6.3.4 (Applying Beaching Correction), the applicant provides the following equation (2.4-15) for "shoreline wave height", *h*:

$$h = A(s)^{4/5} H_s^{1/5}$$

The applicant indicates that this equation is to be applied at the "beach and ocean interface." It is unclear what this means. Is it the interface at the peak run-in of the tsunami (for which case h=runup elevation), or is it the location of the "typical" beach and ocean interface? To be consistent with what is given in FSAR Reference 2.4.6-237, *h* must in fact be the runup elevation. The above reference is the most recent publication and summary of the various approaches of Ward and others, and states:

> "Using the methods above, I propagate tsunami to a position close to shore in shallow water where it can be considered a long wave, but not so shallow that its amplitude *A(h)* exceeds water depth *h* there. I estimate run up height η, on shore by $\eta = A(h)^{4/5} h^{1/5}$ (19). Because *A(h)*<*h*, run up always exceeds the offshore wave amplitude."

Note that this equation for runup is identical in form to that given by FSAR Equation 2.4.15 above. Thus, this equation should be used for runup, and is a function of a nearshore wave amplitude, *A(h)*, evaluated at a nearshore depth, *h*, such that at this location, the amplitude is less than the depth.

It is again reiterated that the application of equation 2.4.15 in the applicant's study is inconsistent with the equation presented in the studies by Ward and others. This equation form should and can be used directly for runup, not a "shoreline wave height" as indicated in the revised FSAR by the applicant.

Thus, proceeding with the "correct" expression as given above by Ward (2010) (FSAR Reference 2.4.6-237), one needs the amplitude and depth combination for any source to determine its runup. Assuming that the faster Mississippi Canyon slide is the PMT source, the applicant provides a source amplitude of 73 m (revised FSAR Table 2.4.6-206). At a distance of 640 km (revised FSAR Table 2.4.6-206), the offshore height is given as 7.17 m (revised FSAR Table 2.4.6-207). Note that according to the equations used by the applicant, this variable should actually be wave amplitude, rather than wave height as indicated in the revised FSAR. As noted clearly in RAI 2.4.6-016, in order to now proceed and use the runup equation of Ward (2010), the local depth when the wave height is 7.17 m must be provided, and must, according to the description given by Ward, be greater than the amplitude of 7.17 m. Using Google Earth, the water depth at this distance is, very approximately, 10 m. Thus, according to the approach of Ward (2010), the runup elevation = (7.17 m)^0.8 (10 m)^0.2 = 7.66 m. There is no need for the additional run-in distance equations, which are extremely empirical in form, and would be difficult to justify for a required site-specific analysis such as needed here.

In conclusion, the revised nearshore equations as given in the newest applicant response are now incorrect, according to the most recent review article of Ward (2010) (FSAR Reference 2.4.6-237). In the previous FSAR revision, the source depth was being used for "*h*" in Ward's equation 19 above, rather than the proper shallow water depth. This yielded erroneously high runup elevations. The applicant is having the same issue now with their "Shoreline Wave Height" as shown in Table 2.4.6-207. Note that (7.17 m)^0.8 (1689 m)^0.2 = 21.4 m. Again, 7.17 m is the wave amplitude in the 10 m depth, while 1689 m is the depth at the landslide source.

It is extremely conflicting that the applicant in their current analysis can develop a method to give them a 2.3 m runup elevation (Table 2.4.6-208) using a 21 m shoreline height, while the proper application of the Ward approach gives a 7.7 m runup height using a 7.1 m amplitude in 10 m of water. This is a very strong indication that a more detailed, site-specific analysis may be justified.

Supplemental RAI 2.4.6-17 issued.

Supplemental RAI 2.4.6-17: To meet the requirements of GDC 2, 10 CFR 52.17, and 10 CFR Part 100, PEF should provide an assessment of the Probable Maximum Tsunami (PMT) by providing the following information:

(a) An analysis of the PMT event using a technically sound and conservative approach such as those predicted by a site and region specific model approach applicable to tsunami waves to calculate tsunami water levels at or near the site. Such a model avoids approximations of source geometry, bathymetry between the source and offshore of site, and topography near the site inherent in the applicant's current approach. For example, shallow water wave equation models (COMCOT, ComMIT, Delft3D) and Boussinesq-type Models (Coulwave, Funwave, Geowave) could be used for earthquake and earthquake/landslide/impact generated tsunamis, respectively.

If a numerical model is used, provide a clear presentation of all equations used, discussion of assumptions inherent in these equations and the associated conservatism, and the procedure to calculate the water-level values. Please provide all input data sources, calculation packages, and any associated modeling input files.

(b) If the existing approach which relies on the Ward et al publication is used, proper usage of these methods must be checked, and a complete presentation of the theoretical assumptions, as relevant to propagation modeling of a landslide-generated wave and runup/inundation, should be provided. The applicant must provide site-specific justification as to why the Ward (2010) equations are applicable and conservative for the Levy site. This would typically involve presenting the theoretical assumptions behind the generation, attenuation, shoaling, and runup equations, and why these assumptions are valid and conservative with respect to site-specific conditions. Specifically:

Tsunami Generation: (1) Provide the reference for wave amplitude Equation 2.4.6-3, along with relevant assumptions used to develop that equation. (2) Provide references for

the expressions of slide velocity and a clear indication as to which expressions were used to calculate the slide velocities listed in Table 2.4.6-206. (3) Provide the rationale and justification for using Equation 2.4.6-8 derived for impact tsunami sources to model landslide tsunamis, particularly with regard to differences in wave characteristics between landslide and impact tsunamis. (4) Explain how diameter listed for each source in Table 2.4.6-206 relates to landslide parameters.

Tsunami Propagation: (1) Explain how the "measurement point" is chosen to determine R, the distance of measurement point from the source. (2) Because the "measurement point" is a nearshore location, justify the use of Equation 2.4.6-11 that is derived for constant water depth, considering the broad continental shelf offshore of western Florida. (3) If in a revised procedure applicant applies the propagation and shoaling terms at the edge of the continental shelf, provide an expression for propagation across the continental shelf. (4) The equation for the attenuation curves (2.4.6-8) is miss-cited. Provide the correct reference, domain of applicability of these fitted curves, and assumptions used to derive these curves.

Tsunami Runup: (1) Definition of h in Equation 2.4.15 is inconsistent with the definition indicated in FSAR References 2.4.6-228 and 2.4.6-237, from which this equation was taken. In the revised FSAR, applicant indicates that h represents "shoreline wave height" whereas it is intended to represent runup as described in the aforementioned References. Provide clarification of the use of Equation 2.4.15. (2) Provide the theoretical assumptions behind the equation 2.4.15, and why these assumptions are valid and conservative with respect to site-specific conditions. (3) If revised Equation 2.4.15 is used to calculate runup, confirm that revised section 2.4.6.6.3.5 is not necessary. (4) Provide the geographic location (lat, long) and water depth where the shoaled amplitude *A(R)* in Table 2.4.6-207 is calculated. (5) Provide location information for revised figure 2.4.6-230 "Landward Topographic Profile", for example, in a map figure.

Resolution of RAI 2.4.6-17 and issuance of Open Items: In response to RAI 2.4.6-17 and in the corresponding update to FSAR Section 2.4.6, the applicant uses numerical methods to simulate tsunami generation, propagation, and runup. This contrasts to the applicant's original method of using various analytic expressions and empirical relations to estimate tsunami water levels at the site as described in the original FSAR.

The applicant simulates the tsunamis from 3 source regions: (1) a seismogenic tsunami from the Venezuela convergence zone; (2) a landslide from the Mississippi Canyon region; and (3) a landslide from the Florida Escarpment region. For the landslide sources, the applicant uses two types of initial conditions as input to the tsunami propagation models: (a) static initial conditions calculated from the difference between the initial and final position of the landslide (i.e., hot-start conditions) and (b) dynamic conditions for a moving landslide in which the near-source wave and velocity history is calculated with a fully non-hydrostatic Navier-Stokes model (NHWAVE). The model used to calculate tsunami propagation and runup is FUNWAVE-TVD. Static initial conditions are input to FUNWAVE-TVD for the seismogenic source and the static

characterization of the landslide sources. Output from NHWAVE is used as input to FUNWAVE-TVD for the dynamic characterization of the landslide sources.

FUNWAVE-TVD is an update to the original FUNWAVE hydrodynamic model, which solves the weakly-nonlinear, weakly-dispersive Boussinesq equations in spherical coordinates. The volume conservation and horizontal momentum equations are depth-integrated. The model includes attenuation from bottom friction and turbulent mixing. Overland flow is directly calculated in FUNWAVE-TVD, modeling tsunami inundation and runup.

NHWAVE solves the fully non-hydrostatic Navier-Stokes equations in a sigma coordinate system, which accommodates a moving water surface and water bottom. Turbulence is incorporated using an eddy viscosity closure scheme, although turbulent stresses are not modeled for this case. It should be noted that a kinematic vertical velocity is ascribed to the landslide and that landslide flow dynamics are not explicitly modeled in this analysis.

The applicant provided an extensive verification and validation document for these two models.

RAI Status (2.4.6-08 and Supplemental RAIs 2.4.6-15, 2.4.6-16, 2.4.6-17): Closed.

Request for Additional Information (RAI) 2.4.6-09: Section C.I.2.4.6.4 of Regulatory Guide 1.206 (RG 1.206) provides specific guidance with respect to tsunami analysis. This includes providing a complete description of the analysis procedure used to calculate tsunami wave height and period at the site.
Provide clarification in the updated FSAR to resolve the inconsistency of the statement that the Gulf of Mexico contains no sources of reverse faults (first sentence, section 2.4.6.4.1.2, pg. 2.4-52) given the mechanism of the September 10, 2006 Mw=5.8 in the NE Gulf of Mexico (third sentence). (Discussion Items #29)

Resolution of RAI 2.4.6-09 and issuance of Open Items: In response to RAI 2.4.6-09, the applicant clarifies that they meant to indicate that there are no subduction zone faults in the Gulf of Mexico, without adding specific explanation for the possibility of intra-plate reverse faults, such as the September 20, 2006 earthquake. RAI Status: Closed.

Results of Contractor's Independent Confirmatory Analysis

Background

Numerical simulations of tsunami propagation have made great progress in the last thirty years. Several tsunami computational models are currently used in the National Tsunami Hazard Mitigation Program, sponsored by the National Oceanic and Atmospheric Administration, to produce tsunami inundation and evacuation maps for Alaska,

California, Hawaii, Oregon, and Washington. The computational models include MOST (Method Of Splitting Tsunami), developed originally by researchers at the University of Southern California (Titov and Synolakis, 1998); COMCOT (Cornell Multi-grid Coupled Tsunami Model), developed at Cornell University (Liu et al., 1995); and TSUNAMI2, developed at Tohoko University in Japan (Imamura, 1996). All three models solve the same depth-integrated and 2D horizontal (2HD) non-linear shallow-water (NSW) equations with different finite-difference algorithms. There are a number of other tsunami models as well, including the finite element model ADCIRC (ADvanced CIRCulation Model For Oceanic, Coastal And Estuarine Waters) (e.g., Myers and Baptista, 1995).

The applicant did not perform hydrodynamic modeling according to any of the aforementioned methods in establishing tsunami water levels at the site.

Dispersive, Non-Linear Modeling of Tsunami Runup and Inundation

For a given source region condition, existing models can simulate propagation of a tsunami over a long distance with sufficient accuracy, provided that accurate bathymetry data exist. Figure 2.4.6.4.4-1 shows the snapshots of free surface elevations at one hour and 44 minutes after the 2004 Sumatra earthquake occurred.

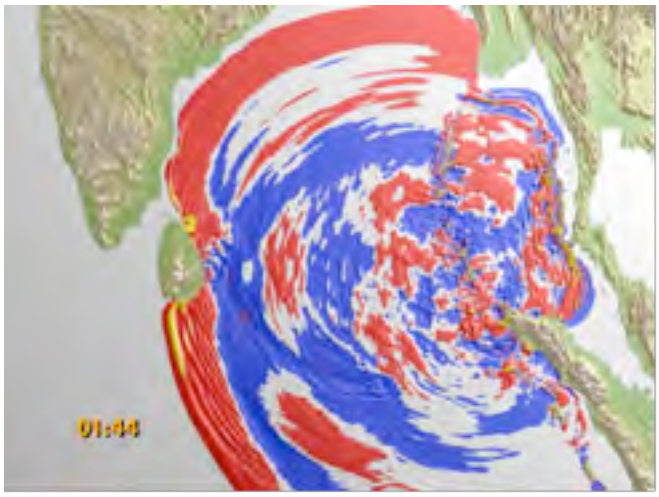

Figure 2.4.6.4.4-1: Snapshots of free surface elevations at one hour and forty four minutes after the 2004 Sumatra earthquake occurred. Yellow and red colors denote positive elevations, blue denotes negative depressions (numerical results based on COMCOT).

The shallow-water equation models lack the capability of simulating dispersive waves, which could be the dominating features in landslide-generated tsunamis and for tsunamis traveling a long distance. Several high-order depth-integrated wave hydrodynamics models (Boussinesq models) are now available for simulating non-linear and weakly dispersive waves, such as COULWAVE (Cornell University Long and Intermediate Wave Modeling Package) (Lynett and Liu, 2002) and FUNWAVE (Kennedy et al., 2000). The major difference between the two is their treatment of moving shoreline

boundaries. Lynett et al. (2003) applied COULWAVE to the 1998 PNG tsunami with the landslide source; the results agreed well with field survey data. Recently, several finite element models also have been developed based on Boussinesq-type equations (e.g., Woo and Liu, 2004). Boussinesq models require higher spatial and temporal resolutions, and therefore are more computationally intensive. Moreover, most of model validation work was performed for open-ocean or open-coast problems. In other words, the models have not been carefully tested for wave propagation and oscillations in semi-enclosed regions
– such as a harbor or bay
– especially under resonant conditions.

Being depth-integrated and horizontally 2D, NSW and Boussinesq models lack the capability of simulating the details of many coastal effects, such as wave overturning and the interaction between tsunamis and coastal structures, which could be either stationary or movable. At present, stationary coastal structures are parameterized as bottom roughness and contribute to frictional effects in these 2HD models. Although by adjusting the roughness and friction parameter satisfactory results can be achieved for maximum runup and delineation of the inundation zone (e.g., Liu et al., 1995), these models cannot provide adequate information concerning wave forces acting on coastal structures, nor can they estimate bottom stress, which is essential in determining sediment erosion and deposition.

As a tsunami propagates into the nearshore region, the wave front undergoes a non-linear transformation while it steepens through shoaling. If the tsunami is large enough, it can break at some offshore depth and approach land as a bore – the white wall of water commonly referenced by survivors of the Indian Ocean tsunami. Wave breaking in traditional NSW tsunami models has not been handled in a satisfactory manner. Numerical dissipation commonly is used to mimic breaking, and thus, results become grid dependant. Numerical dissipative approaches most notably include shock capturing schemes. In these schemes, energy dissipation is related to the local smoothness of the solution, which is strongly related to the grid length near the shock. With shock capturing methods, the numerical results tend to be very smooth. However, the dissipation is entirely numerical, and although the general form of the dissipative terms may be of the proper physical form, the dissipation will inevitable be related to the grid length and time step. In Boussinesq models, breaking is still handled in an approximate manner due to the fact that the depth-integrated derivation does not allow for an overturning wave; however these breaking schemes have been validated for a wide range of nearshore conditions (e.g., Lynett, 2006).

Being depth-integrated, NSW and Boussinesq models lack the capability of simulating the vertical details of many coastal effects, such as strong wave breaking/overturning and the interaction between tsunamis and irregularly shaped coastal structures. To address this deficiency, several 2D and 3D computational models based on Navier-Stokes equations have been developed, with varying degrees of success. For example, Professor Liu and his students at Cornell University developed a 2D computational model, COBRAS (Cornell Breaking waves and Structures model) (Lin and Liu, 1998a, b; Lin et al., 1999), which is capable of describing the interactions between breaking waves and

structures that are either surface piercing or submerged (Chang et al., 2001; Hsu et al., 2002). COBRAS uses the Volume of Fluid (VOF) method to track free surface movement along with a turbulence closure model. Several other computational models using different free surface tracking methods are also in use, such as the micro surface cell technique developed by Johnson et al. (1994).

While a moving shoreline is readily included in VOF-type models, due to the computational costs of these models, it is often not practical to use them for large-scale inundation problems like tsunami runup. The NSW and Boussinesq models are conventionally used for this purpose. Researchers generally use a fixed grid, finite difference or finite element method to solve these depth-integrated equations. Using a fixed grid numerical model to solve a moving boundary problem can lead to difficulties related to the loss of mass conservation and instabilities in the computations (Leendertse, 1987) as a result of imposing discrete fixed increments to the extent of wetting and drying areas (Balzano, 1998).

To eliminate the difficulties related to shoreline location being locked onto a grid, Zelt (1991) used a Lagrangian model to simulate shoreline movement due to solitary wave runup. This model produced maximum runup values that compared well with experimental values, but the shape of the wave as it traveled up the slope did not compare as favorably. A handful of others have utilized Lagrangian techniques with depth-integrated equation models to simulate a moving shoreline (e.g., Gopalakrishnan, 1989; Petera and Nassehi, 1996). Another treatment of the moving boundary problem is employing a slot or permeable-seabed technique (Tao, 1983, 1984). The first application of the permeable slot with a Boussinesq-type model (Madsen et al., 1997) yielded runup errors on the order of ten percent of the maximum. Modifications have been made to this permeable slot technique (Kennedy et al., 2000), increasing the accuracy, but it was also shown that the empirical coefficients that govern the technique cannot be universally determined due to numerical stability problems (Chen et al., 2000). Lynett et al. (2002) developed an extrapolation method runup scheme, allowing for the shoreline to exist at any arbitrary location in-between grid points and negating the major drawback of using fixed grids. This method is shown to be accurate for a wide range of 1HD and 2HD problems including the shoreline motion due to breaking and non-breaking waves (e.g., Pedrozo-Acuña et al., 2006).

Technical Approach Used in Confirmatory Analysis

Earthquake generated tsunamis, with their very long wavelengths, are ideally matched with NSW for transoceanic propagation. Models such as those used by Titov and Synolakis (1995) and Liu et al. (1995) have been shown to be reasonably accurate throughout the evolution of a tsunami, and are in widespread use today. However, when examining tsunamis generated by submarine mass failures, the NSW can lead to significant errors (Lynett et al., 2003). The length scale of a submarine failure tends to be much less than that of an earthquake, and thus, the wavelength of the created tsunami is shorter. To correctly simulate the shorter wave phenomenon, one needs equations with excellent shallow to intermediate water properties, such as the Boussinesq equations.

While Boussinesq models have accuracy limitations on how deep (or short) the landslide can be (Lynett and Liu, 2002), they are able to simulate the majority of tsunami generating landslides. Thus, for the work proposed here, the Boussinesq-based numerical model COULWAVE (Lynett and Liu, 2002) will be used. (See Appendix for reprints of peer-reviewed papers that form the foundation of COULWAVE.) This model solves the fully non-linear extended Boussinesq equations on a Cartesian grid. A particular advantage of the model is the use of fully non-linear equations for both deep and shallow water. This avoids the common problem of "splitting" the analysis when the wave reaches shallow water. Applications for which COULWAVE has proven very accurate include wave evolution from intermediate depths to the shoreline, including parameterized models for wave breaking and bottom friction.

Wave Propagation

COULWAVE is based on the Boussinesq-type equations, which are known to be accurate for inviscid wave propagation from fairly deep water (wavelength/depth ~2) all the way to the shoreline (Wei et al., 1995). The equation model consists of a fairly complex set of partial differential equations which are integrated in time to solve for the free surface elevation and the horizontal velocity vector, $\mathbf{u}$. A 4th order Adams-Bashforth-Moulton predictor-corrector time integration scheme is required, and the spatial derivatives are approximated with 4th order, centered finite differences. The high order scheme is required due to the inclusion of first to third order derivatives in the model equations. Waves are generated in the numerical domain with an internal source (Wei et al., 1999), which can use as input a wave energy spectrum to create a directional, random wave field. In conjunction with the internal source generator, sponge layers are placed along the outgoing lateral boundaries, and provide excellent wave absorption across a wide range of frequencies and amplitudes.

Fundamentally, the Boussinesq equations are inviscid. To accommodate frictional effects, viscous submodels are integrated into COULWAVE. Bottom friction is calculated with the quadratic friction equation:

$$R_{BottomFriction} = f \frac{\mathbf{u}_b |\mathbf{u}_b|}{H},$$

where $\mathbf{u}_b$ is the velocity evaluated at the seafloor, and f is a bottom friction coefficient, typically in the range of 0.001 to 0.01. As noted in Lynett et al. (2002), maximum runup is sensitive to the value of f, particularly for very large, breaking waves. (See Appendix for further explanation of the theory described above.)

Wave Breaking

The wave breaking model has received much attention and has undergone numerous validation exercises. The wave breaking model is based on the "eddy-viscosity" scheme, where energy dissipation is added to the momentum equation when the wave slope exceeds some threshold value, and continues to dissipate until the wave slope reaches some minimum value when the dissipation is turned off.

One set of comparisons is shown in Figure 2.4.6.4.4-2 for a number of regular waves breaking and running up a slope. As can be seen, COULWAVE captures the mean values of height and water level to a high degree of accuracy.

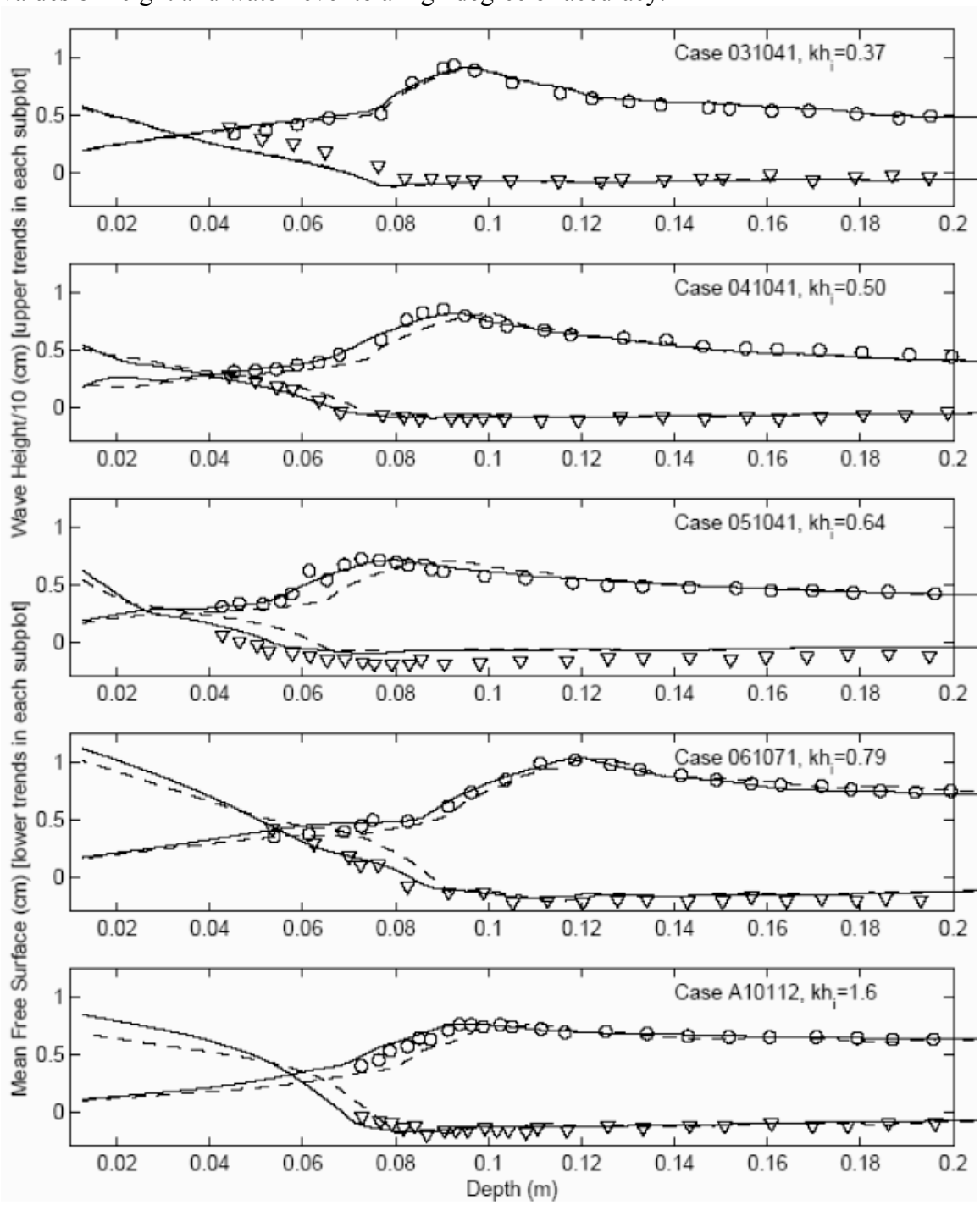

Figure 2.4.6.4.4-2: Wave height and mean free surface measurements from the experiments of Hansen and Svenson (1979) symbols, the traditional Boussinseq model (dashed-line), and COULWAVE (solid line). Trials are for monochromatic waves breaking on a planar 1/20 slope.

While these comparisons show that the model is capable of capturing a simplified, laboratory setup, it also is necessary to gauge the accuracy against real, field conditions. COULWAVE has been compared with a number of field sites; one such comparison is given in Figure 2.4.6.4.4-3. As can be seen, the model captures the spectral transformation of random waves through the surf zone. Note that the breaking model uses a single set of parameters (eddy viscosity, etc.) for all trials, so there is no individual case optimization.

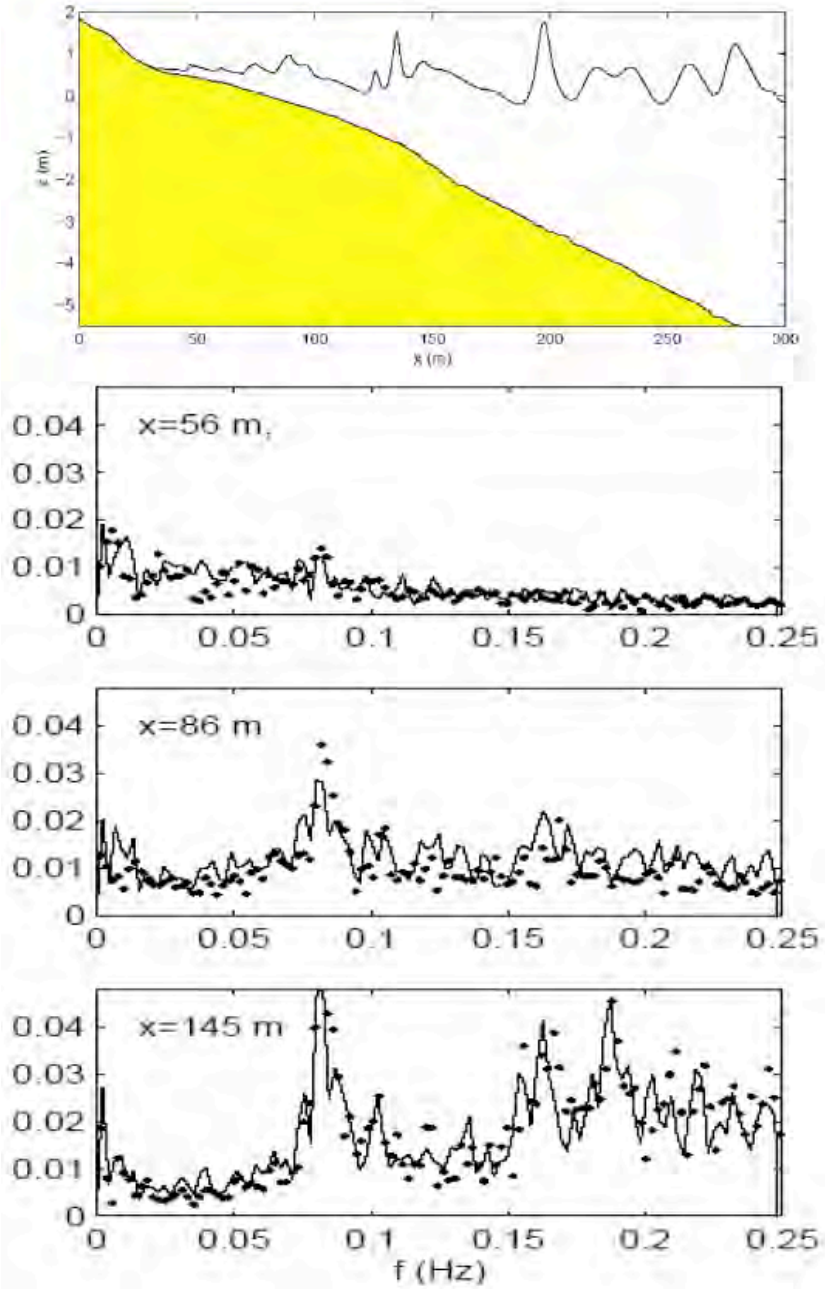

Figure 2.4.6.4.4-3: COULWAVE random wave comparison with field data. The lower subplots show the spectrum comparisons at three different locations. Dots are the field data from Raubenhiemer (2002); solid lines are the COULWAVE results.

The horizontal velocity profile under breaking waves is a necessary component that needs to be captured accurately for transport-related physics. Using a process of superposition of velocity profiles (Lynett, 2006), instantaneous and mean profiles under breaking waves is predicted well (see Figure 2.4.6.4.4-4).

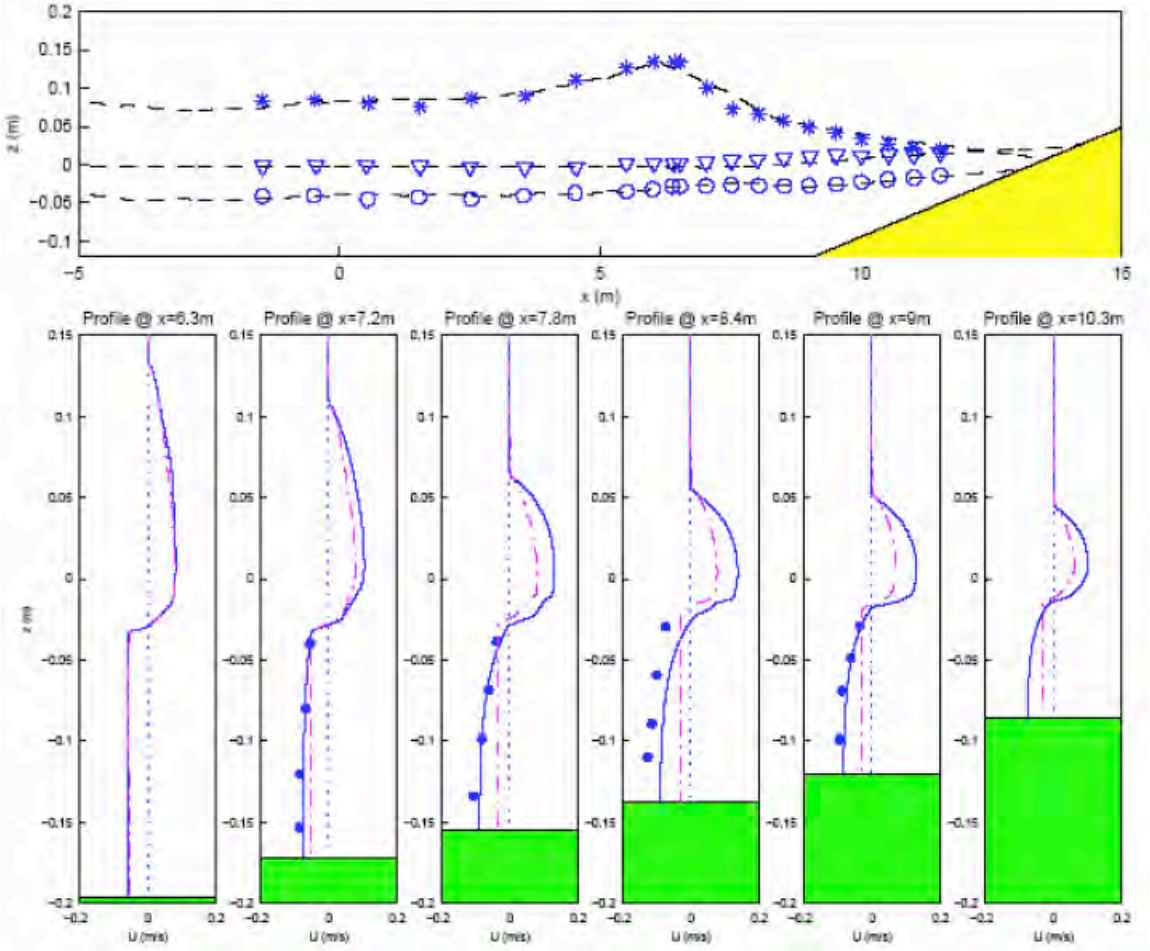

Figure 2.4.6.4.4-4: Comparison with data of Ting and Kirby (1995) spiller. The top plot shows the mean crest level (stars), mean water level (triangles), and mean trough level (circles) for the experiment as well as the numerical simulation. The lower subplots are the time-averaged horizontal velocities, where the experimental values are shown with dots, COULWAVE results are indicated by the solid lines, and the standard Boussinesq results are indicated by the dashed-dotted lines.

Publications which specifically use COULWAVE to simulate wave breaking include Lynett and Liu (2002), Lynett et al. (2003), Korycansky and Lynett (2005), Cheung et al. (2003), Lynett and Liu (2006), Lynett (2006), Lynett (2007), and Korycansky et al. (2007).

Wave Runup and Inundation

The moving shoreline condition has shown to capture shoreline motion due to a wide range of wave frequencies, wave heights, and beach slopes. The shoreline algorithm was

originally developed to simulate the important motion of tsunami runup (Lynett et al., 2002), and uses a variation of the so-called "extrapolation" technique. The extrapolation method has its roots in Sielecki and Wurtele (1970), with extensions by Hibberd and Peregrine (1979), Kowalik and Murty (1993), and Lynett et al. (2002). The basic idea behind this method is that the shoreline location can be extrapolated using the nearest wet points, such that its position is not required to be locked onto a fixed grid point; it can move freely to any location. The numerical results evaluated at the extrapolated waterline are used to update the solution for the next time step. This moving-boundary technique is numerically stable and does not require any artificial dissipation mechanisms.

Recently, extensive comparisons have been made with empirical runup laws and existing experimental data for runup due to regular waves (Korycansky and Lynett, 2005). Figure 2.4.6.4.4-5 shows how COULWAVE compares with the so-called Irribaren scaling for runup, an established coastal engineering relation based on deep water properties of the waves.

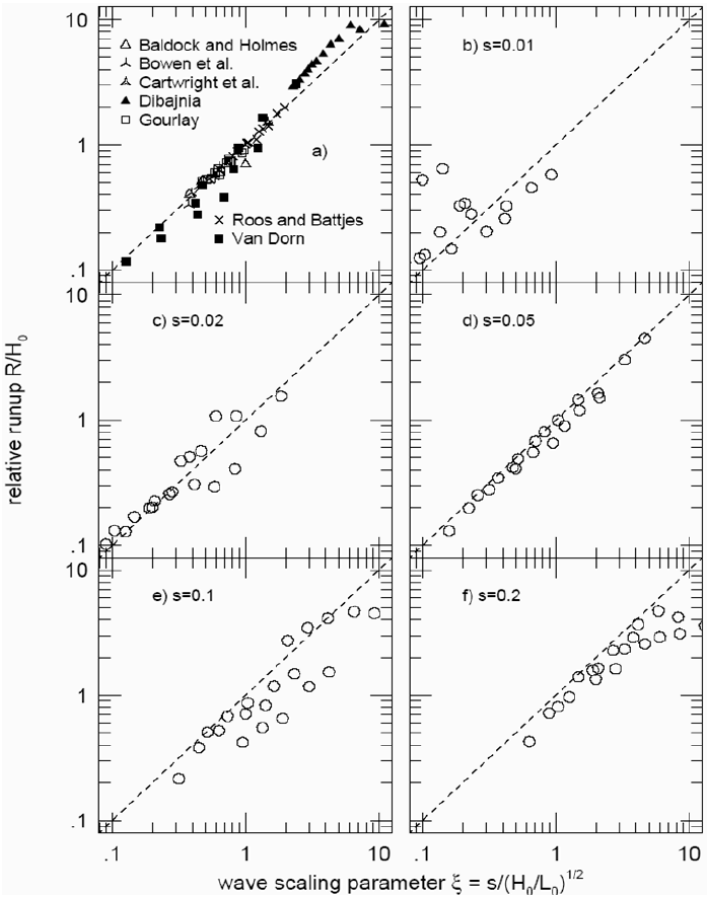

Figure 2.4.6.4.4-5: Wavetank experimental measurements of runup from the literature and COULWAVE runup results (open circles).

Publications which specifically use COULWAVE for runup or the moving shoreline algorithm developed by Lynett include Lynett et al. (2002), Lynett et al. (2003),

Korycansky and Lynett (2005), Cheung et al. (2003), Pedrozo-Acuña et al. (2006), Lynett and Liu (2006), Lynett (2006), Lynett (2007), and Korycansky and Lynett (2007).

Overtopping of Sloping Structures

Quality, time-dependent data for wave overtopping of levees and dikes is sparse. Thus, as with existing published numerical models (e.g., Dodd, 1998), the large majority of comparisons provided here will use time-averaged experimental data. First, a comparison is made with the data of Saville (1955). This data set is one of the standard comparisons found in the literature (e.g., Kobayashi and Wurjanto, 1989; Dodd, 1998; Hu et al., 2000). An example of the physical setup for these trials is given in Figure 2.4.6.4.4-6, a spatial snapshot for a numerical simulation.

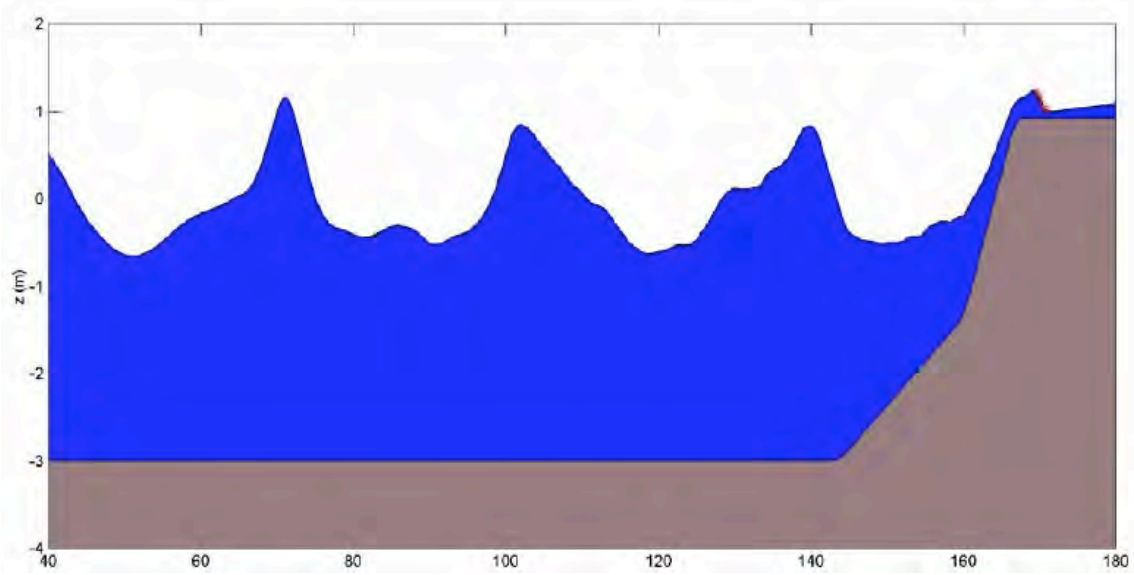

Figure 2.4.6.4.4-6: COULWAVE snapshot from a recreation of the Saville (1955) experiments. The general setup is a wavemaker depth ~ 3m, a flat portion leading up to a 1/10 slope, which connects to the "structure". In these experiments, the structure has either a 1/3 or 1/1.5 slope.

A range of freeboard and wave conditions was tested. A summary of the comparisons is given in Table 2.4.6-2.

Table 2.4.6-2: Numerical comparisons with data from the Saville (1955) experiments. Ho is the wave height at the wavemaker, T is the wave period, Htoe is the wave height at the toe of the structure, R is the distance between the structure crest and the still water level, d_toe is the water depth at the toe, slope is the 1/slope of the structure, Q_meas is the measured overtopping flux, Q_K&W is the simulated overtopping by Kobayashi and Wurjanto (1989), and Q_Bous is the COULWAVE simulated flux.

Run	Ho (m)	T (s)	Htoe (m)	R (m)	d_toe (m)	slope	Q'_meas (m2/s)	Q'_K&W (m2/s)	Q'_Bous (m2/s)
1	1.83	6.39	1.74	0.91	1.37	3	0.51	0.21	0.35
2	1.83	6.39	1.74	1.83	1.37	3	0.32	0.02	0.21
3	1.83	6.39	1.74	0.91	2.74	3	0.50	0.41	0.49
4	1.83	6.39	1.74	1.83	2.74	3	0.28	0.11	0.16
5	1.37	7.67	1.36	0.92	2.74	3	0.45	0.41	0.44
6	1.83	10.8	1.94	0.91	1.37	3	0.47	0.42	0.42
7	1.83	10.8	1.9	1.83	1.37	3	0.13	0.12	0.12
8	1.83	10.8	1.94	2.74	1.37	3	0.31	0.02	0.04
9	1.83	10.8	1.94	0.91	2.74	3	0.73	0.71	0.68
10	1.83	10.8	1.94	1.83	2.74	3	0.31	0.35	0.35
11	1.83	10.8	1.94	2.74	2.74	3	0.06	0.12	0.11
12	1.37	14.97	1.62	0.92	1.37	3	0.46	0.49	0.46
13	1.37	14.97	1.62	0.92	2.74	3	0.65	0.57	0.63
14	1.37	14.97	1.62	1.82	2.74	3	0.39	0.26	0.33
15	1.37	14.97	1.62	2.74	2.74	3	0.13	0.08	0.09
16	1.37	14.97	1.62	3.66	2.74	3	0.06	0.08	0.03
17	1.83	10.8	1.88	0.91	1.37	3	0.38	0.51	0.44
18	1.83	10.8	1.86	2.74	1.37	1.5	0.10	0.06	0.09
19	1.83	10.8	1.88	0.91	0	1.5	0.30	0.31	0.31
20	1.83	10.8	1.88	1.83	0	1.5	0.16	0.05	0.09

Overall, the agreement between the Boussinesq simulations and the experiments is quite good. Where the two diverge, the Boussinesq results tend to agree with the published numerical results of Kobayashi and Wurjanto (1989).

The Boussinesq model results must also exhibit agreement with well established empirical formulas, such as those given by Owen (1980) and Van der Meer and Janssen (1995). For these tests, a wide range of wave and levee configurations are tested. Ranges of parameters are: levee slope from 1/3 - 1/8, freeboard from 1' - 4', wave height at the structure toe from 2'-8', and wave period from 8s-16s. The incident wave condition is a shallow water TMA spectrum using a gamma value of 3.0. Approximately 500 Boussinesq simulations were performed, and the comparisons with the formula of van der Meer and Janssen (1995) are shown in Figure 2.4.6.4.4-7. Agreement is quite good.

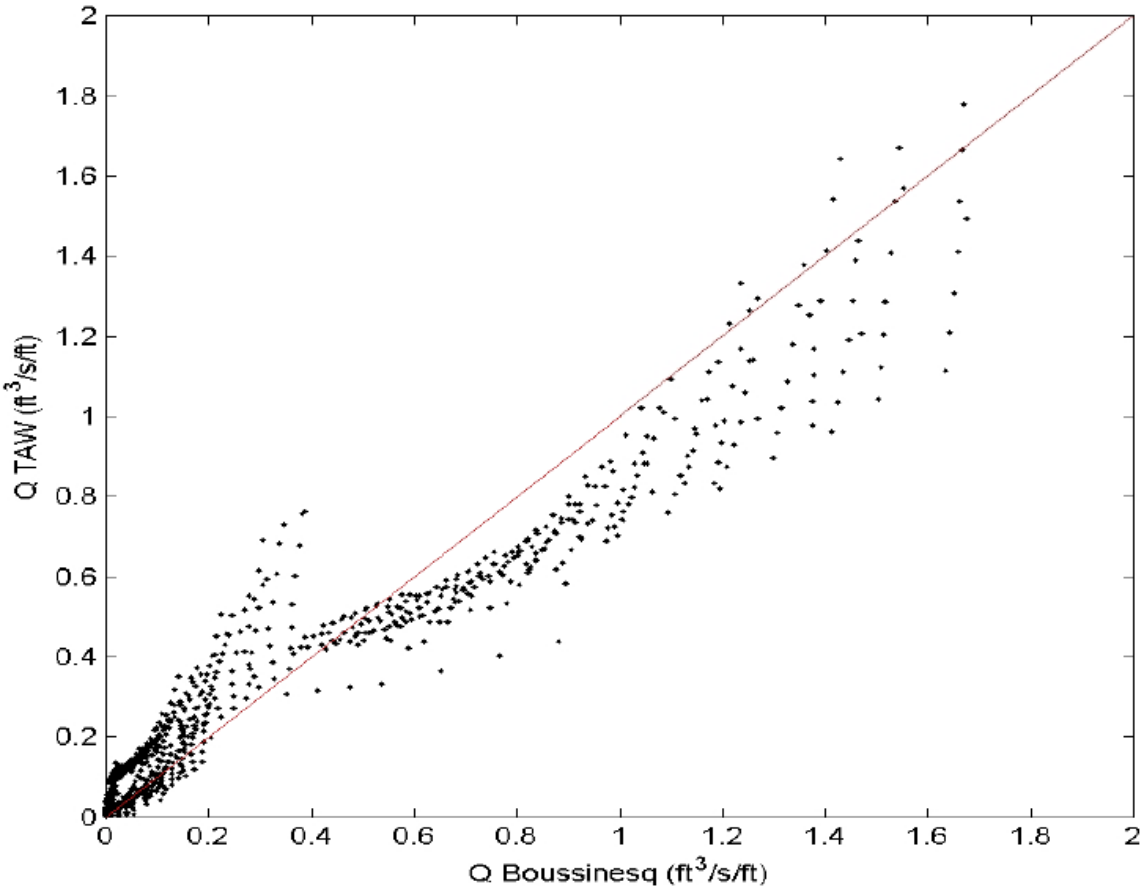

Figure 2.4.6.4.4-7: Comparison of Boussinesq overtopping rates with the formula given in the TAW design guidance.

Conclusion

In response to RAI 2.4.6-17 and in the corresponding update to FSAR Section 2.4.6, the applicant uses numerical methods (FUNWAVE-TVD and NHWAVE) to simulate tsunami generation, propagation, and runup. Water level analysis to establish the PMT conducted under the independent confirmatory analysis primarily uses the COULWAVE model above that includes the effects of non-linearity and dispersion.

2.4.6.4.5 Tsunami Water Levels

In the original version of the FSAR, various methods of tsunami analysis used by the applicant to estimate tsunami water levels at the Levy County Nuclear Plant site are described at the beginning of Section 2.4.6.4.4. Most of the water level estimates are taken directly from previously published studies. The exception is the analysis for the East Breaks landslide in the Gulf of Mexico, where the applicant uses a tsunami attenuation function and Monte Carlo analysis to establish the maximum water level.

In response to RAI 2.4.6-17 and in the corresponding update to FSAR Section 2.4.6, the applicant uses numerical methods to simulate tsunami generation, propagation, and runup. The applicant simulates the tsunami water levels near the site from 3 source regions: (1) a seismogenic tsunami from the Venezuela convergence zone; (2) a landslide from the Mississippi Canyon region; and (3) a landslide from the Florida Escarpment region. The geometry of the sources is based on the USGS Administrative Report: ten Brink et al. (2009). The applicant uses three nested grids based on the ETOPO1 DEM (open-ocean grid-Grid A), the NGDC Coastal Relief Model (Grid B), and local LIDAR data for the highest resolution grid near the site (Grid C). The vertical datum used for all simulations includes the effects of long-term sea-level rise and 10 percent exceedance high tide. Because of nonlinearity in tsunami propagation and runup, the effects on the simulations of using a higher water level datum may be significant, in comparison to adding the sea-level rise and tide effects after the fact. The drag coefficient used by the applicant for overland flow is Cd=0.001 and is fairly conservative. In the FSAR, it is unclear what drag coefficient was used by the applicant for propagation. However, in the input files the applicant provided, it looks like the applicant used Cd=0.0001 (10^{-4}) for Grid A (also conservative) and Cd=0.001 for Grids B and C.

Model results by the applicant indicate the tsunami from a Mississippi Canyon landslide yields the highest water levels near the site and is therefore the Probable Maximum Tsunami. The water levels from the Venezuela seismogenic source and the Florida Escarpment landslide are significantly less. In addition, the static (hot-start) landslide characterization produces tsunami water levels slightly higher at the site than the dynamic characterization.

Request for Additional Information (RAI) 2.4.6-10: Section C.I.2.4.6.5 of Regulatory Guide 1.206 (RG 1.206) provides specific guidance with respect to tsunami water levels. This includes describing the ambient water levels, including tides, sea level anomalies, and wind waves assumed to be coincident with the tsunami.
Provide a discussion in the updated FSAR of the value for 10% exceedance high-tide and long-term sea-level rise coincident with maximum tsunami water levels at the Levy County site.

Resolution of RAI 2.4.6-10 and issuance of Open Items: The applicant provides details of high spring tide, sea-level anomaly and sea-level rise in the calculation of PMT water levels. RAI Status: Closed.

Results of Contractor's Independent Confirmatory Analysis

Introduction

Numerical modeling of three different types of tsunami sources has been performed to determine their impact on the Levy County site. The three source types are (1) distant earthquake sources; (2) a regional earthquake source in the Gulf of Mexico; and (3) regional submarine landslide sources in the Gulf of Mexico. Most of the analysis

described in this section is focused on source type (3) for determination of the PMT. For all conditions, the most conservative source parameters were employed, even when arguably unphysical, to provide an absolute upper limit on the possible tsunami effects at the Levy County site.

Distant Earthquake Sources

Regional tsunami propagation patterns in the Gulf of Mexico have been computed for a number of distant earthquake sources located in the Caribbean as reported in ten Brink et al. (2008). In Chapter 8 of that study, earthquake scenarios along five fault systems were examined: (1) west Cayman oceanic transform fault (OTF); (2) east Cayman OTF; (3) northern Caribbean subduction zone; (4) north Panama Oceanic Convergence Boundary; and (5) the northern South America convergent zone. In that report, tsunami propagation was modeled using the leap-frog, finite-difference approximation to the linear-long wave equations computed using Cartesian coordinates. Bottom friction, wave breaking, and runup were not modeled—computations were restricted to water depths of 250 m or greater. Results for the western Gulf of Mexico indicate that offshore tsunami amplitudes were less than 1.0 m for each earthquake scenario.

For comparative purposes, we re-compute here the offshore tsunami water levels for earthquake scenarios (3) and (5) using the COMCOT model. The COMCOT model is more accurate than the model used in ten Brink et al. (2008) since it includes non-linear terms in the propagation equations (hence, the computations can be carried into shallower water than in ten Brink et al., 2008), a moving boundary condition at the shoreline, and is computed in spherical coordinates. Bottom friction is also included, but is set at a low, conservative value ($f = 10^{-4}$) in this case. Figures 2.4.6.4.5-1 and 2.4.6.4.5-2 show the peak tsunami amplitude for M~9 earthquakes along the northern Caribbean subduction zone and northern South America convergent zone, respectively.

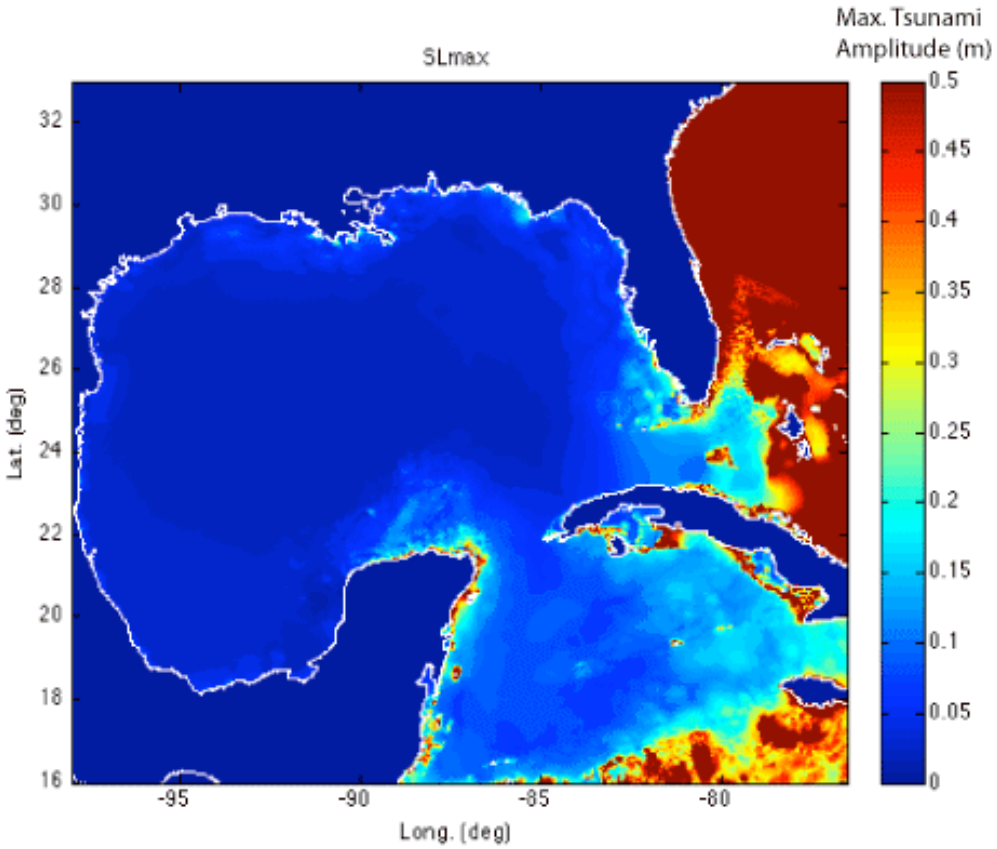

Figure 2.4.6.4.5-1: Peak tsunami amplitude over 12 hours of propagation time for a M~9 earthquake along the northern Caribbean subduction zone. Amplitudes are clipped at 0.5 m.

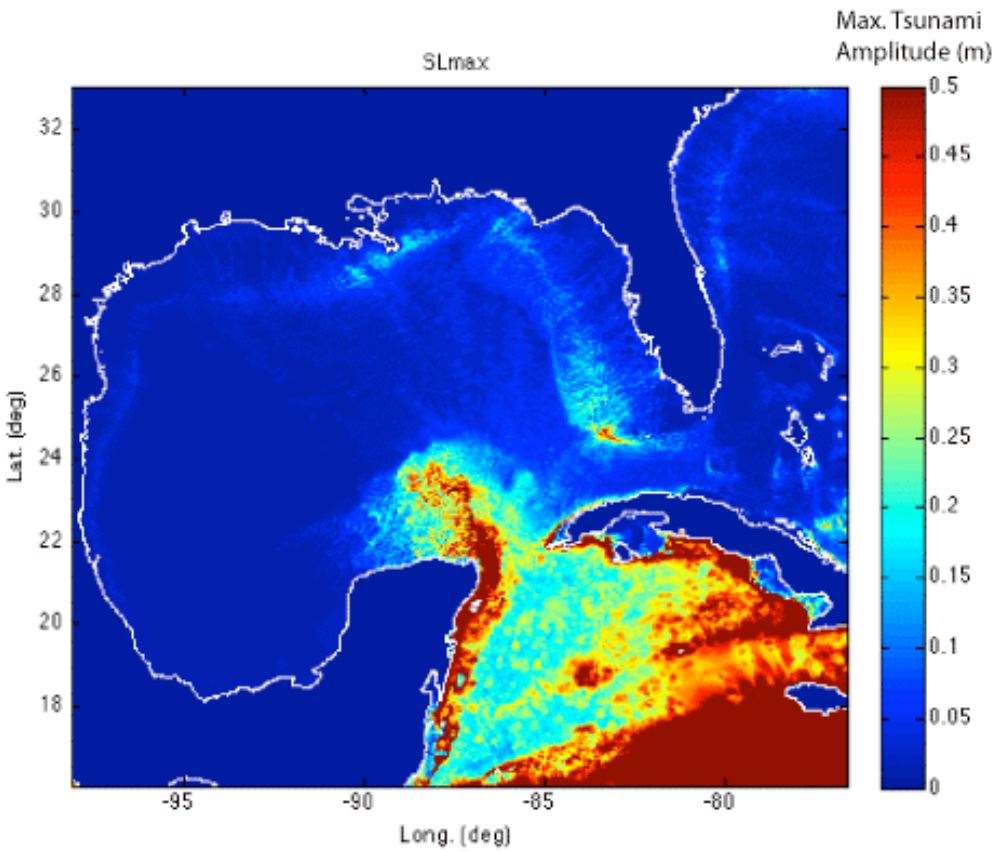

Figure 2.4.6.4.5-2: Peak tsunami amplitude over 12 hours of propagation time for a M~9 earthquake along the northern South America convergent zone. Amplitudes are clipped at 0.5 m.

These results confirm that tsunami amplitudes from distant Caribbean earthquakes are less than 1.0 m near the Levy County site. Tsunami amplitudes from earthquakes along the Azores-Gibraltar oceanic convergence boundary are also likely to be less than 1 m in the Gulf of Mexico (Mader, 2001; Barkan et al., 2009).

Regional Earthquake Sources

Regional tsunami propagation patterns in the Gulf of Mexico (GOM) have been computed for a local earthquake near the location of the September 10, 2006 M=6.0 earthquake. For this scenario, probable maximum fault dimensions and slip similar to an M_{max}=7.5 earthquake (Petersen et al., 2008; Wheeler, 2009; Mueller, 2010) was determined from the empirical scaling relationships for intra-plate earthquakes of Wells and Coppersmith (1994). Conservative values were allowed within 1 standard deviation of the empirical estimates of all fault types (empirical relationships for reverse faults only are not statistically reliable). This resulted in the following rupture parameters: length = 150 km, width = 30 km, and average slip = 5 m. The corresponding magnitude, assuming a shear modulus of 30 GPa, is M_w=7.8 - slightly greater than M_{max}=7.5 because of the conservative assumptions. The geometric parameters of the earthquake were taken

from the nodal plane of the September 10, 2006 M=6.0 earthquake that optimized the radiation of tsunami energy toward the site: dip = 47°; strike=346°; latitude=27.3°N; longitude 86.3°W.

The offshore tsunami water levels for this local earthquake scenario were computed using the COMCOT model as described for the distant earthquake sources above. Bottom friction is also included, but is set at a low, conservative value ($f = 10^{-4}$) in this case. Figure 2.4.6.4.5-3 shows the peak tsunami amplitude (note the change in amplitude scale from the previous figures). In general, tsunami amplitudes from the local M_w=7.8 sources are larger than the distant M~9 earthquake sources, with peak tsunami amplitudes near 1 m. These amplitudes are significantly less than the tsunami amplitudes produced by the regional submarine landslide sources described below.

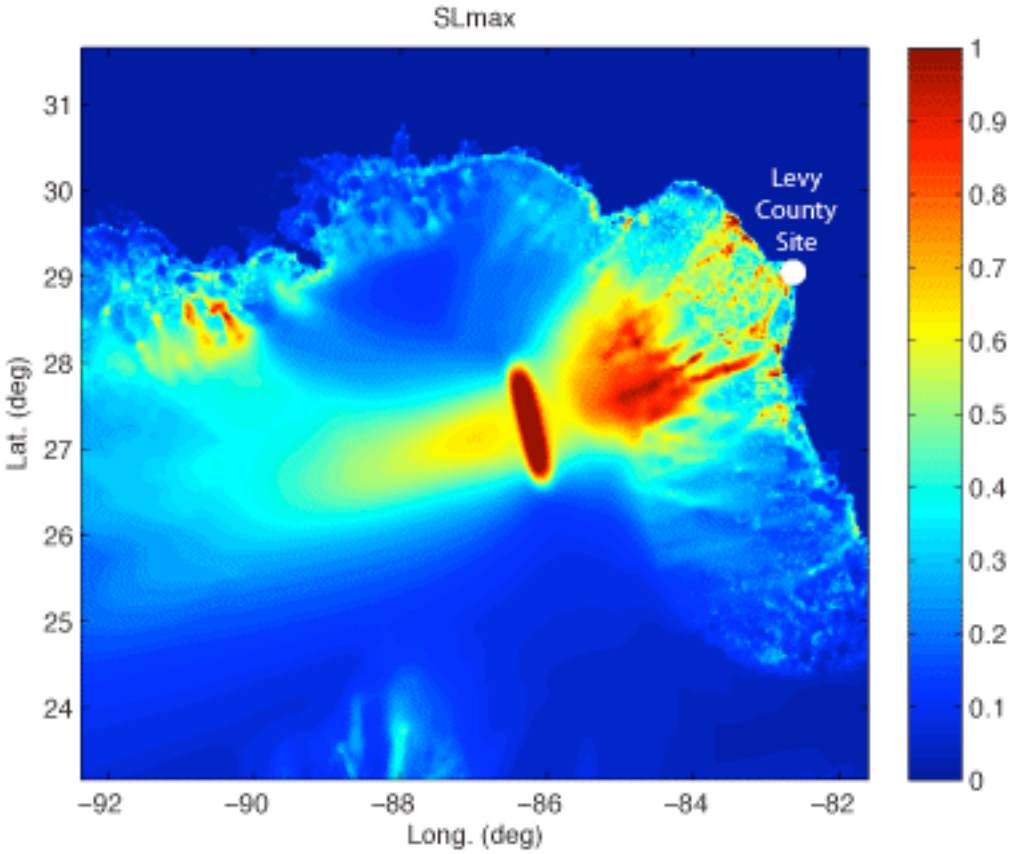

Figure 2.4.6.4.5-3: Peak tsunami amplitude over 12 hours of propagation time for a local M_w=7.8 dip-slip earthquake located in the deep Gulf of Mexico, near the location of the September 10, 2006 M=6.0 earthquake. Amplitudes are clipped at 1.0 m.

Regional Submarine Landslide Sources

Five different landslide tsunami sources in the GOM (Figure 2.4.6.4.5-4) are investigated to determine their impact at the Levy County site. First, all sources are simulated as one-horizontal-dimension (1HD) transects, and thus conservatively neglect radial spreading of wave energy. Additionally, each source is simulated with a wide range of frictional

coefficients, from no friction to likely in-situ friction, to provide both an upper limit and a realistic estimate of the runup. From these 1HD simulations, the Mississippi Canyon source clearly has the greatest potential to bring a large wave to the Levy County site, with 1HD water elevations near the site in excess of +30 m. This source and a local Florida Shelf landslide source are chosen for additional analysis by means of two-horizontal-dimension (2HD) simulations, where radial spreading is explicitly included. Interestingly, both of these sources predict a wave of similar maximum elevation at the 30 m depth offshore of the site, approximately 7 m. However, the Mississippi Canyon wave is longer in period and has a longer train of large waves, and thus is designated as the PMT for the Levy County site. Highly refined nearshore simulations show that this source, even when including high tide and future sea level rise, does not produce a tsunami that reaches the Levy County site ground elevation.

Numerical Grid Development

The bathymetry/topography grid required by the hydrodynamic model is created via three main sources: (1) the Smith and Sandwell (SS) 2-minute global elevation database, (2) a recent GOM grid created by the U.S. Army Corps of Engineers for use with the storm surge model ADCIRC, and (3) a blend of available bathymetry and topography for the west coast of Florida. Sources (2) and (3) are a combination of numerous databases, including recent lidar surveys and digitized elevation maps. These two sources were used for bathymetry and topography at locations with bottom elevations shallower than -500 m. For depths greater than this (or elevations lower), the SS was primarily used.

Figure 2.4.6.4.5-4 shows the entire GOM grid coverage, with the five tsunami landslide source locations outlined. The high level of detail near the Levy County site is not evident in this image. In Figures 2.4.6.4.5-5 and 2.4.6.4.5-6, this detail can be seen; Figure 2.4.6.4.5-5 shows the entire Florida coastline, while Figure 2.4.6.4.5-6 is a zoom-in near the Levy County site location. Barrier islands, coastal waterways, and rivers are all well resolved.

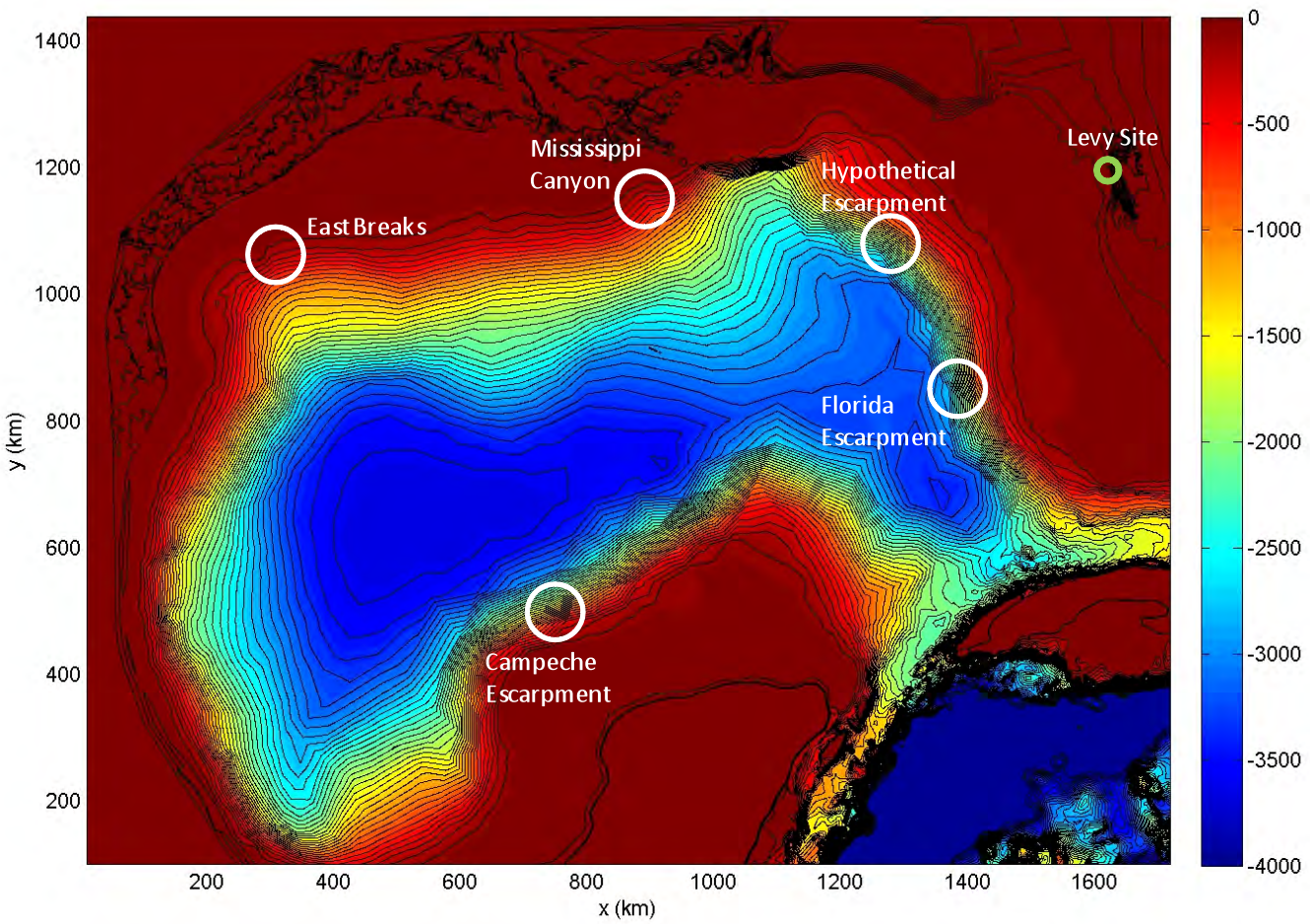

Figure 2.4.6.4.5-4. Bathymetry/topography contour surface of the GOM domain used for the tsunami hydrodynamic modeling. General locations of the five potential tsunami sources are shown by the white circles and the Levy County site is shown by the green circle. Bottom elevations are indicated by colors following the colorbar, with units in meters.

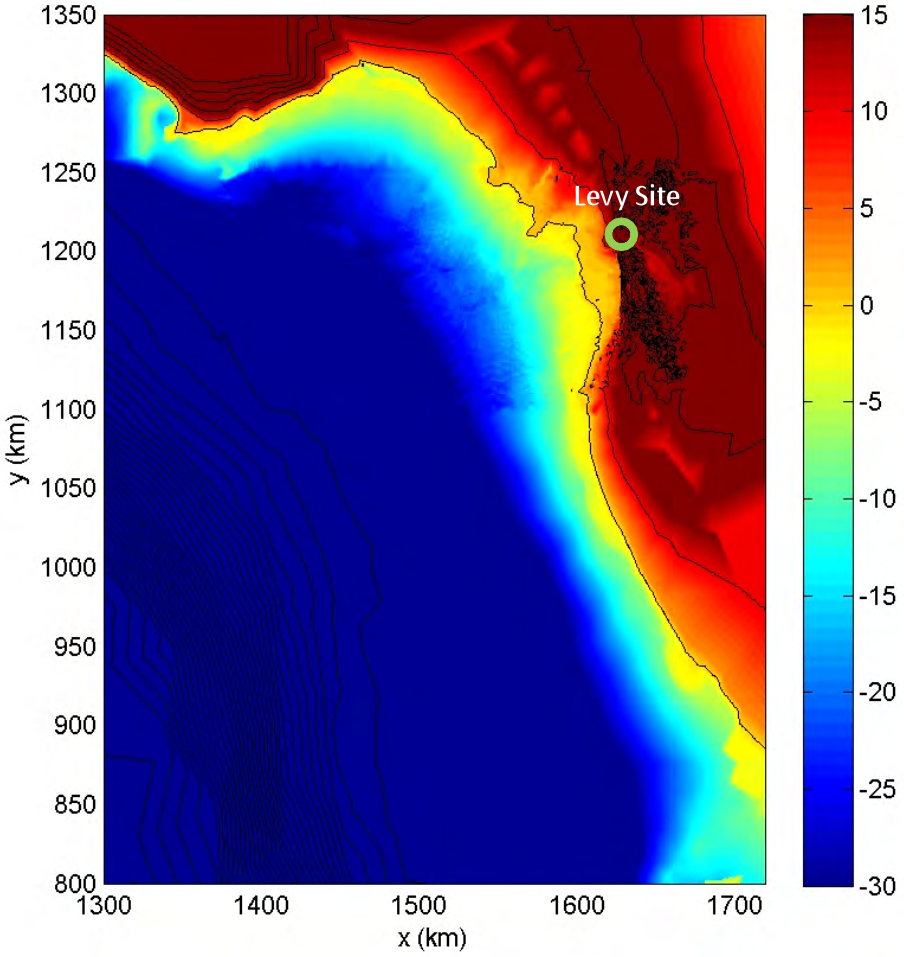

Figure 2.4.6.4.5-5. Zoom-in of the bathymetry/topography contour surface on the Florida coastline, where the Levy County site is indicated by the green circle. Bottom elevations are indicated by colors following the colorbar, with units in meters.

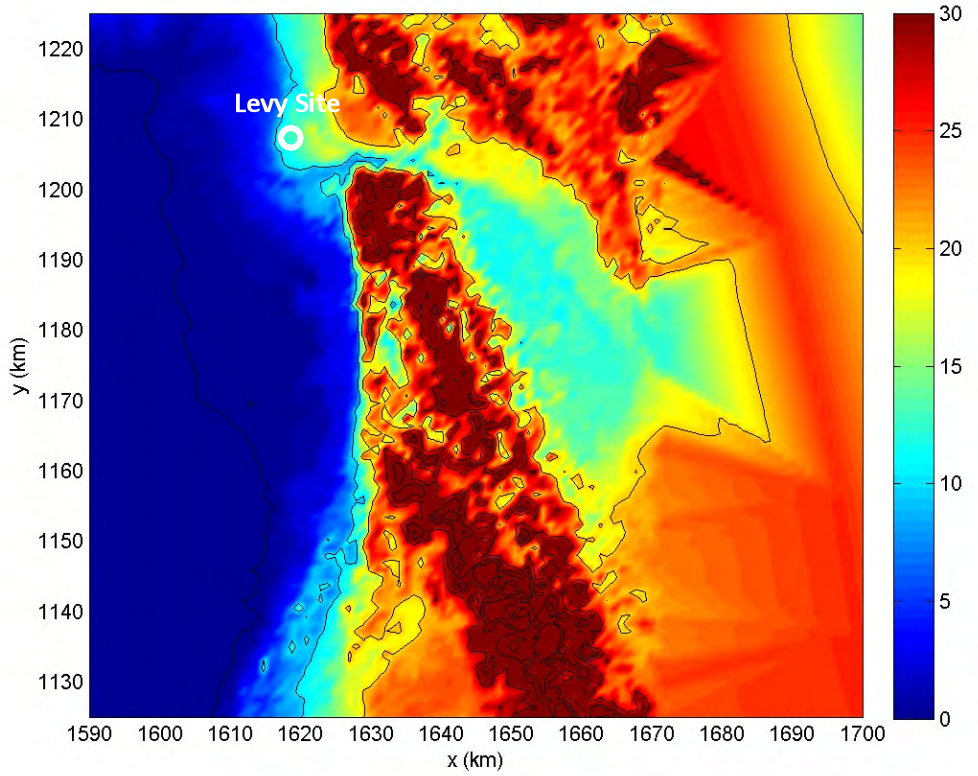

Figure 2.4.6.4.5-6. Zoom-in of the bathymetry/topography contour surface at the Levy County site. Bottom elevations are indicated by colors following the colorbar, with units in meters.

Initial Numerical Simulations - Physical Limits

The purpose of these initial simulations is to provide an absolute upper limit of the tsunami wave height that could be generated by the potential tsunami sources. Note that these limiting simulations use physical assumptions that are arguably unreasonable; the results of these simulations will be used to filter out tsunami sources that are incapable of adversely impacting the Levy County site under even the most conservative assumptions. Specifically, these assumptions are:

1. Time scale of the seafloor motion is very small compared the period of the generated water wave (tsunami).
2. Bottom roughness, and the associated energy dissipation, is negligible in locations that are initially wet (i.e., locations with negative bottom elevation, offshore).

Assumption (1) simplifies the numerical analysis considerably. With this assumption, the free water surface response matches the change in the seafloor profile exactly. This type of approximation is used commonly for subduction-earthquake-generated tsunamis, but is known to be very conservative for landslide tsunamis (Lynett and Liu, 2002). The modeling simplification arises because the need to include the landslide time evolution is removed. The initial pre-landslide bathymetric profile, as estimated by examination of neighboring depth contours, is subtracted from the post (existing) landslide bathymetric

profile. This difference surface is smoothed and then used directly as a "hot-start" initial free surface condition in the hydrodynamic model.

Assumption (2) does not simplify the analysis significantly; however is does prevent the use of an overly high bottom roughness coefficient, which could artificially reduce the tsunami energy reaching the shoreline. Note that while the offshore regions are assumed to be without bottom friction, such an assumption is too physically unrealistic to be acceptable for the inland regions where the roughness height may be of the same order as the flow depth. For tsunami inundation, particularly for regions such as this project location where the wave would need to inundate long reaches of densely vegetated land to reach the site, inclusion of some measure of bottom roughness is necessary.

If any of these initial simulations indicated the need for more precise descriptions of the source motion, these will be incorporated into a subsequent analysis. Source physics description and modeled motion will be given only if needed for this analysis. The most likely reason for more precise source physics would be if one of the initial simulation shows flooding at the site in exceedance of the PMF elevation determined elsewhere.

One-Horizontal Dimension (Transect) Simulations
First, 1HD simulations are performed for all potential sources. The 1HD simulations require a small fraction of the CPU time of the 2HD runs, but do not include radial spreading and refraction. The lack of radial spreading will lead to a conservative result in 1HD. Refraction can have either a constructive or destructive effect on the wave height, depending on the shallow water depth contours. 1HD simulations will provide an upper limit on the inundation distance and information on the relative importance of overland bottom friction, while the 2HD simulations provide insight into radial spreading and refraction. Results from the 1HD simulations will be used to filter all the sources down to a few possible candidates for the PMT; then a 2HD simulation will be run for each of these candidates.

•East Breaks Landslide Source:

As provided in the landslide characterization section, the excavation depth of this slide is approximately 160 m. This length provides the trough elevation (i.e., -160 m) of the hot-start initial water surface condition. The horizontal dimensions of the slide source region are ~12 km in width and 50 km in length. With this information, and knowledge of characteristic slide-generated waves taken from the literature (Lynett and Liu, 2002; Lynett and Liu, 2005), the hot-start initial condition is constructed as shown in Figure 2.4.6.4.5-7.

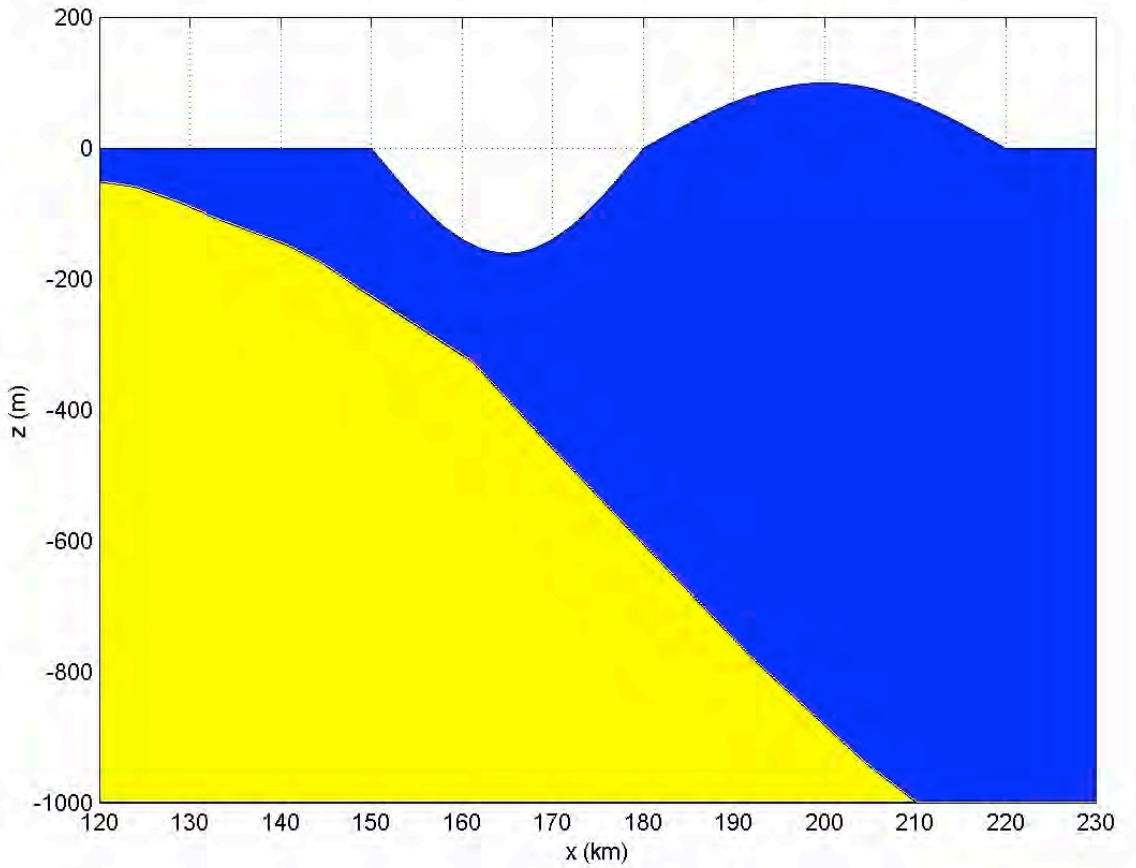

Figure 2.4.6.4.5-7. Centerline profile of the hot-start water surface condition used for the limiting East Breaks landslide tsunami simulations.

The depth transect is taken from the source location directly to the Levy County site, as shown in Figure 2.4.6.4.5-8. A constant spatial grid size of 200 m is used across the transect for the 1HD cases. Predictions from three 1HD simulations are given for **(A)** no bottom friction, **(B)** bottom friction due to moderate roughness characteristic of grass/turf ($f = 0.01$), and **(C)** bottom friction due to large roughness characteristic of the trees and dense shrub-like vegetation currently existing seaward of the Levy County site ($f = 0.05$). Note that the three different bottom friction values are only applied over initially dry land; for all simulations the initially submerged portions of the transect use no bottom friction.

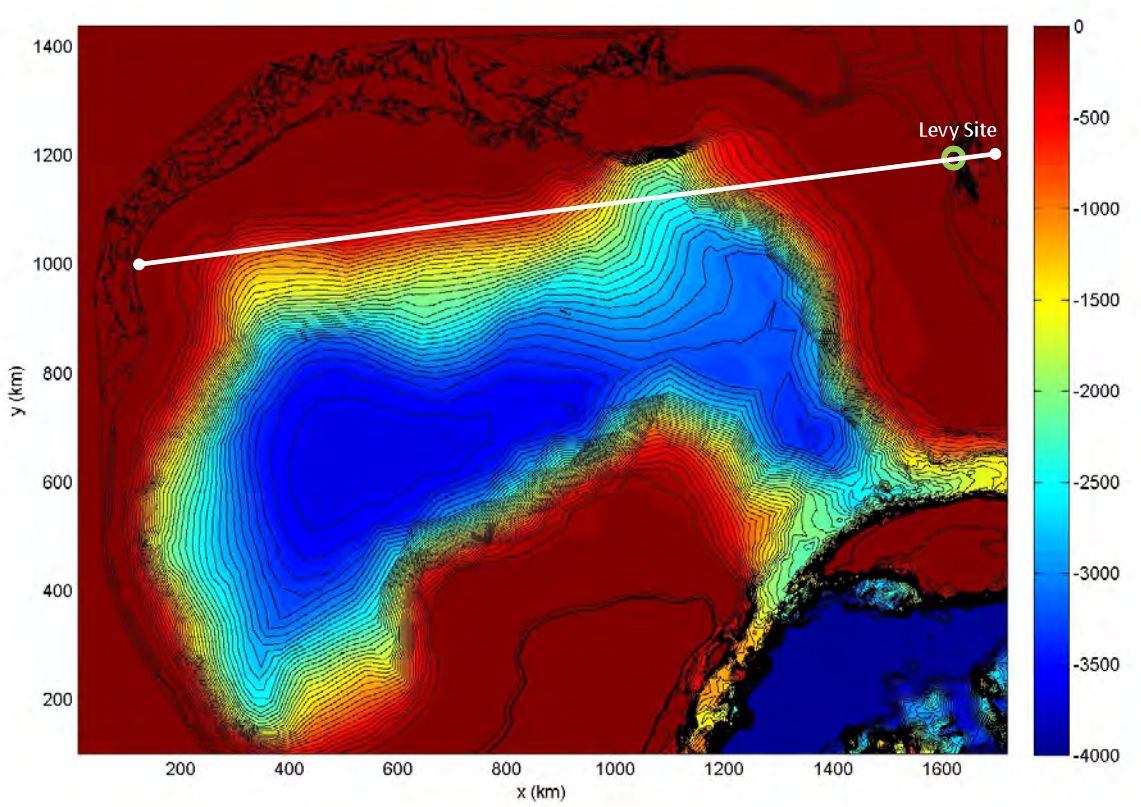

Figure 2.4.6.4.5-8. Bathymetry/topography contour surface in the GOM; the white line shows the transect used for the 1HD simulations. This transect passes through the East Breaks source location as well as the Levy County site.

A series of figures showing the evolution of this wave is provided in Figures 2.4.6.4.5-9 through 2.4.6.4.5-15. In the top subplot of all these figures, the entire transect is given, scaled vertically to show the limits of depth; due to this scaling the free surface wave appears small. The offshore evolution of the East Breaks wave can be seen in this top plot in Figures 2.4.6.4.5-9 and 2.4.6.4.5-10. The dispersive effects are clear from the long train of waves that reaches the Florida shelf. The wave in the nearshore zone is shown in the three lower subplots, which show a zoom-in of the transect near the site. For perspective, the red box in the top figure outlines the area shown in the lower three plots in these figures. All of the simulations provide identical results for the tsunami prior to reaching the shoreline because all the simulations start with the same wave, use the same bathymetry, and are frictionless offshore. This is most evident in Figure 2.4.6.4.5-11, which shows the tsunami approaching the site.

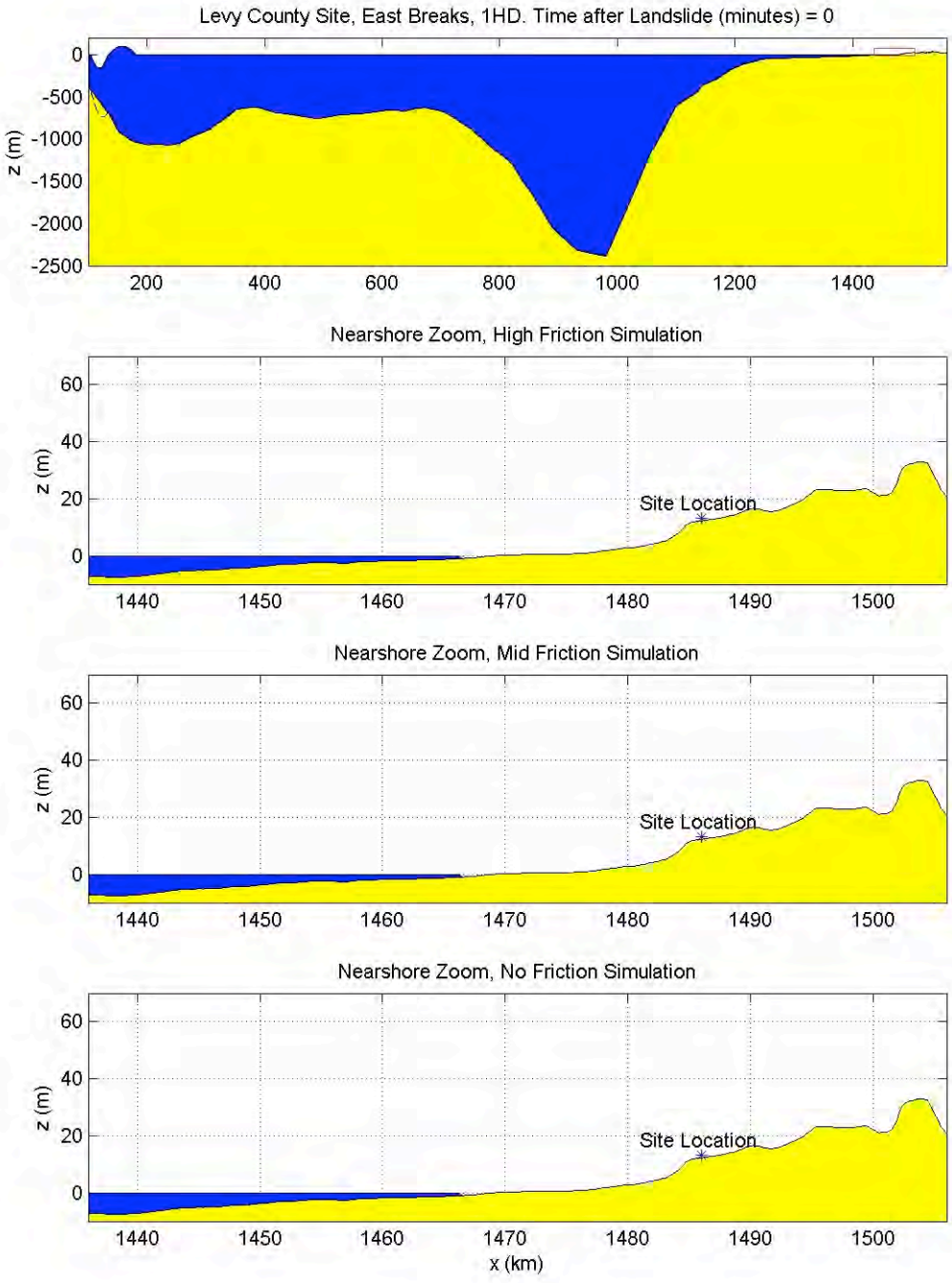

Figure 2.4.6.4.5-9. The offshore evolution of the hot-start tsunami condition for East Breaks. The top plot is the entire simulation transect, and the lower plots are zoom-in's of the nearshore areas, with each subplot showing the results using a different friction factor, as given in the title. Note that the vertical scale changes among the plots. Time shown is t=0 s.

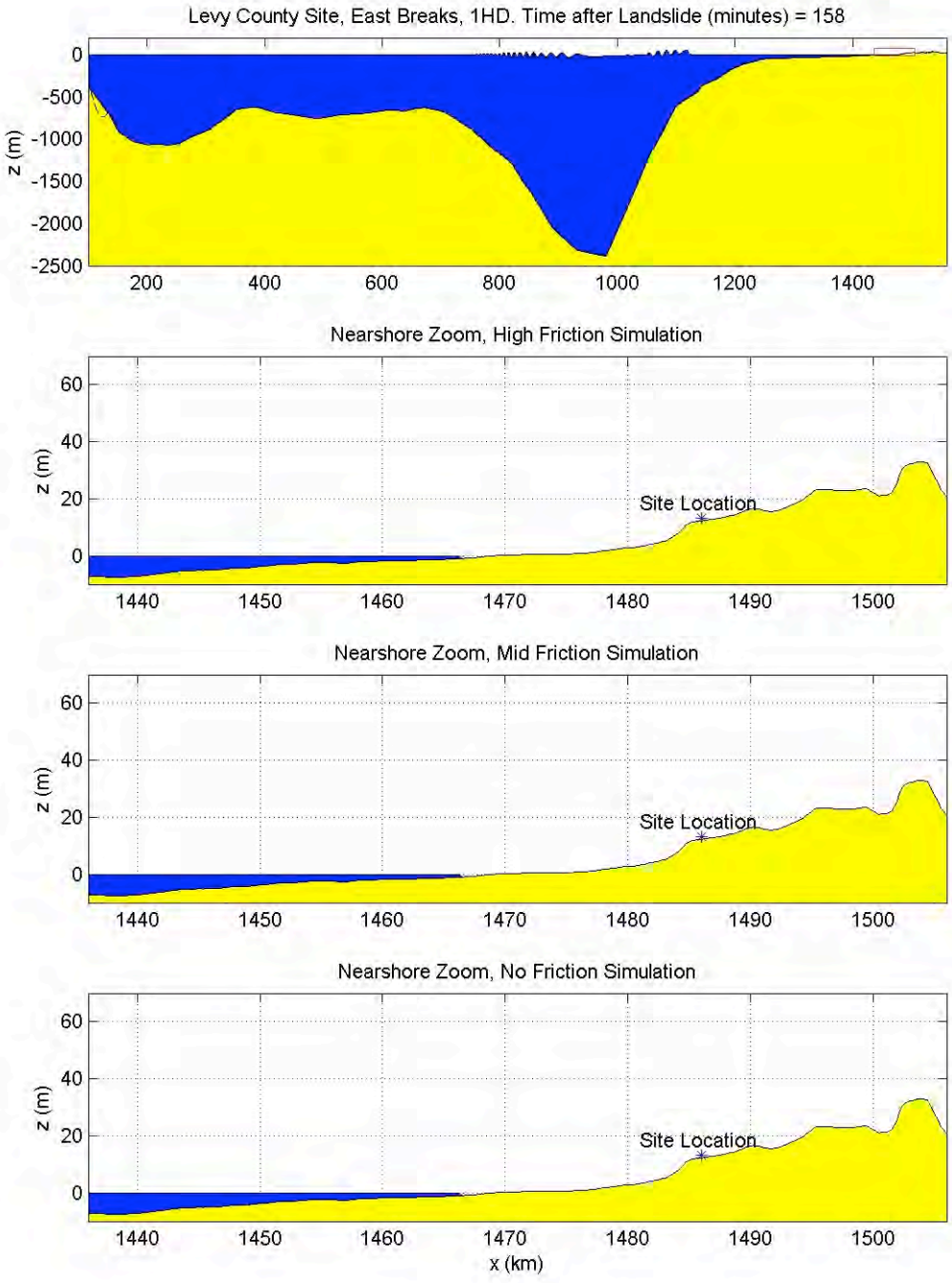

Figure 2.4.6.4.5-10. Same caption as Fig. 2.4.6.4.5-9. Time shown is t=158 min.

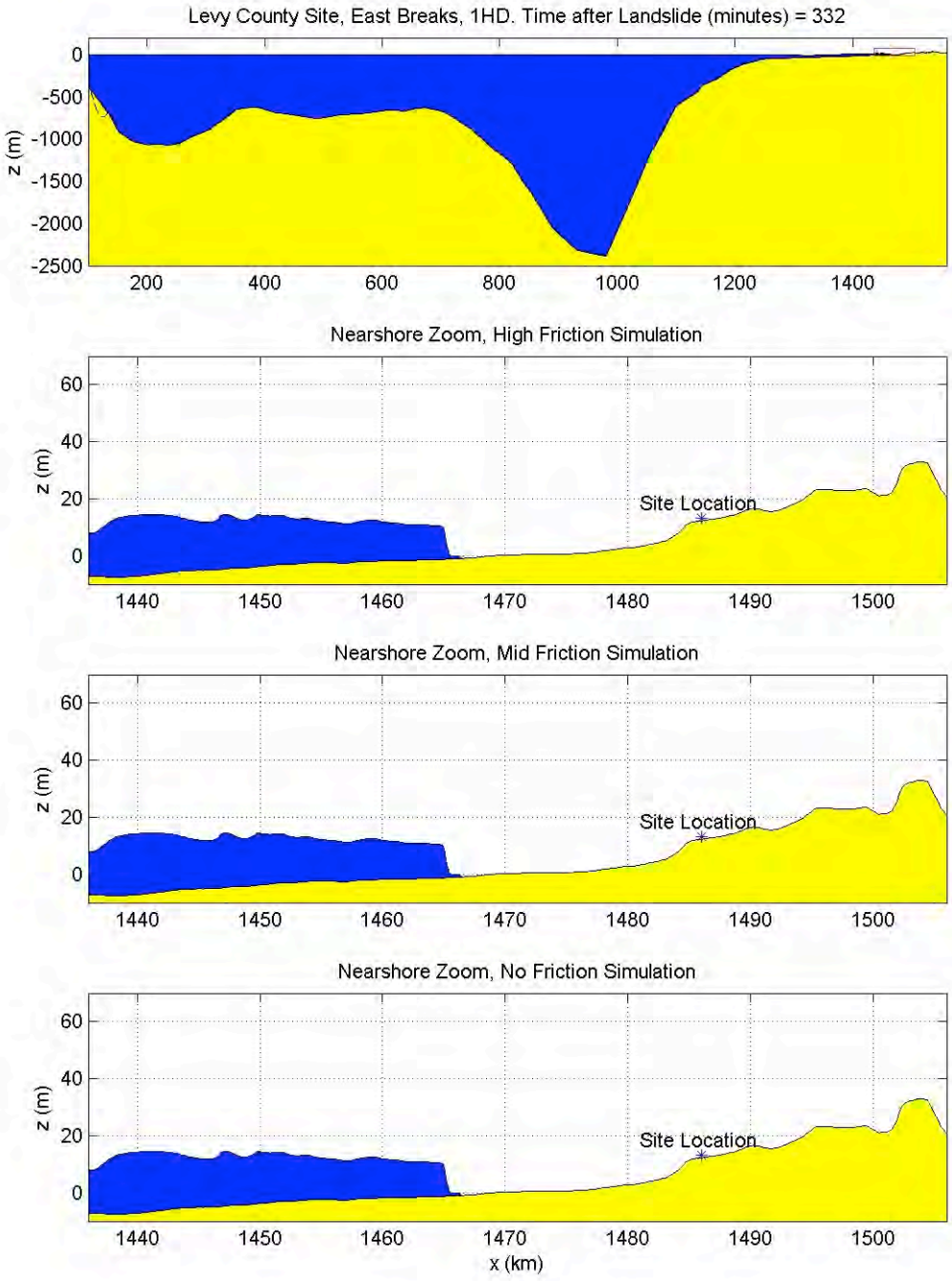

Figure 2.4.6.4.5-11. Same caption as Fig. 2.4.6.4.5-9. Time shown is t=332 min.

As the wave starts inundating dry land, friction becomes important and the results of the three simulations diverge, shown in Figures 2.4.6.4.5-12 through 2.4.6.4.5-15. The no-friction case (A) shows a fast moving bore front that easily reaches the Levy County site ground elevation, with maximum water surface elevations approaching +25 m at the site. Despite the modest friction value used in case (B), here the tsunami wave front is slowed significantly but does reach the site, and maximum water elevations at the site are approximately +22 m. Finally, for case (C), the large, realistic friction retards the flow considerably, and the tsunami wave front stops 3 km seaward of the site. Note that in all these figures, the horizontal and vertical scales are distorted, and that even the realistic friction tsunami case travels 15 km inland. A conclusion of this 1HD East Breaks study is that a tsunami approaching the site, with a bore height up to +12 m at the still water shoreline, will not adversely impact the site if the vegetation roughness is properly accounted for. However, the site is flooded with the moderate friction assumption (case B), and thus it may be necessary to investigate this site further.

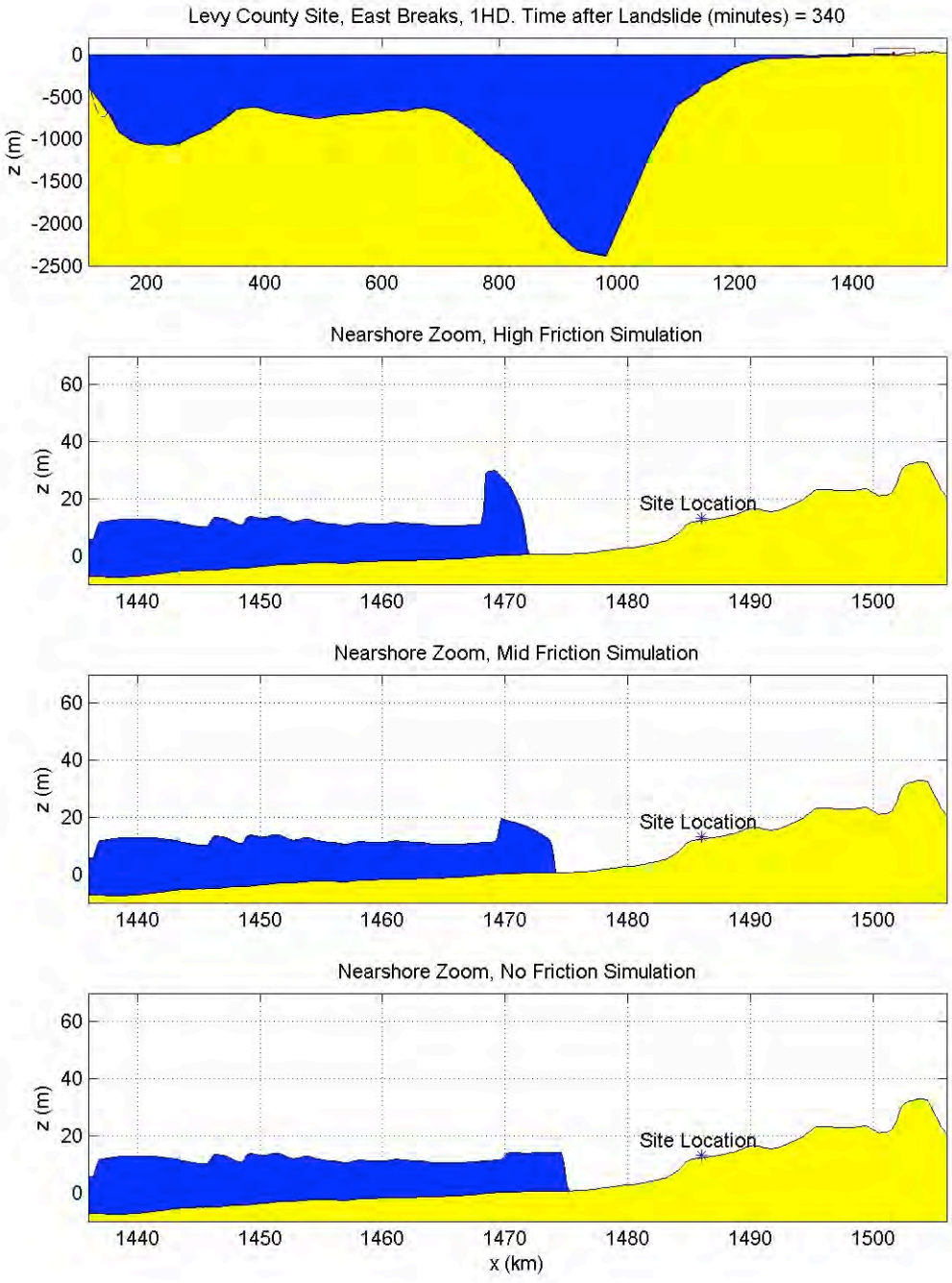

Figure 2.4.6.4.5-12. Same caption as Fig. 2.4.6.4.5-9. Time shown is t=340 min.

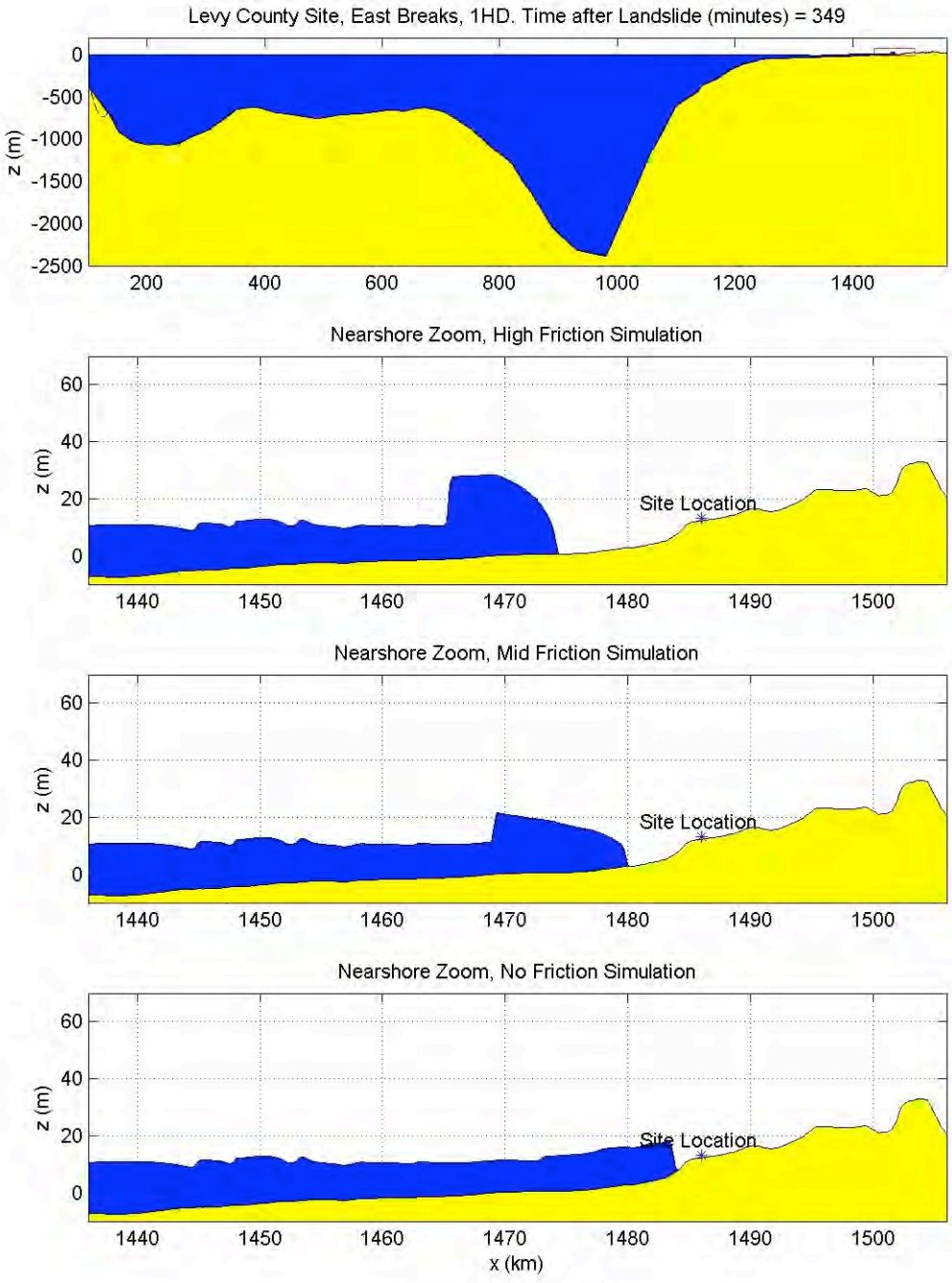

Figure 2.4.6.4.5-13. Same caption as Fig. 2.4.6.4.5-9. Time shown is t=349 min.

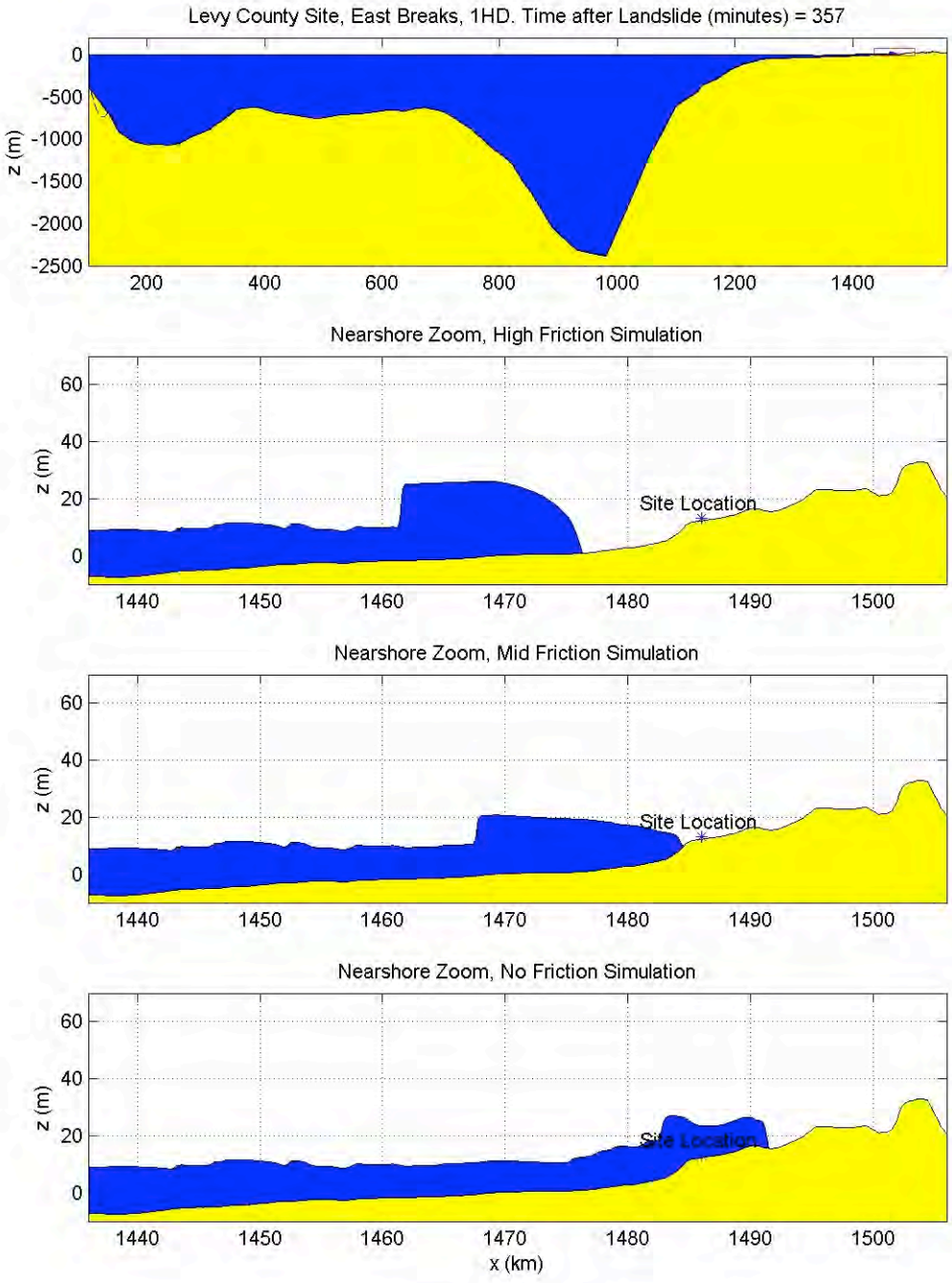

Figure 2.4.6.4.5-14. Same caption as Fig. 2.4.6.4.5-9. Time shown is t=357 min.

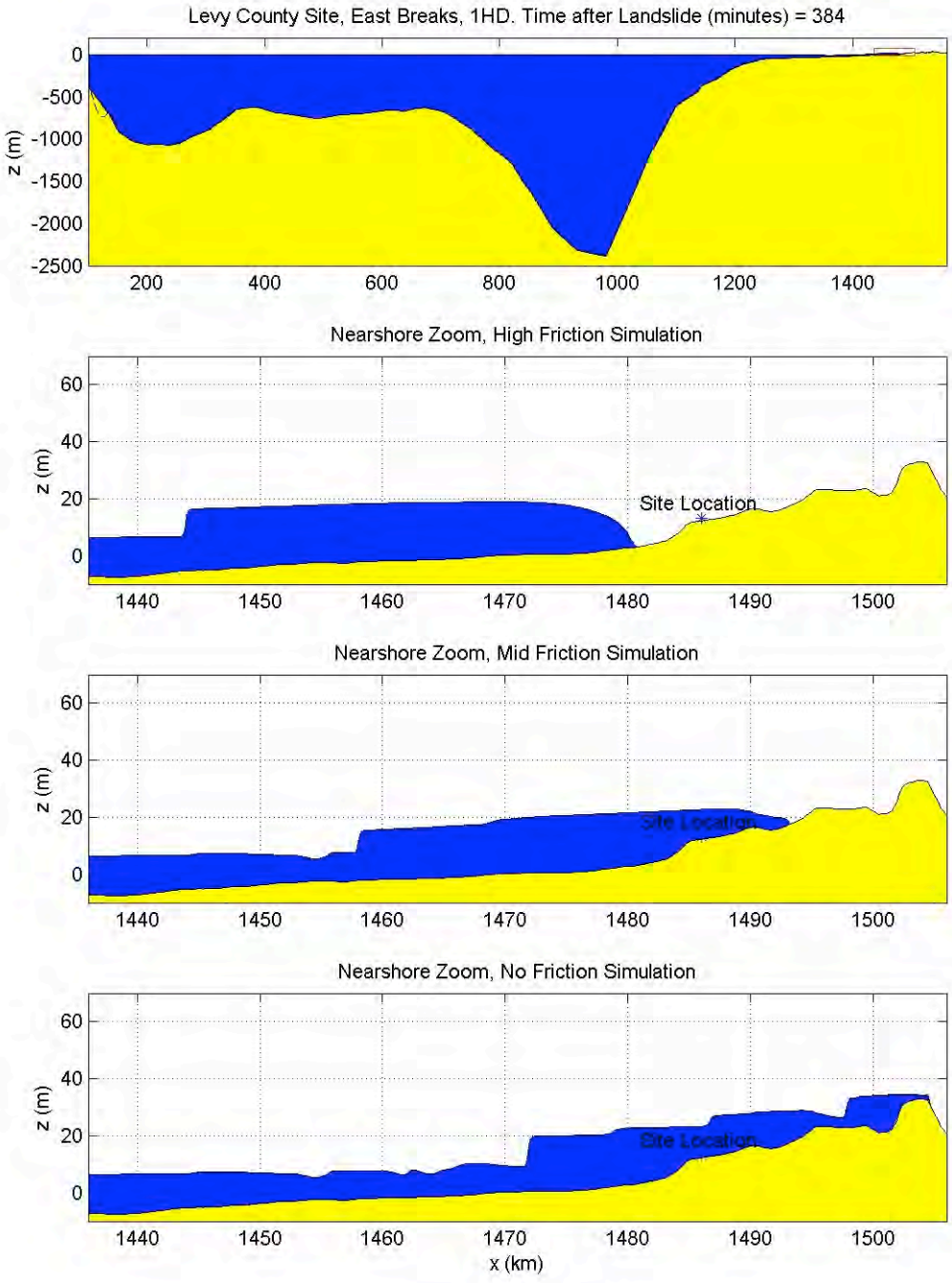

Figure 2.4.6.4.5-15. Same caption as Fig. 2.4.6.4.5-9. Time shown is t=384 min.

•Campeche Landslide Source:

Unfortunately, as noted in the landslide description section, there is no available data with which to constrain a Campeche submarine landslide source. In the absence of any quantitative guidance, it is assumed that a slide in this region will share geometric properties with the slope above the Florida Escarpment, owing to their similar geologic characteristics. As provided in the landslide characterization section, the excavation depth of this slide is approximately 150 m. This length provides the trough elevation (i.e., -150 m) of the hot-start initial water surface condition. The horizontal dimensions of the slide source region are assumed to be ~20 km in width and 50 km in length, inferred from the various scarps visible in the multibeam bathymetric data. With this information, and knowledge of characteristic slide-generated waves taken from the literature (Lynett and Liu, 2002; Lynett and Liu, 2005), the hot-start initial condition is constructed as shown in Figure 2.4.6.4.5-16.

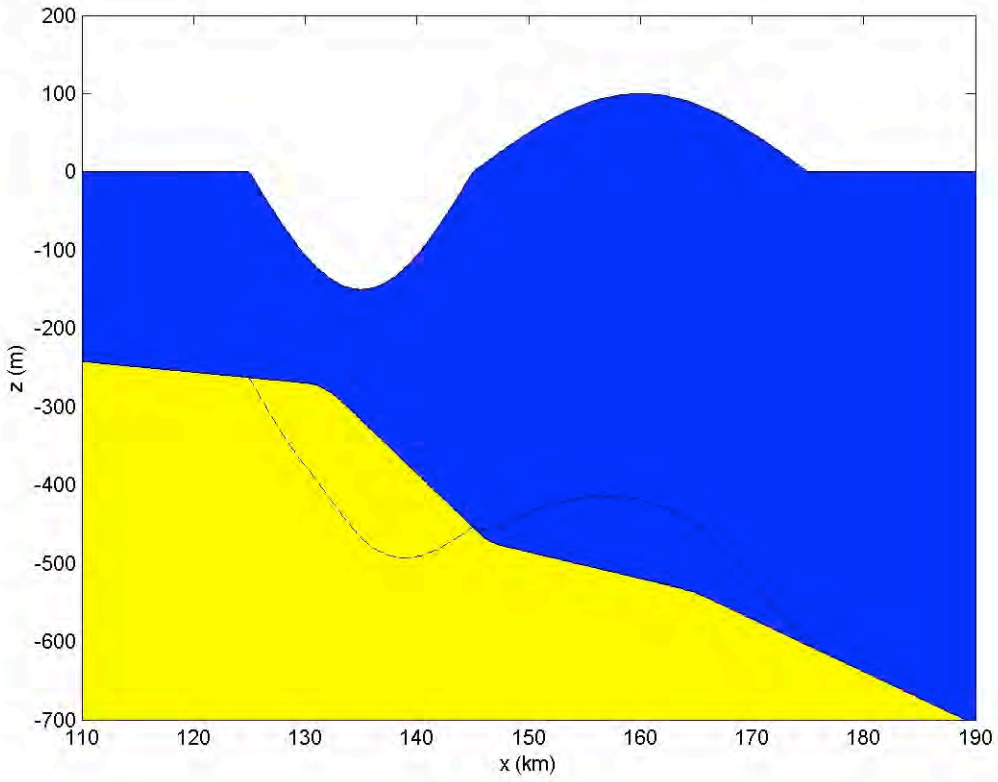

Figure 2.4.6.4.5-16. Centerline profile of the hot-start water surface condition used for the limiting Campeche Escarpment landslide tsunami simulations. Black dashed line shows the seafloor profile after mass failure.

The depth transect is taken from the source location directly to the Levy County site, as shown in Figure 2.4.6.4.5-17. A constant spatial grid size of 200 m is used across the transect for the 1HD cases. Predictions from three 1HD simulations are given for **(A)** no bottom friction, **(B)** bottom friction due to moderate roughness characteristic of grass/turf ($f = 0.01$), and **(C)** bottom friction due to large roughness characteristic of the trees and

dense shrub-like vegetation currently existing seaward of the Levy County site (f=0.05). Note that the three different bottom friction values are only applied over initially dry land; for all simulations, the initially submerged portions of the transect use no bottom friction.

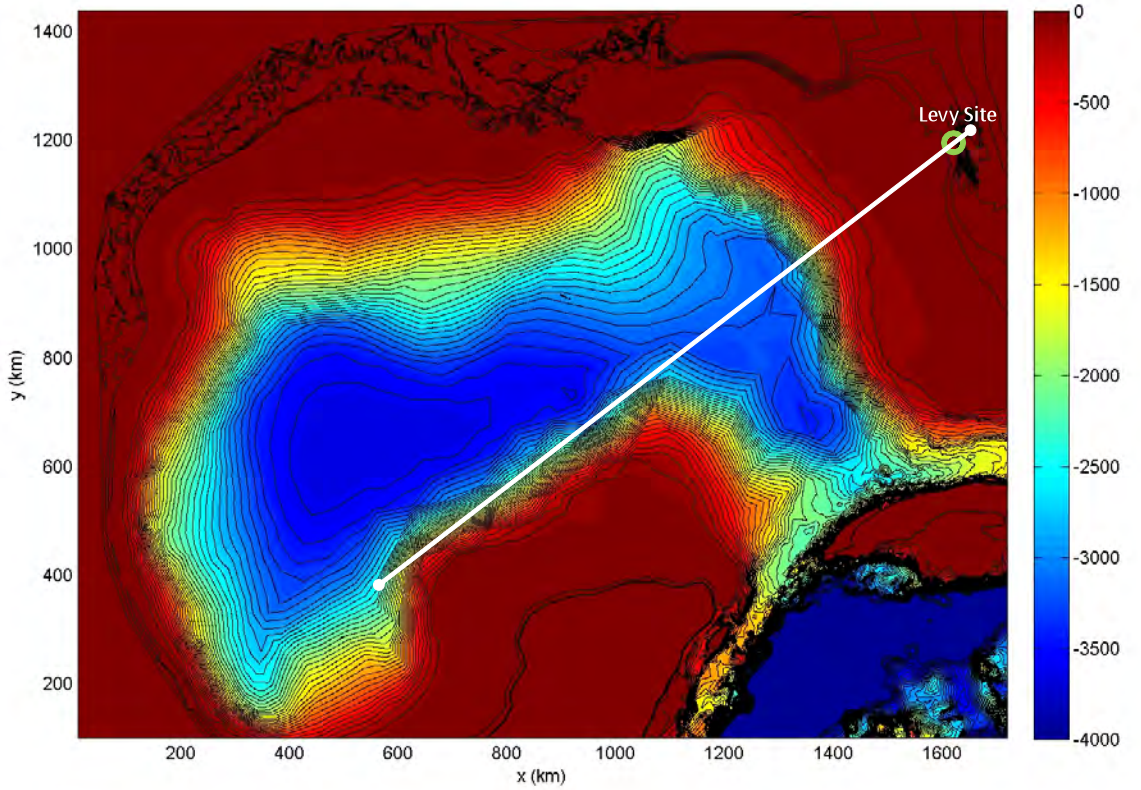

Figure 2.4.6.4.5-17. Bathymetry/topography contour surface in the GOM; the white line shows the transect used for the 1HD simulations. This transect passes through the Campeche Escarpment source location as well as the Levy County site.

A series of figures showing the evolution of this wave are provided in Figures 2.4.6.4.5-18 through 2.4.6.4.5-24. In the top subplot of all these figures, the entire transect is given, scaled vertically to show the limits of depth; due to this scaling the free surface wave appears small. The offshore evolution of the Campeche wave can be seen in this top plot in Figures 2.4.6.4.5-18 and 2.4.6.4.5-19. There are clearly dispersive effects, as shown by the long train of waves that reaches the Florida shelf. The wave in the nearshore zone is shown in the three lower subplots, which show a zoom-in of the transect near the site. For perspective, the red box in the top figure outlines the area shown in the lower three plots in these figures. All of the simulations provide identical results for the tsunami prior to reaching the shoreline, as all the simulations start with the same wave, use the same bathymetry, and are frictionless offshore. This is most evident in Figure 2.4.6.4.5-20, which shows the tsunami approaching the site.

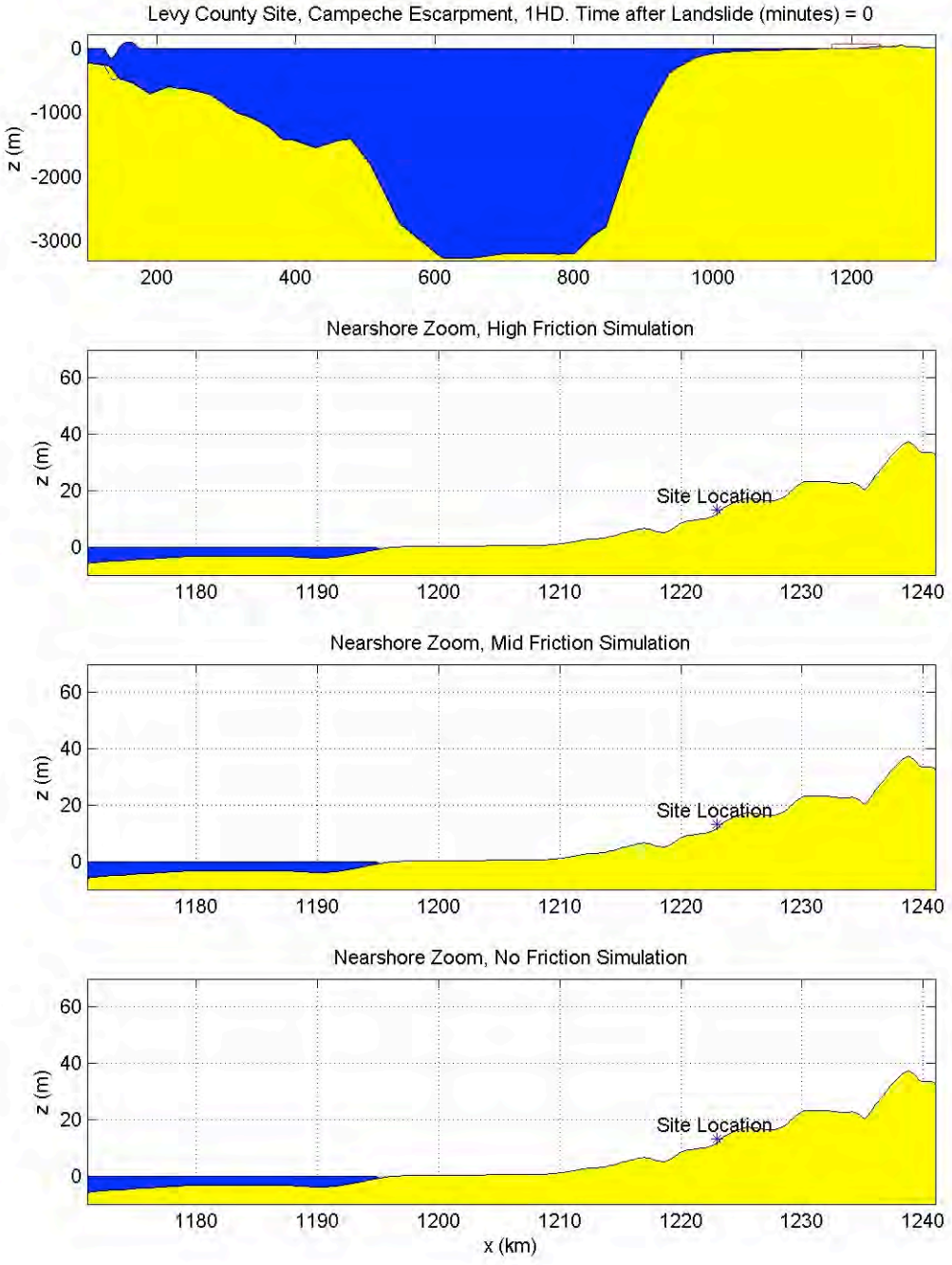

Figure 2.4.6.4.6-18. The offshore evolution of the hot-start tsunami condition for the Campeche Escarpment source. The top plot is the entire simulation transect, and the lower plots are zoom-in's of the nearshore areas, with each subplot showing the results using a different friction factor, as given in the title. Note that the vertical scale changes among the plots. Time shown is t=0 s.

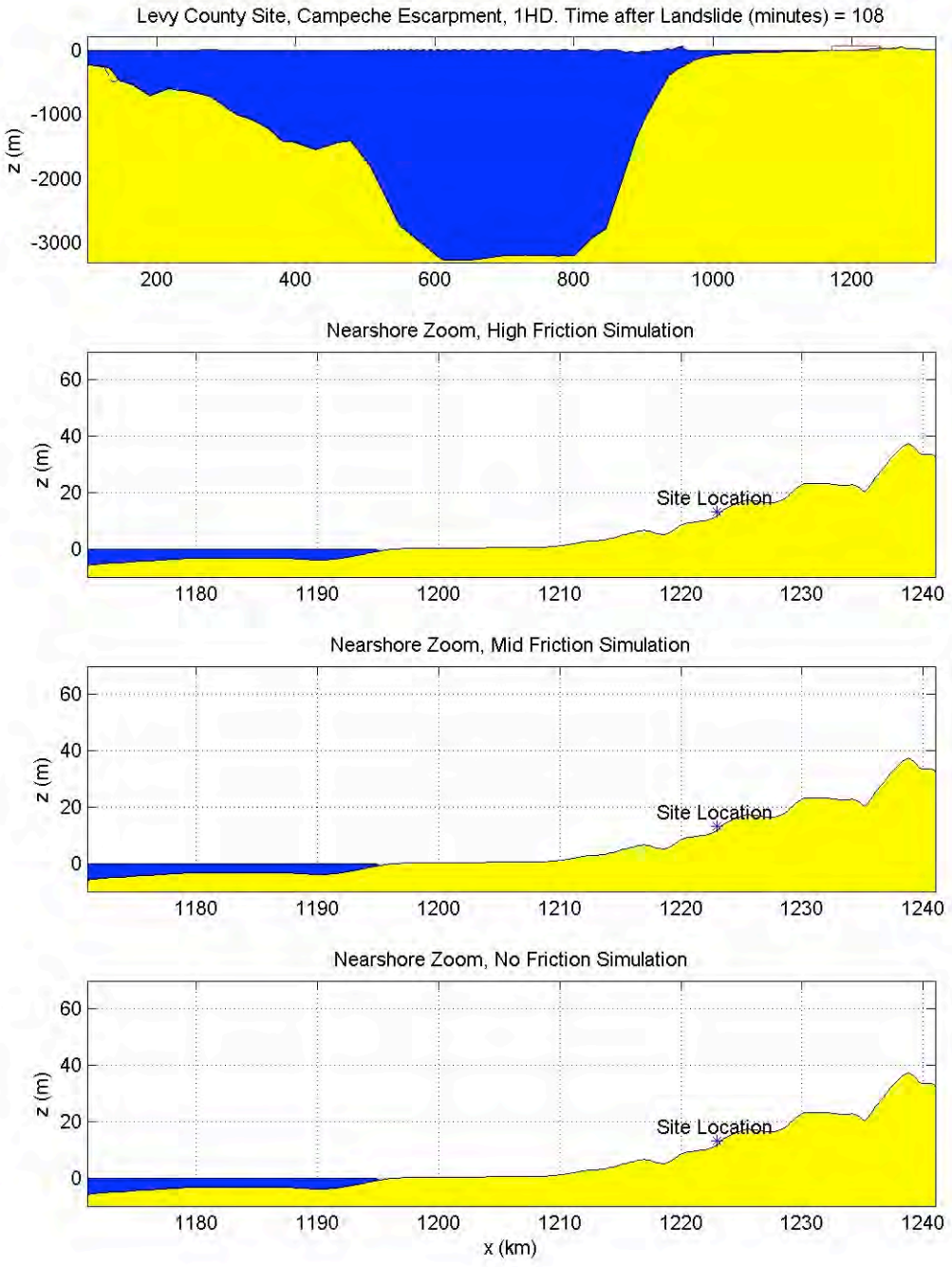

Figure 2.4.6.4.5-19. Same caption as Fig. 2.4.6.4.5-18. Time shown is t=108 min.

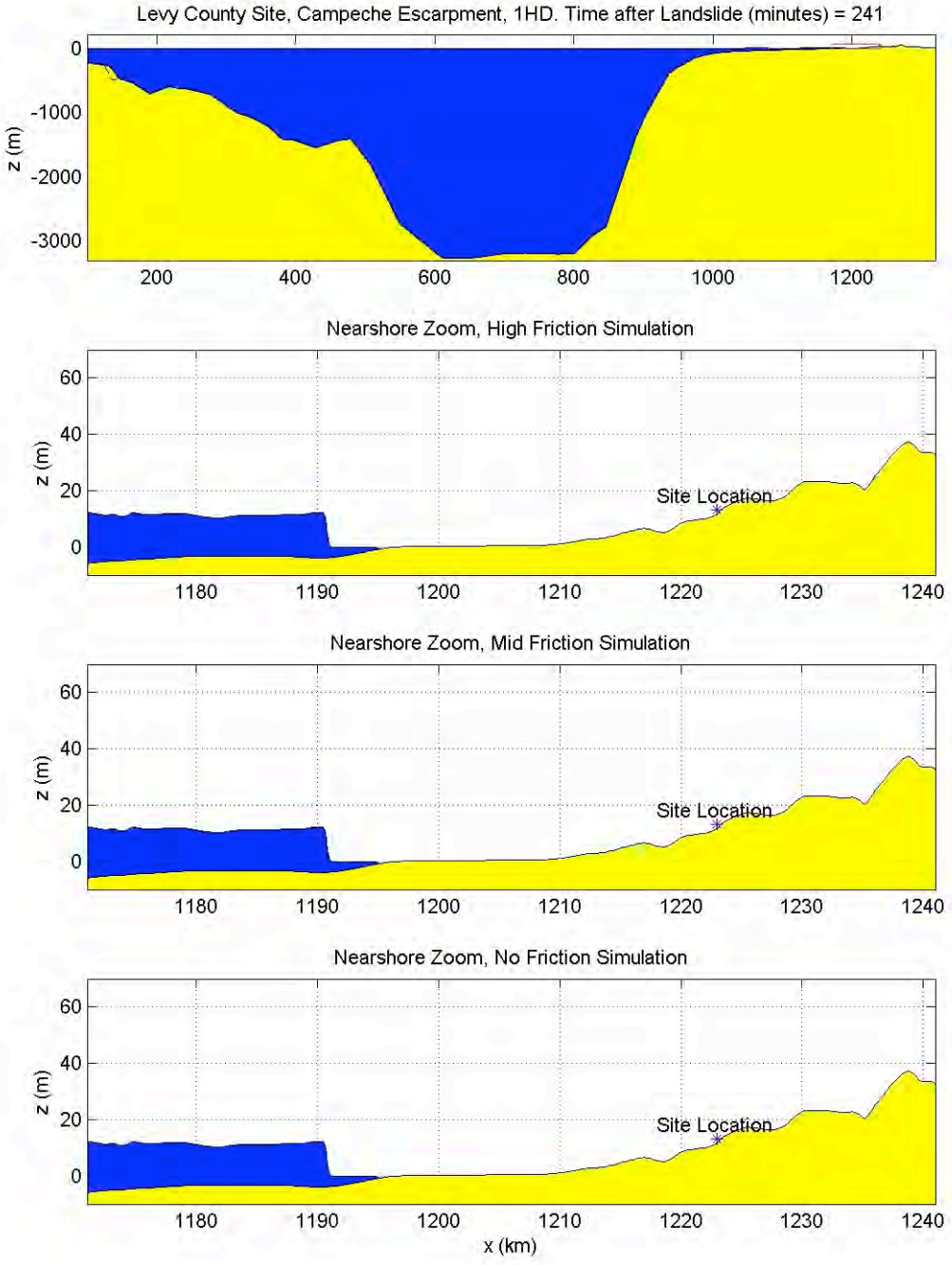

Figure 2.4.6.4.5-20. Same caption as Fig. 2.4.6.4.5-18. Time shown is t=241 min.

As the wave starts inundating dry land, friction becomes important and the results of the three simulations diverge (shown in Figures 2.4.6.4.5-21 through 2.4.6.4.5-24). The no-friction case (A) shows a fast moving bore front that easily reaches the Levy County site ground elevation, with maximum water surface elevations approaching +23 m at the site. Despite the modest friction value used in case (B), the tsunami wave front is slowed significantly but does reach the site, and maximum water elevations at the site are approximately +14 m. Finally, for case (C), the large, realistic friction retards the flow considerably, and the tsunami wave front stops 15 km seaward of the site. Note that in all these figures, the horizontal and vertical scales are distorted, and that the realistic friction tsunami case still manages to travel 15 km inland. A conclusion of this 1HD Campeche study is that a tsunami approaching the site, with a bore height up to +14 m at the still water shoreline, will not adversely impact the site if the vegetation roughness is properly accounted for. However, the site is flooded with the moderate friction assumption (case B), and thus it may be necessary to investigate this site further.

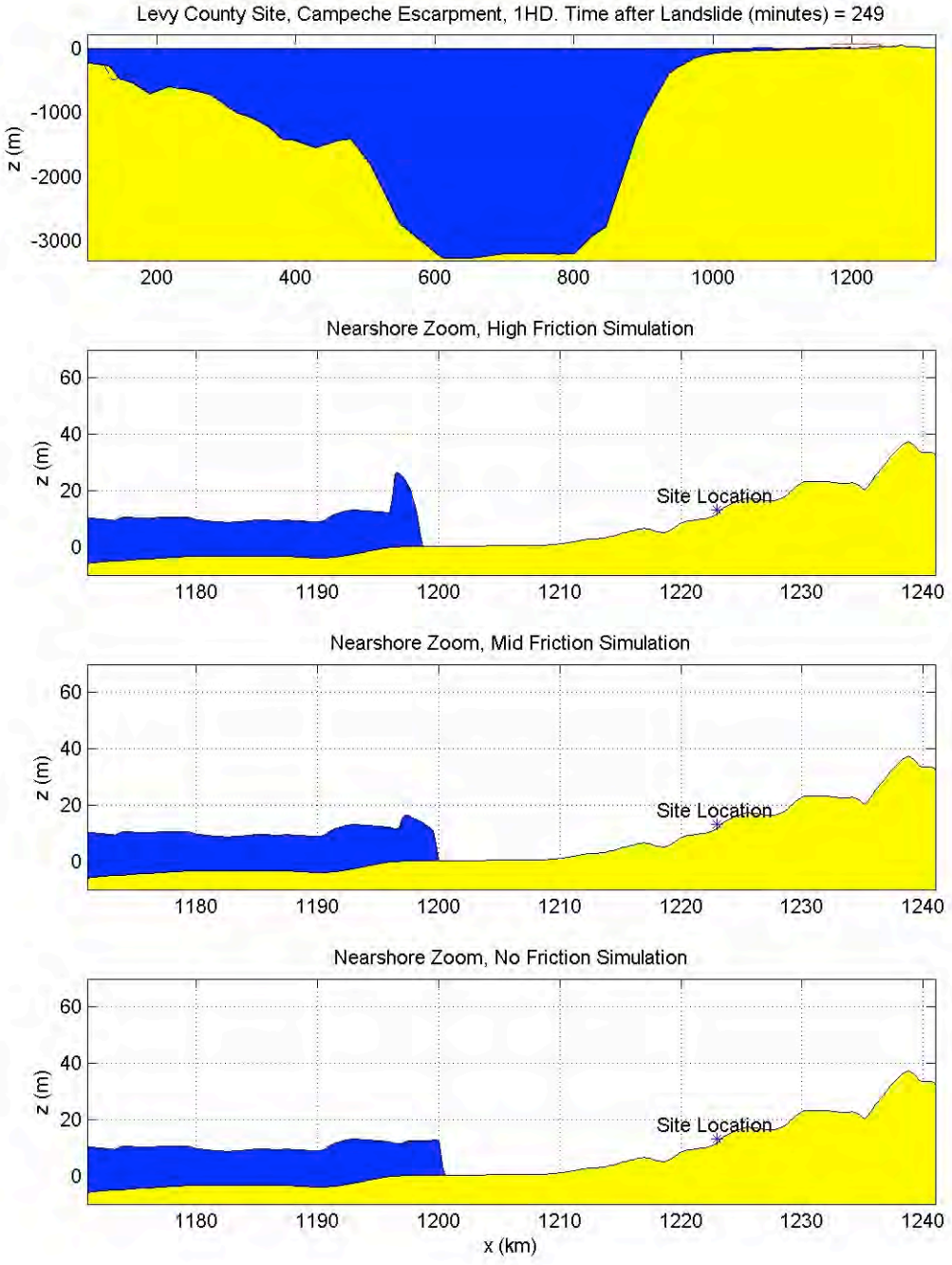

Figure 2.4.6.4.5-21. Same caption as Fig. 2.4.6.4.5-18. Time shown is t=249 min.

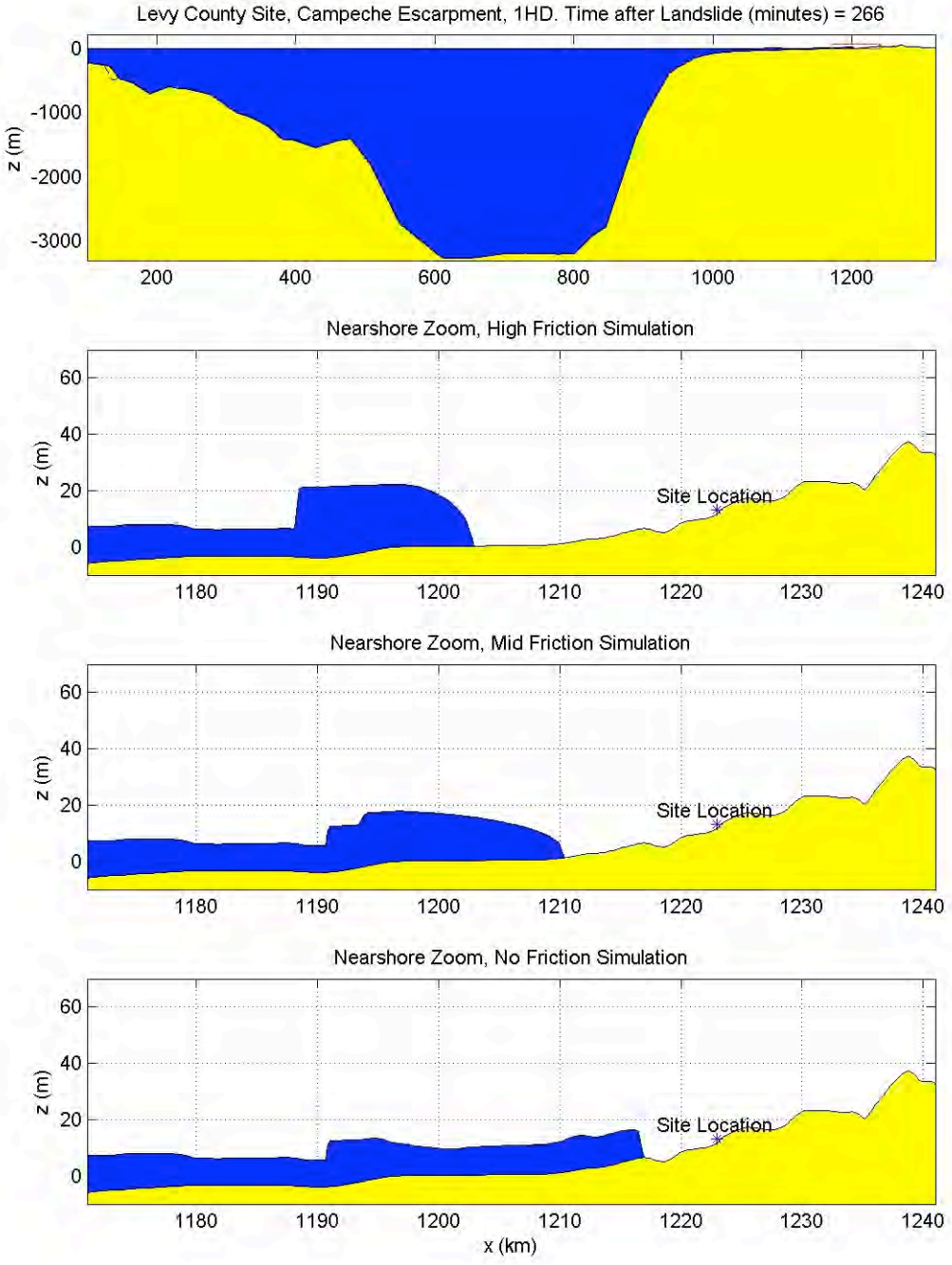

Figure 2.4.6.4.5-22. Same caption as Fig. 2.4.6.4.5-18. Time shown is t=266 min.

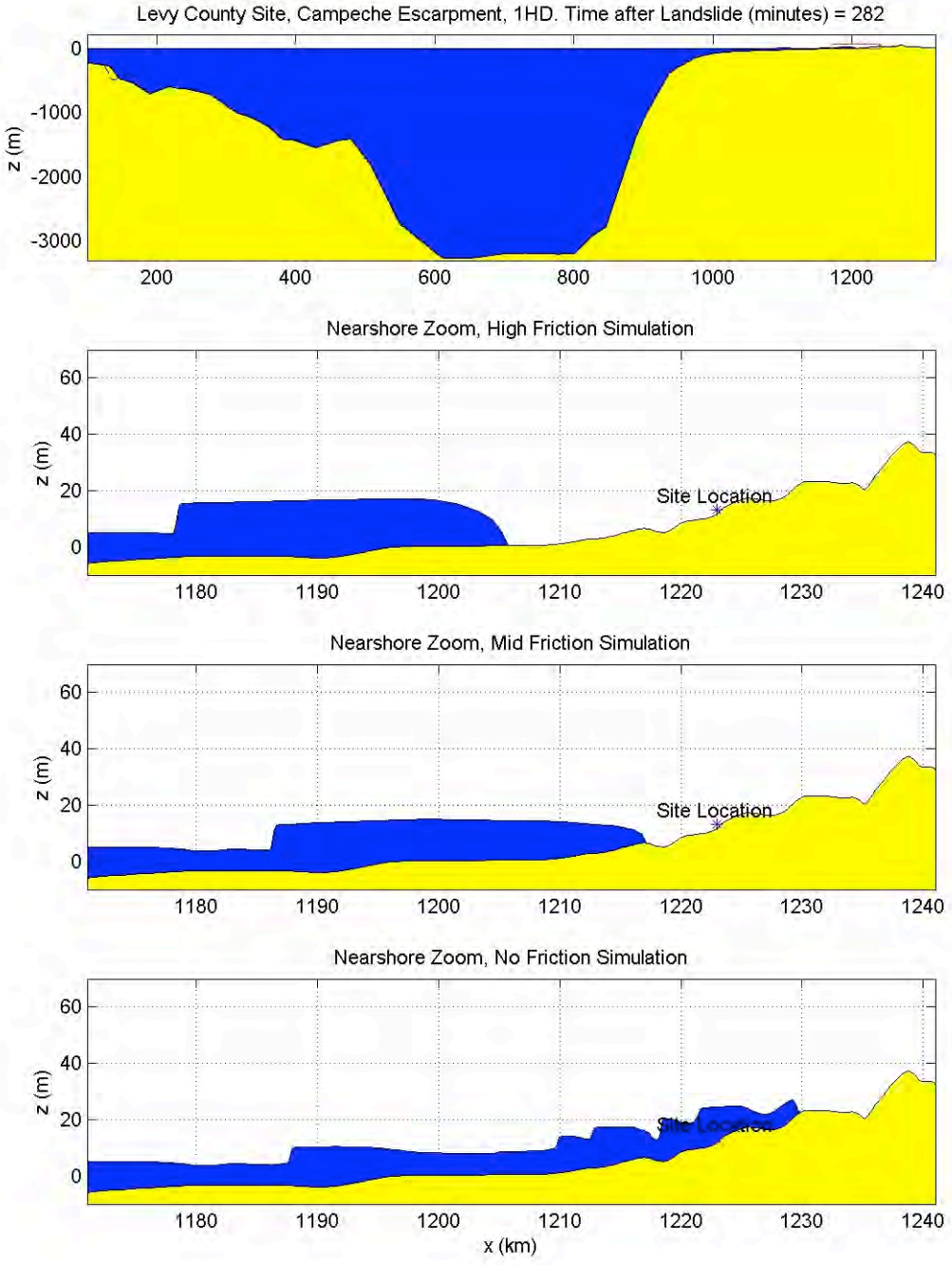

Figure 2.4.6.4.5-23. Same caption as Fig. 2.4.6.4.5-18. Time shown is t=282 min.

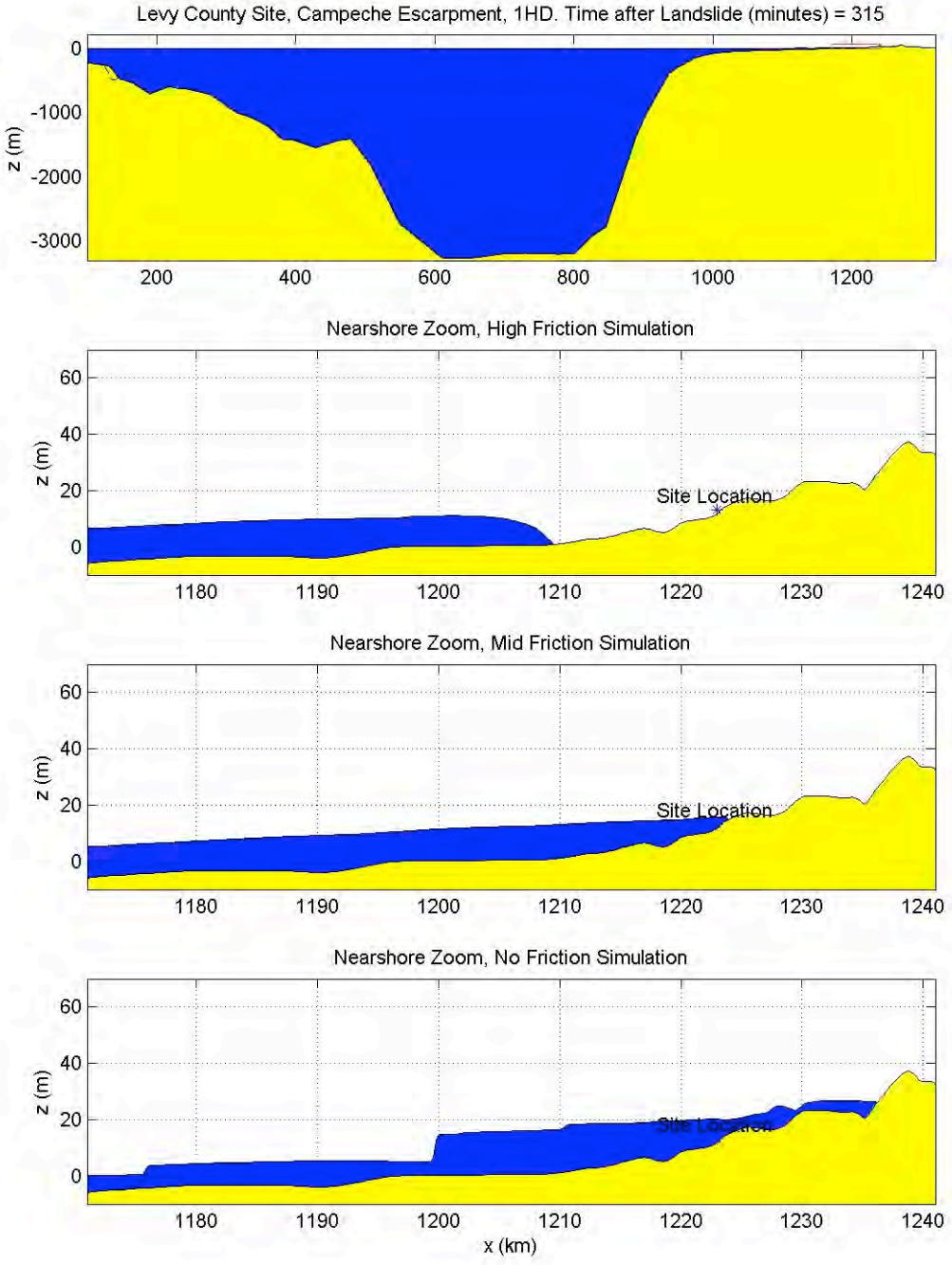

Figure 2.4.6.4.5-24. Same caption as Fig. 2.4.6.4.5-18. Time shown is t=315 min.

•Florida Slope Landslide Source:

As provided in the landslide characterization section, the excavation depth of this slide is approximately 150 m. This length provides the trough elevation (i.e., -150 m) of the hot-start initial water surface condition. The horizontal dimensions of the slide source region are assumed to be ~20 km in width and 50 km in length, inferred from the various scarps visible in the multibeam bathymetric data. With this information, and knowledge of characteristic slide-generated waves taken from the literature (Lynett and Liu, 2002; Lynett and Liu, 2005), the hot-start initial condition is constructed as shown in Figure 2.4.6.4.5-25.

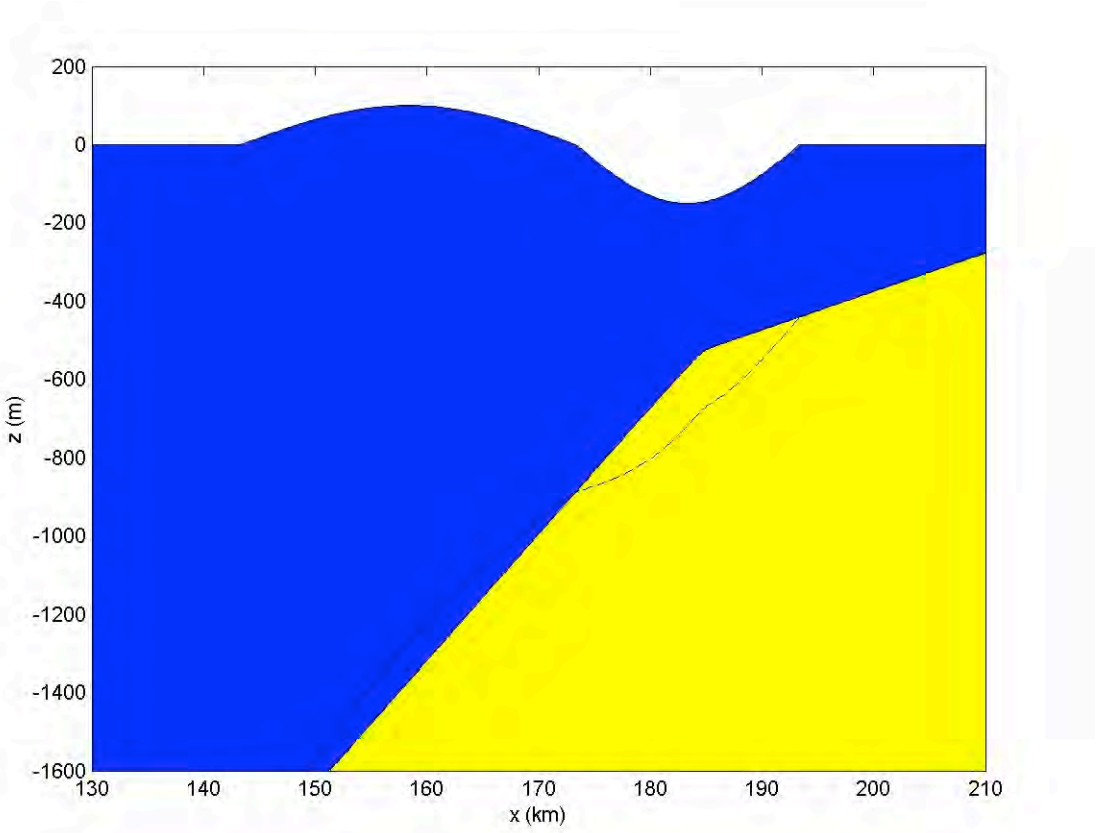

Figure 2.4.6.4.5-25. Centerline profile of the hot-start water surface condition used for the limiting Florida Slope landslide tsunami simulations. Black dashed line shows the seafloor profile after mass failure.

The depth transect is taken from the source location directly to the Levy County site, as shown in Figure 2.4.6.4.6-26. A constant spatial grid size of 200 m is used across the transect for the 1HD cases. Predictions from three 1HD simulations are given for **(A)** no bottom friction, **(B)** bottom friction due to moderate roughness characteristic of grass/turf ($f = 0.01$), and **(C)** bottom friction due to large roughness characteristic of the trees and dense shrub-like vegetation currently existing seaward of the Levy County site ($f = 0.05$). Note that the three different bottom friction values are only applied over initially dry

land; for all simulations, the initially submerged portions of the transect use no bottom friction.

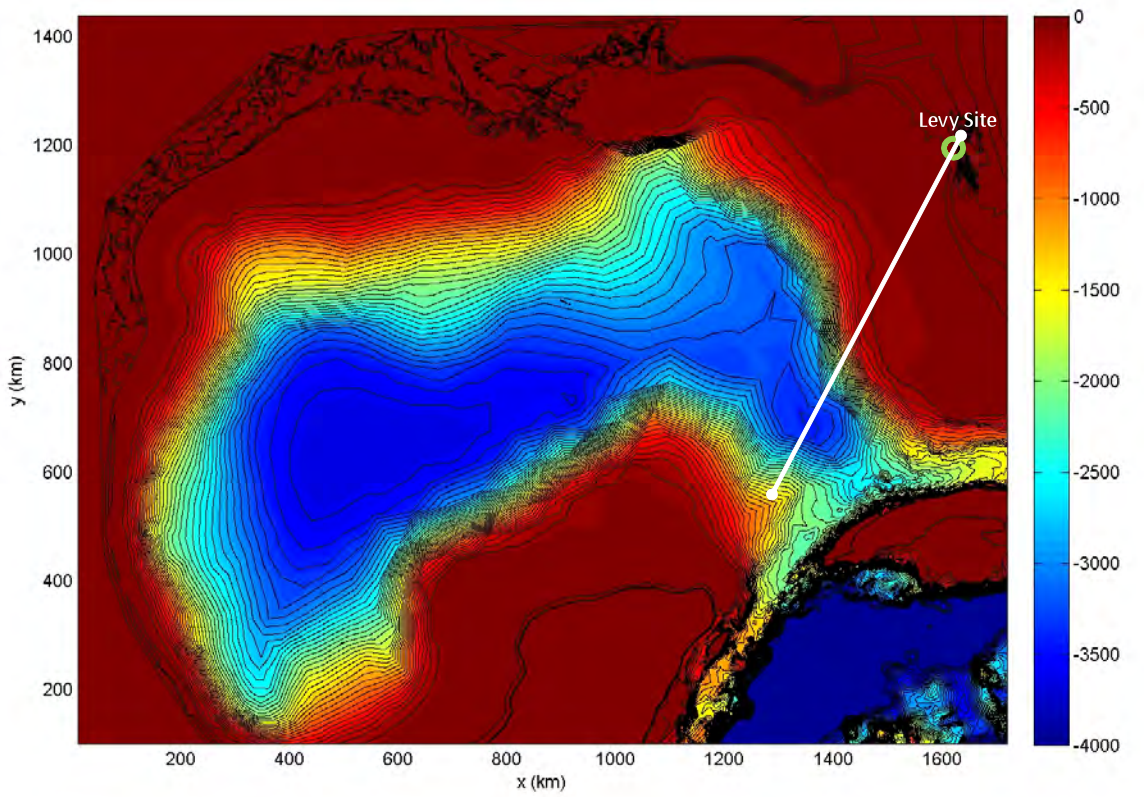

Figure 2.4.6.4.5-26. Bathymetry/topography contour surface in the GOM; the white line shows the transect used for the 1HD simulations. This transect passes through the Florida Slope source location as well as the Levy County site.

A series of figures showing the evolution of this wave are provided in Figures 2.4.6.4.5-27 through 2.4.6.4.5-32. In the top subplot of all these figures, the entire transect is given, scaled vertically to show the limits of depth; due to this scaling the free surface wave appears small. The offshore evolution of the Florida Slope wave can be seen in this top plot in Figures 2.4.6.4.5-27 and 2.4.6.4.5-28. The large, non-linear wave immediately steepens and forms a bore-front once on the shallow shelf. The wave in the nearshore zone is shown in the three lower subplots, which show a zoom-in of the transect near the site. For perspective, the red box in the top figure outlines the area shown in the lower three plots in these figures. All of the simulations provide identical results for the tsunami prior to reaching the shoreline, as all the simulations start with the same wave, use the same bathymetry, and are frictionless offshore. This is most evident in Figure 2.4.6.4.5-29, which shows the tsunami approaching the site.

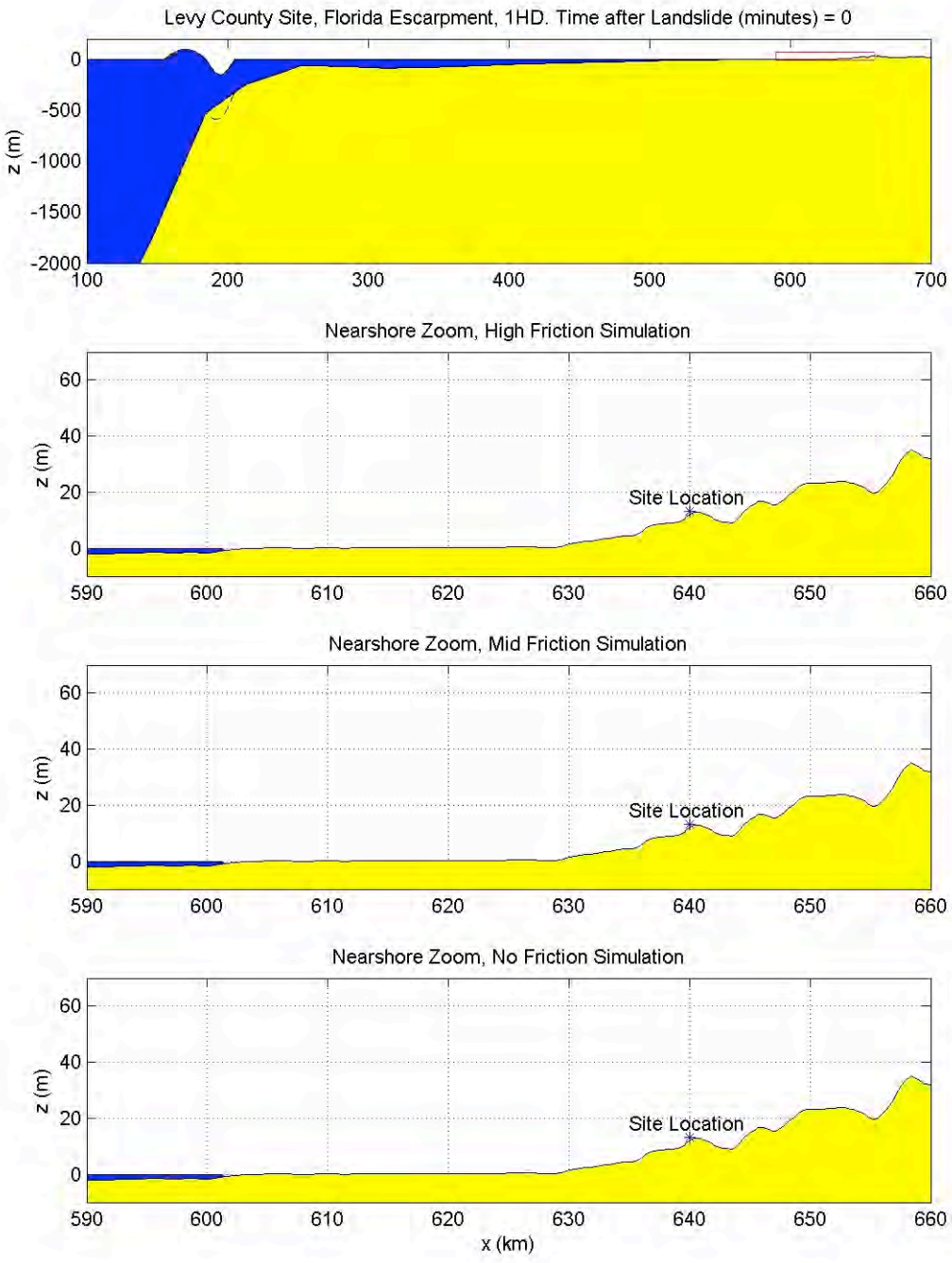

Figure 2.4.6.4.5-27. The offshore evolution of the hot-start tsunami condition for the Florida Slope source. The top plot is the entire simulation transect, and the lower plots are zoom-in's of the nearshore areas, with each subplot showing the results using a different friction factor, as given in the title. Note that the vertical scale changes among the plots. Time shown is t=0 s.

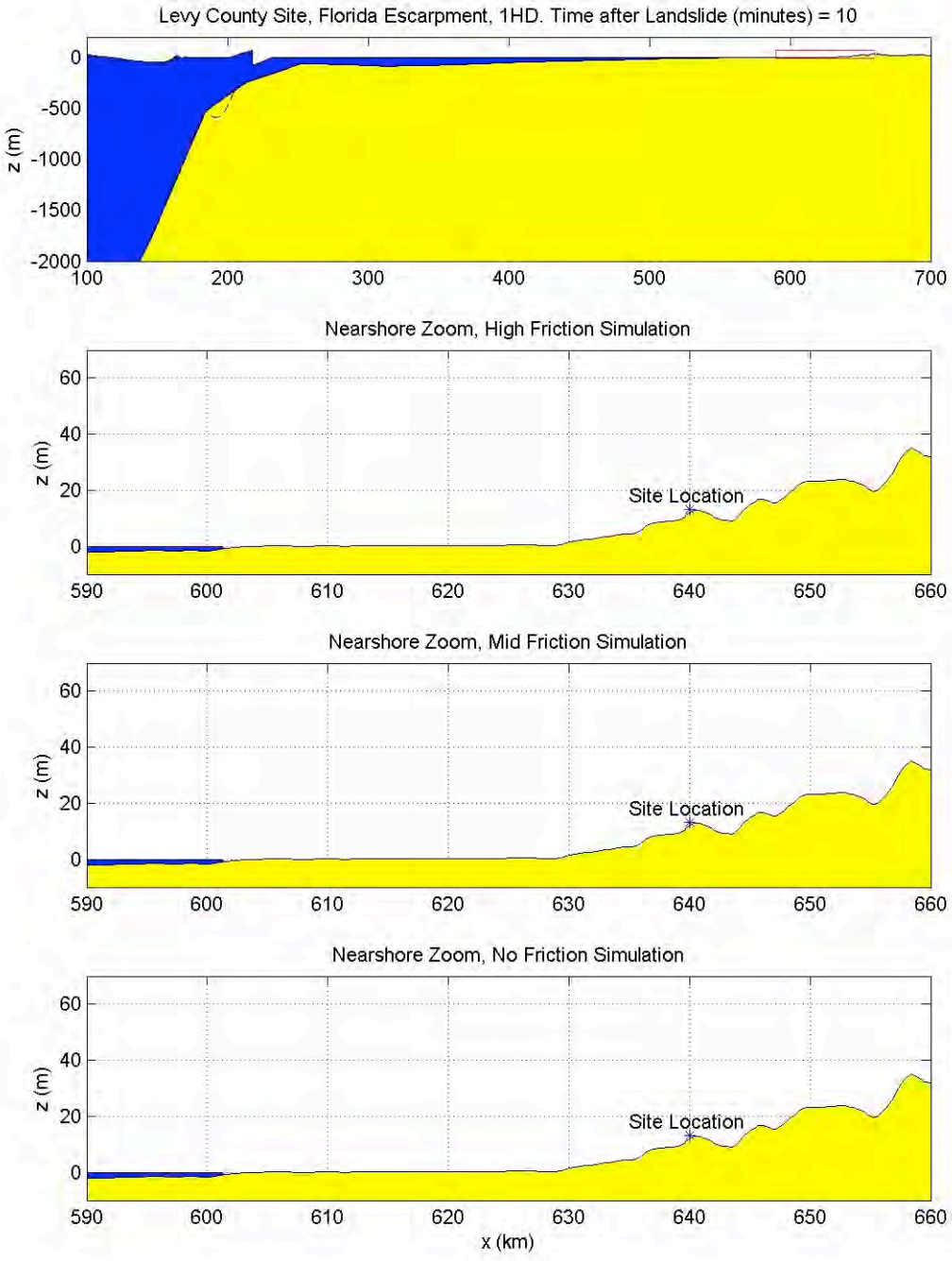

Figure 2.4.6.4.5-28. Same caption as Fig. 2.4.6.4.5-27. Time shown is t=10 min.

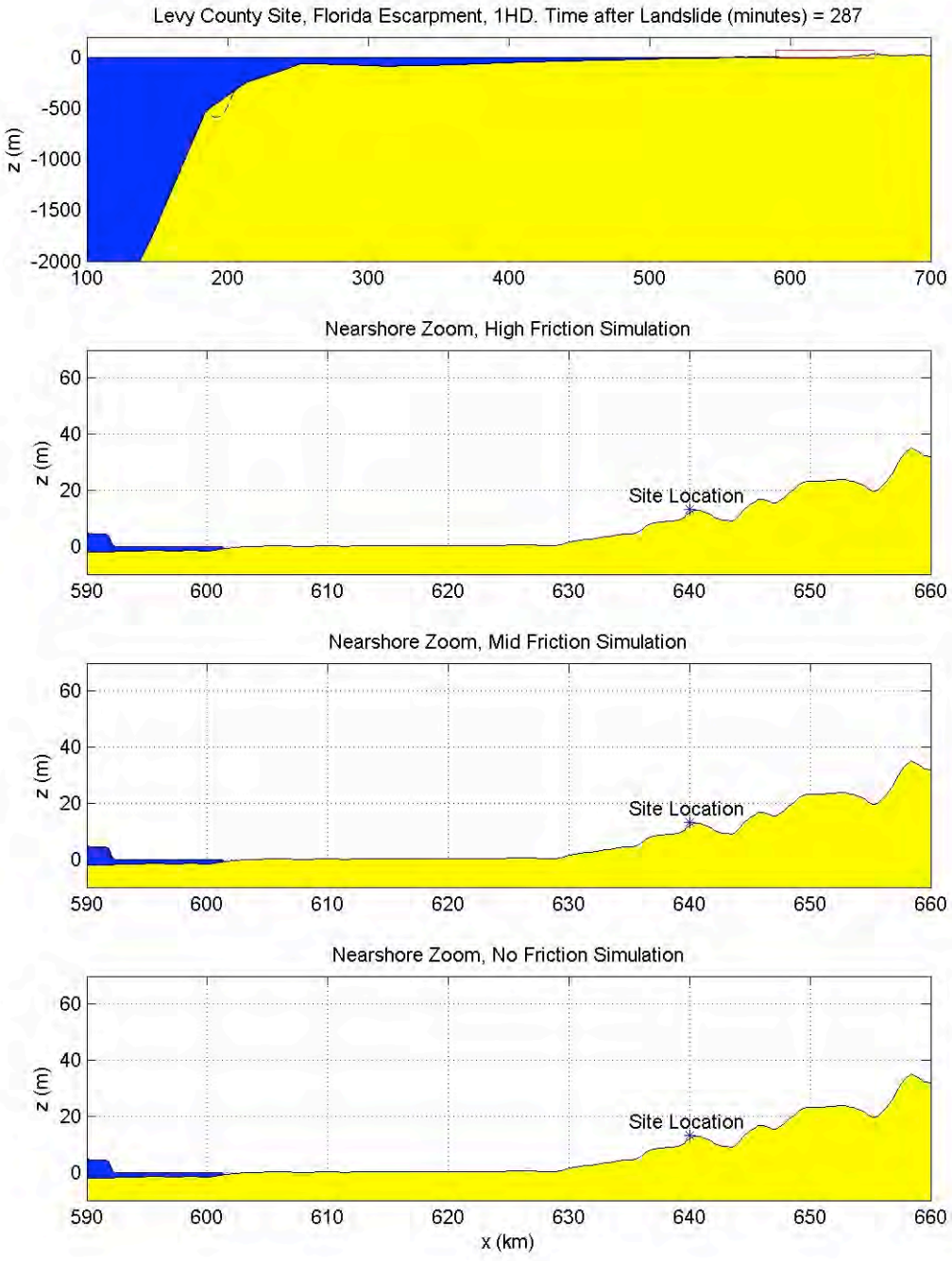

Figure 2.4.6.4.5-29. Same caption as Fig. 2.4.6.4.5-27. Time shown is t=287 min.

As the wave starts inundating dry land, friction becomes important and the results of the three simulations diverge (shown in Figures 2.4.6.4.5-30 through 2.4.6.4.5-32. The no-friction case (A) shows a fast moving bore front that barely reaches the Levy County site ground elevation, with maximum water surface elevations approaching +14 m at the site. With the modest friction value used in case (B), the tsunami wave front is slowed significantly and does not reach the site. Finally, for case (C), the large, realistic friction retards the flow considerably, and the tsunami wave front stops 25 km seaward of the site. A conclusion of this 1HD Florida Slope study is that a tsunami approaching the site, with a bore height up to +6 m at the still water shoreline, will not adversely impact the site if the vegetation roughness is properly accounted for.

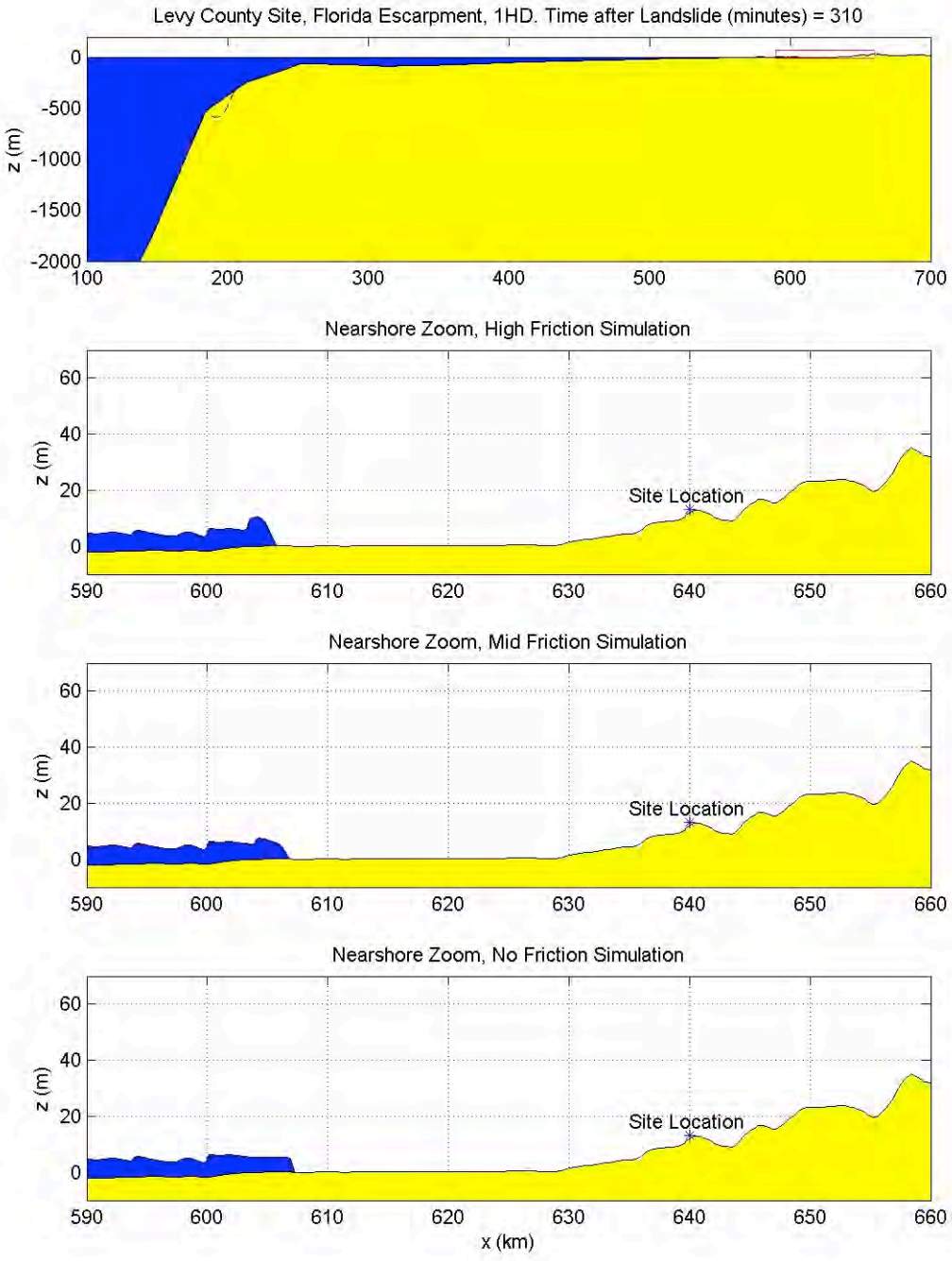

Figure 2.4.6.4.5-30. Same caption as Fig. 2.4.6.4.5-27. Time shown is t=310 min.

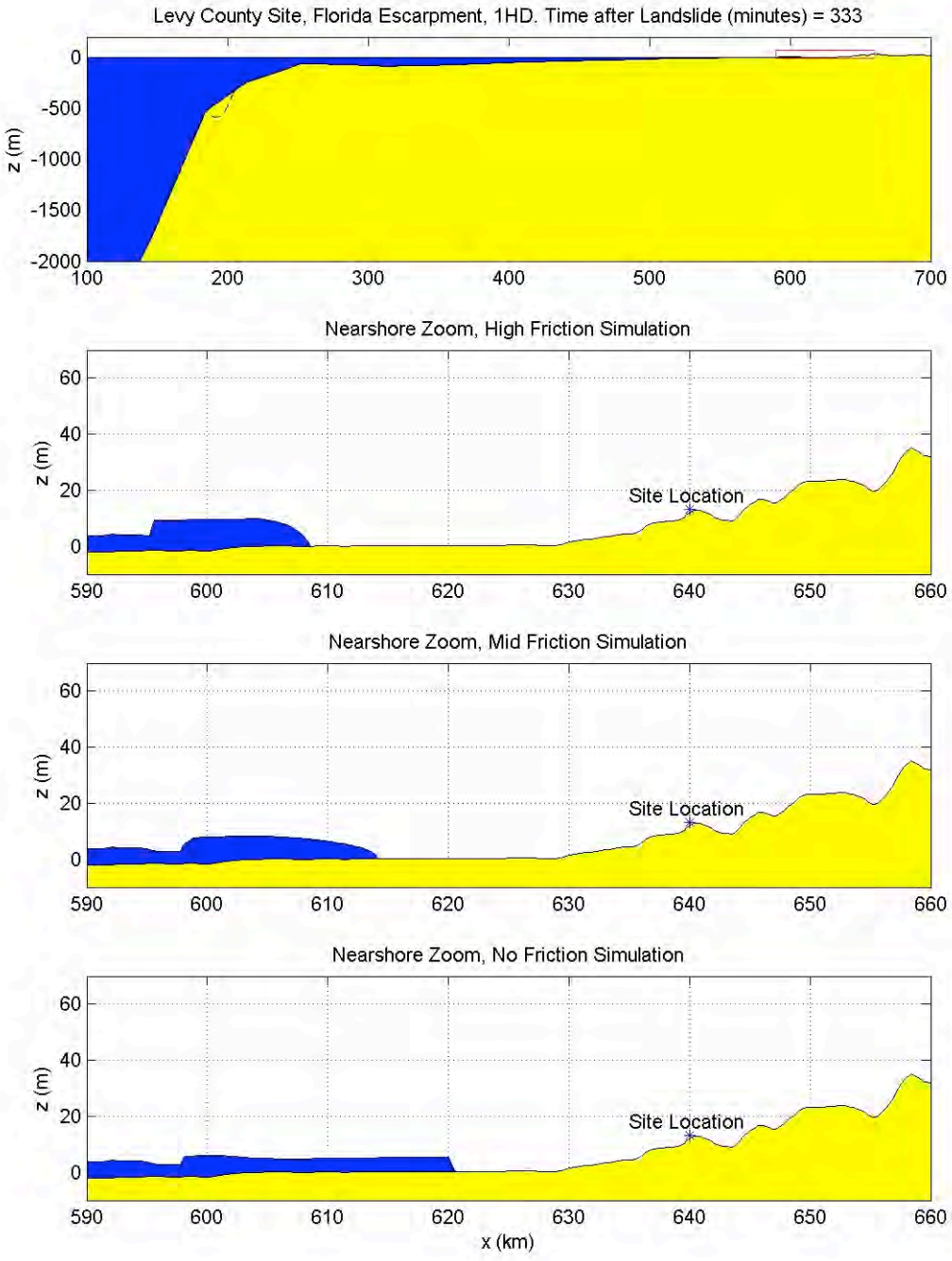

Figure 2.4.6.4.5-31. Same caption as Fig. 2.4.6.4.5-27. Time shown is t=333 min.

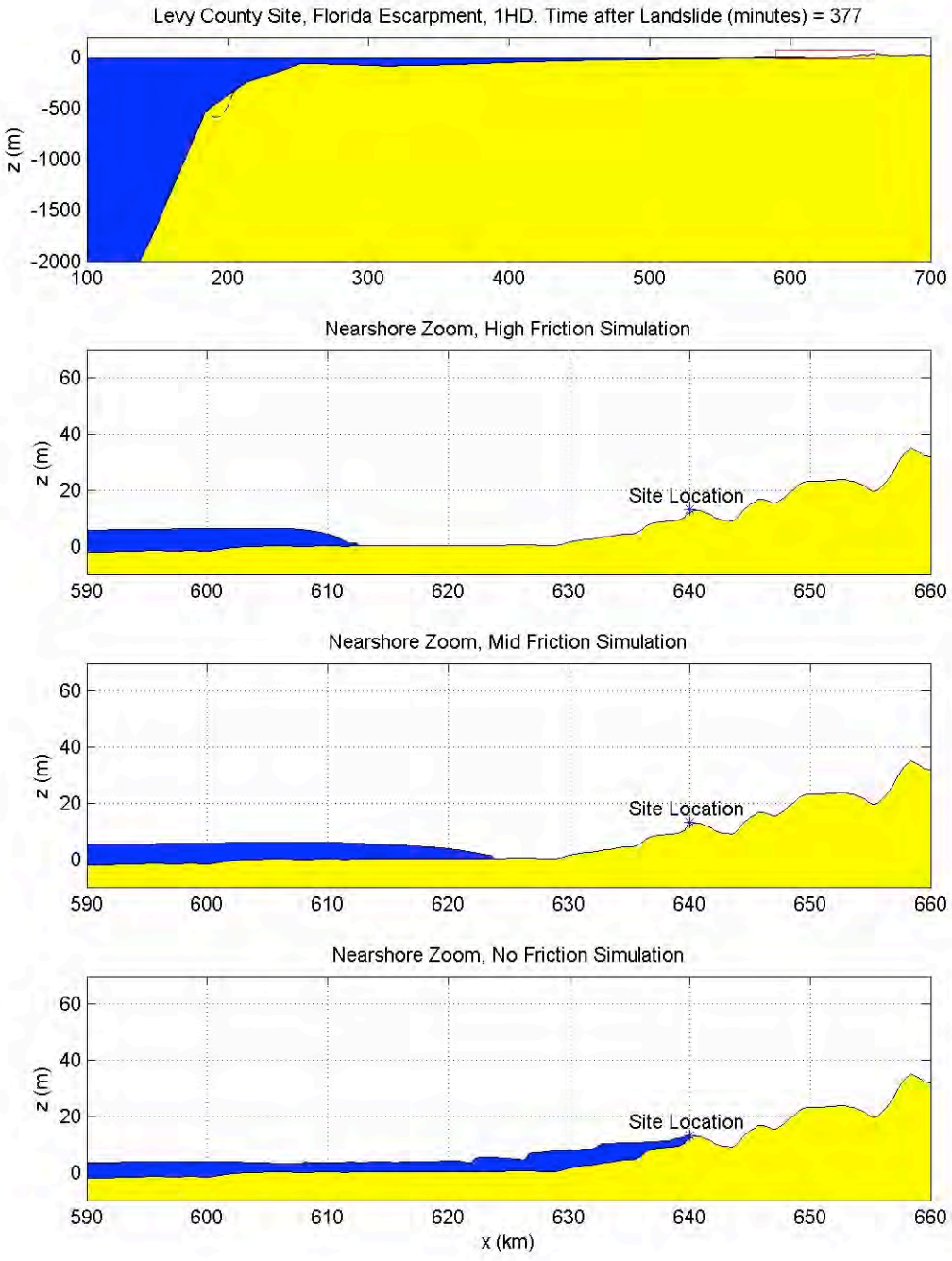

Figure 2.4.6.4.5-32. Same caption as Fig. 2.4.6.4.5-27. Time shown is t=377 min.

It should be noted that one of the reasons for the relatively small wave height produced by this source, as compared to the Campeche source, is the longer length of shelf that this wave must travel over before reaching the shoreline. With the Florida Slope transect, as shown in Figure 2.4.6.4.5-26, the shelf length is 150 km longer than that for the Campeche source (shown in Figure 2.4.6.4.5-17). A second reason for a smaller tsunami, again as compared to Campeche, is the initial wave orientation. For a slide on the Florida shelf, the wave approaching Florida will have a leading depression. For a slide coming from Campeche, the wave approaching Florida will have a leading elevation. Once a leading depression wave is on the shelf, non-linear effects will cause the trailing elevation wave to overrun and partially absorb the depression, equating to a decrease in the absolute elevation of the elevation wave front.

•Florida Slope WORST CASE Landslide Source:

As mentioned in the previous Florida Slope section, the very long shelf length over which a wave must travel from the existing landslide source to the site diminishes the tsunami impact considerably. In this section, a landslide source, identical to the Florida Slope source, is hypothesized to exist immediately offshore of the Levy County site. By minimizing the travel distance over the shallow shelf, this simulation will provide an upper limit of the tsunami impact at the Levy County site due to a Florida Slope-type slide anywhere along the west Florida shelf.

As provided in the landslide characterization section, the excavation depth of this slide is approximately 150 m. This length provides the trough elevation (i.e., -150 m) of the hot-start initial water surface condition. The horizontal dimensions of the slide source region are assumed to be ~20 km in width and 50 km in length, inferred from the various scarps visible in the multibeam bathymetric data. With this information, and knowledge of characteristic slide-generated waves taken from the literature (Lynett and Liu, 2002; Lynett and Liu, 2005), the hot-start initial condition is constructed as shown in Figure 2.4.6.4.5-25.

The depth transect is taken from the source location directly to the Levy County site, as shown in Figure 2.4.6.4.5-33. A constant spatial grid size of 200 m is used across the transect for the 1HD cases. Predictions from three 1HD simulations are given for **(A)** no bottom friction, **(B)** bottom friction due to moderate roughness characteristic of grass/turf ($f = 0.01$), and **(C)** bottom friction due to large roughness characteristic of the trees and dense shrub-like vegetation currently existing seaward of the Levy County site ($f = 0.05$). Note that the three different bottom friction values are only applied over initially dry land; for all simulations, the initially submerged portions of the transect use no bottom friction.

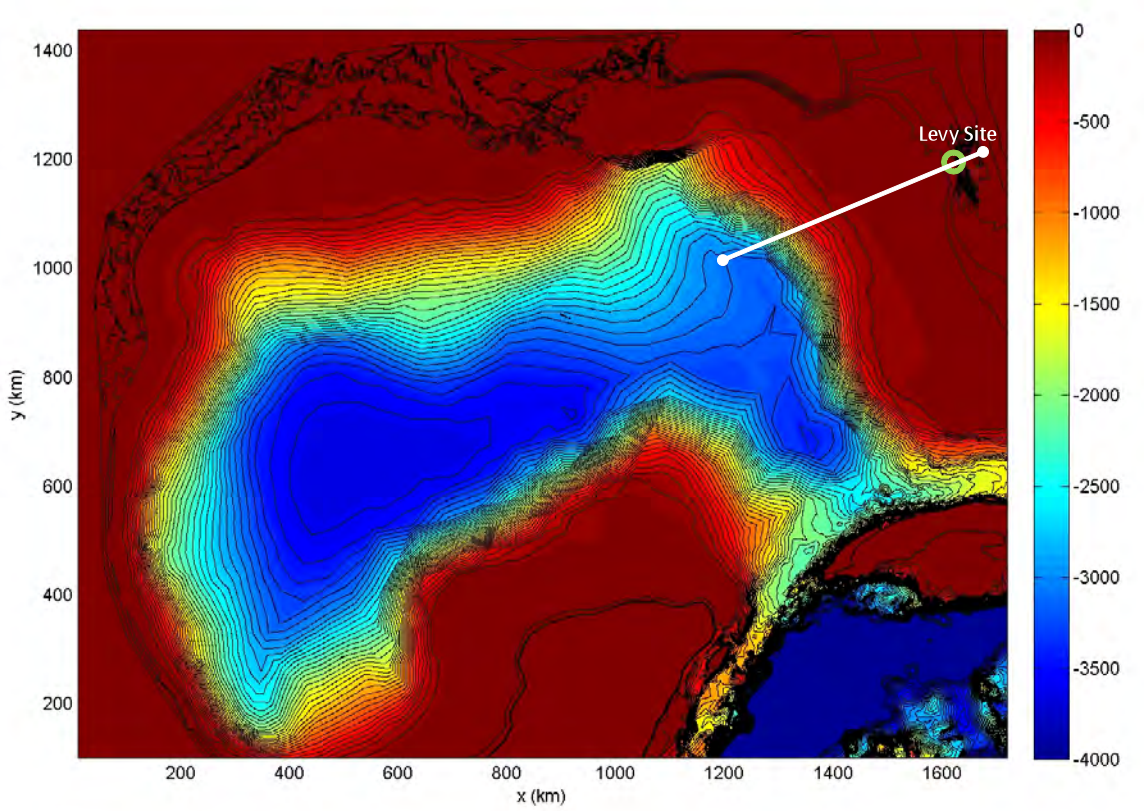

Figure 2.4.6.4.5-33. Bathymetry/topography contour surface in the GOM; the white line shows the transect used for the 1HD simulations. This transect passes through the Florida Slope WORST CASE source location as well as the Levy County site.

A series of figures showing the evolution of this wave are provided in Figures 2.4.6.4.5-34 through 2.4.6.4.5-39. In the top subplot of all these figures, the entire transect is given, scaled vertically to show the limits of depth; due to this scaling the free surface wave appears small. The offshore evolution of the Florida Slope wave can be seen in this top plot in Figures 2.4.6.4.5-34 and 2.4.6.4.5-35. The large, non-linear wave immediately steepens and forms a bore-front once on the shallow shelf. The wave in the nearshore zone is shown in the three lower subplots, which show a zoom-in of the transect near the site. For perspective, the red box in the top figure outlines the area shown in the lower three plots in these figures. All of the simulations provide identical results for the tsunami prior to reaching the shoreline, as all the simulations start with the same wave, use the same bathymetry, and are frictionless offshore. This is most evident in Figure 2.4.6.4.5-36, which shows the tsunami approaching the site.

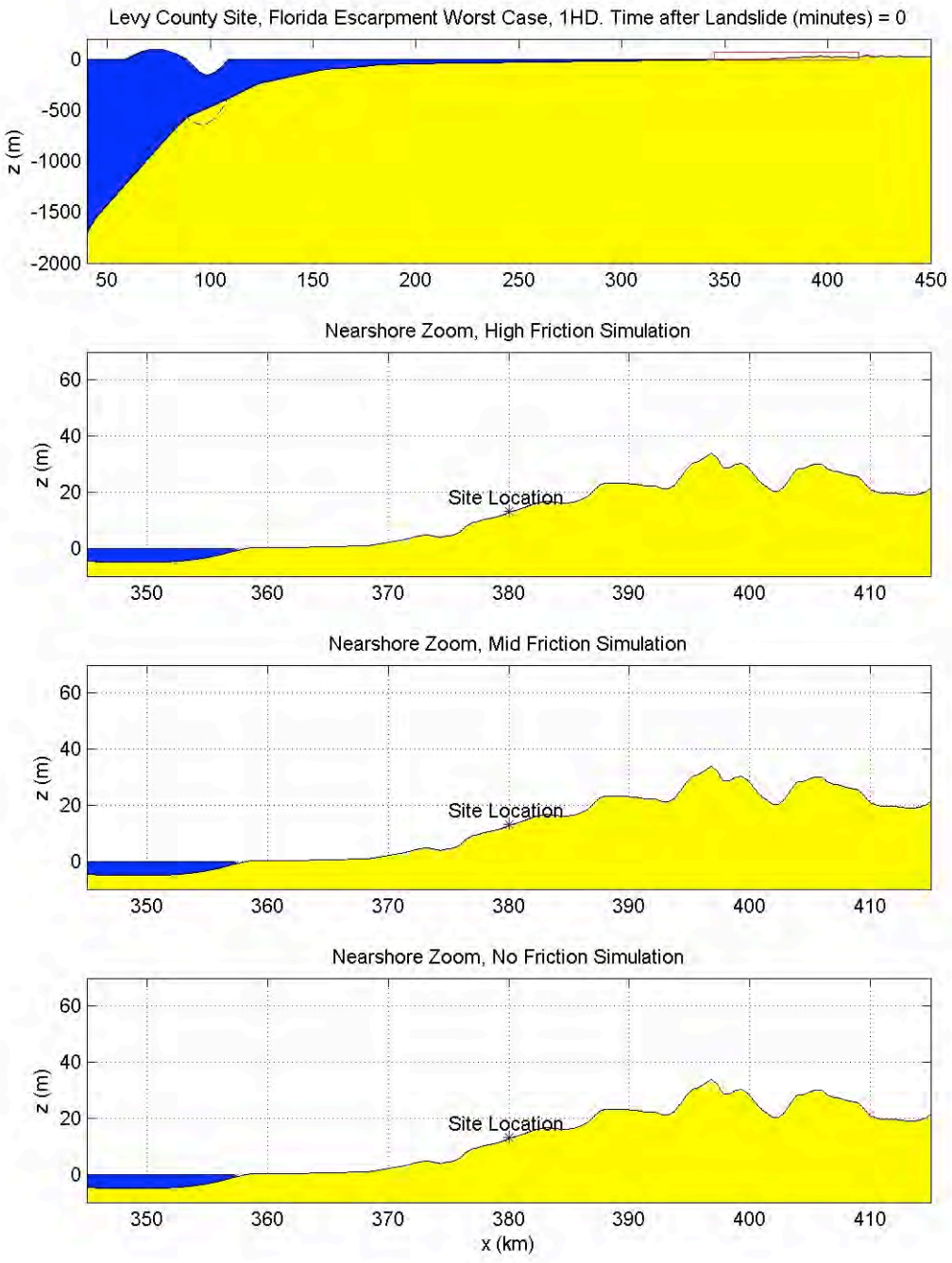

Figure 2.4.6.4.5-34. The offshore evolution of the hot-start tsunami condition for the Florida Slope WORST CASE source. The top plot is the entire simulation transect, and the lower plots are zoom-in's of the nearshore areas, with each subplot showing the results using a different friction factor, as given in the title. Note that the vertical scale changes among the plots. Time shown is t=0 s.

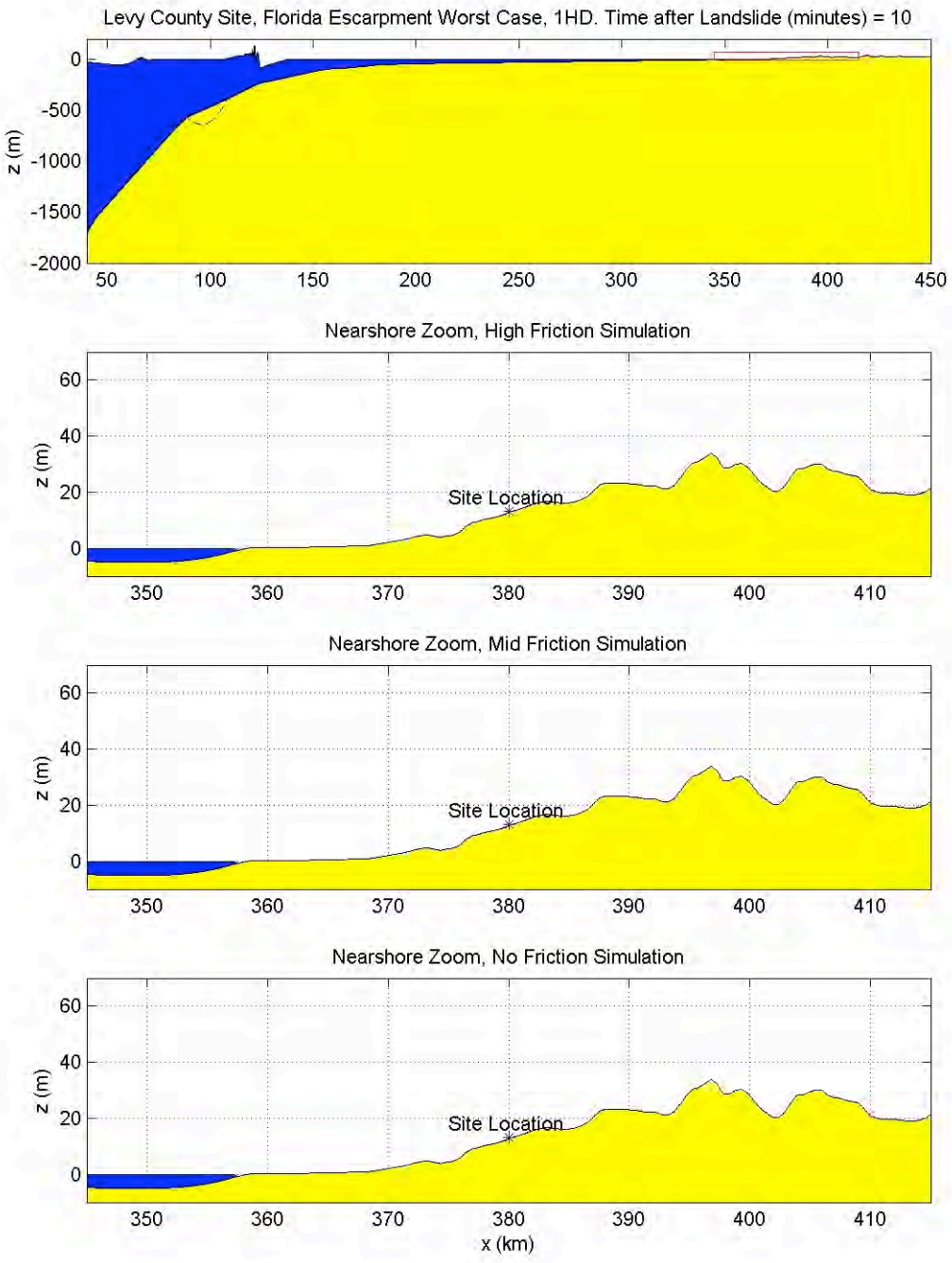

Figure 2.4.6.4.5-35. Same caption as Fig. 2.4.6.4.5-34. Time shown is t=10 min.

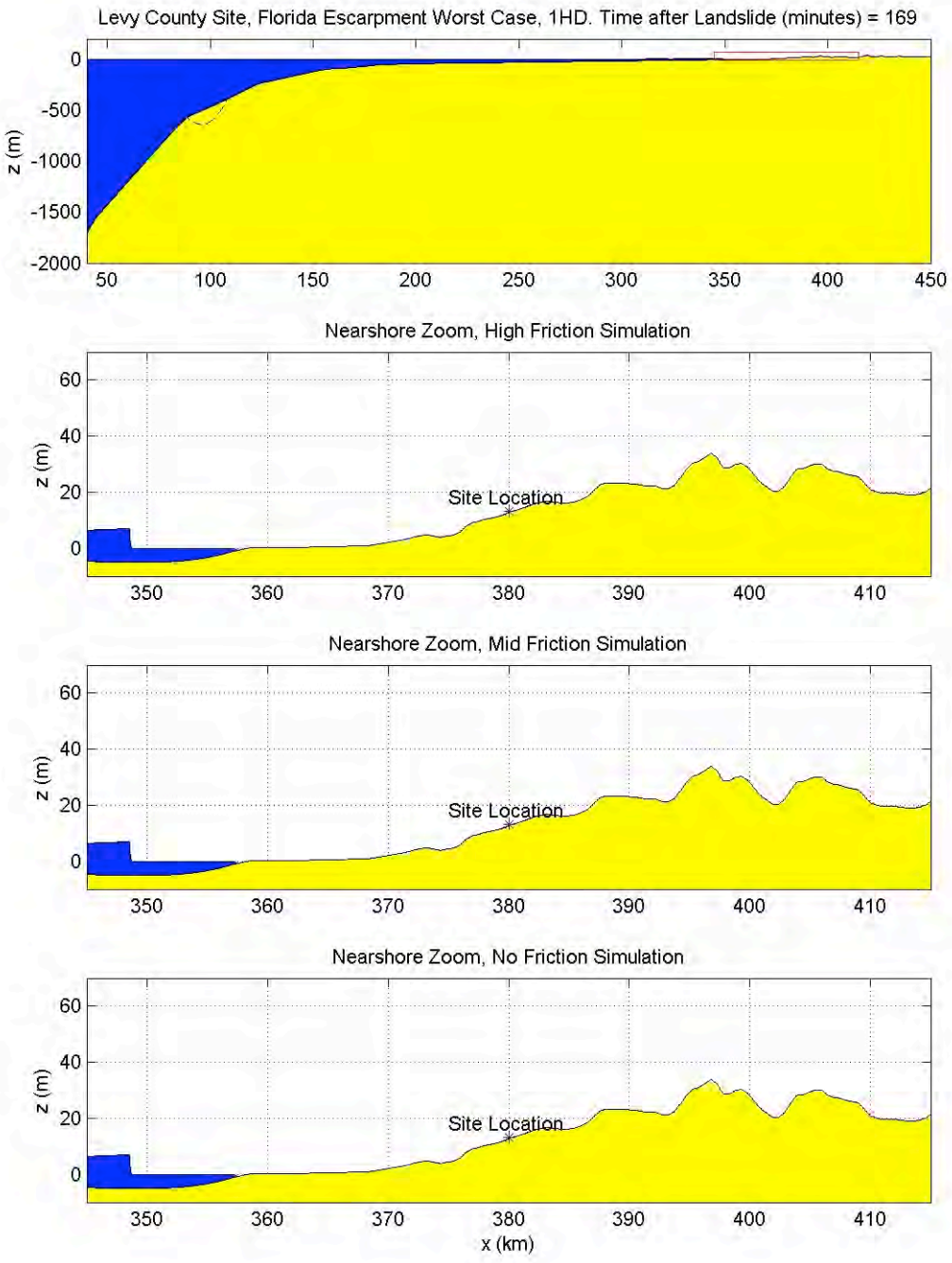

Figure 2.4.6.4.5-36. Same caption as Fig. 2.4.6.4.5-34. Time shown is t=169 min.

As the wave starts inundating dry land, friction becomes important and the results of the three simulations diverge (shown in Figures 2.4.6.4.5-37 through 2.4.6.4.5-39). The no-friction case (A) shows a fast moving bore front that reaches the Levy County site ground elevation, with maximum water surface elevations approaching +15 m at the site. With the modest friction value used in case (B), the tsunami wave front is slowed significantly and does not reach the site. Finally, for case (C), the large, realistic friction retards the flow considerably, and the tsunami wave front is stopped 15 km seaward of the site. A conclusion of this 1HD Florida Slope WORST CASE study is that a tsunami approaching the site, with a bore height up to +9 m at the still water shoreline, will not adversely impact the site if the vegetation roughness is properly accounted for. Despite the 50% larger nearshore wave elevation from the Florida Slope WORST CASE, as compared to the Florida Slope, the impact at the Levy County site is not considerably different, owing to depth-limiting effects.

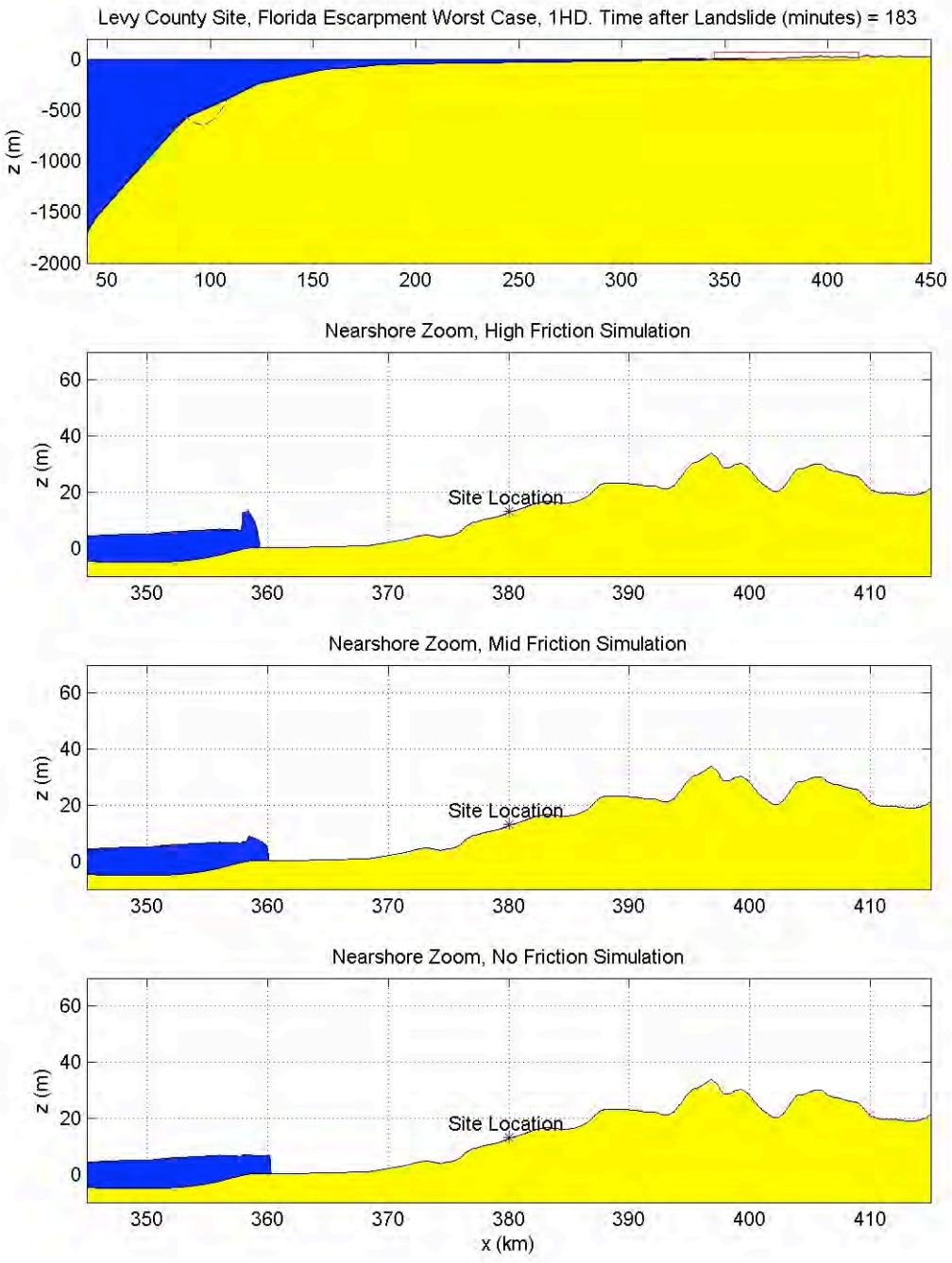

Figure 2.4.6.4.5-37. Same caption as Fig. 2.4.6.4.5-34. Time shown is t=183 min.

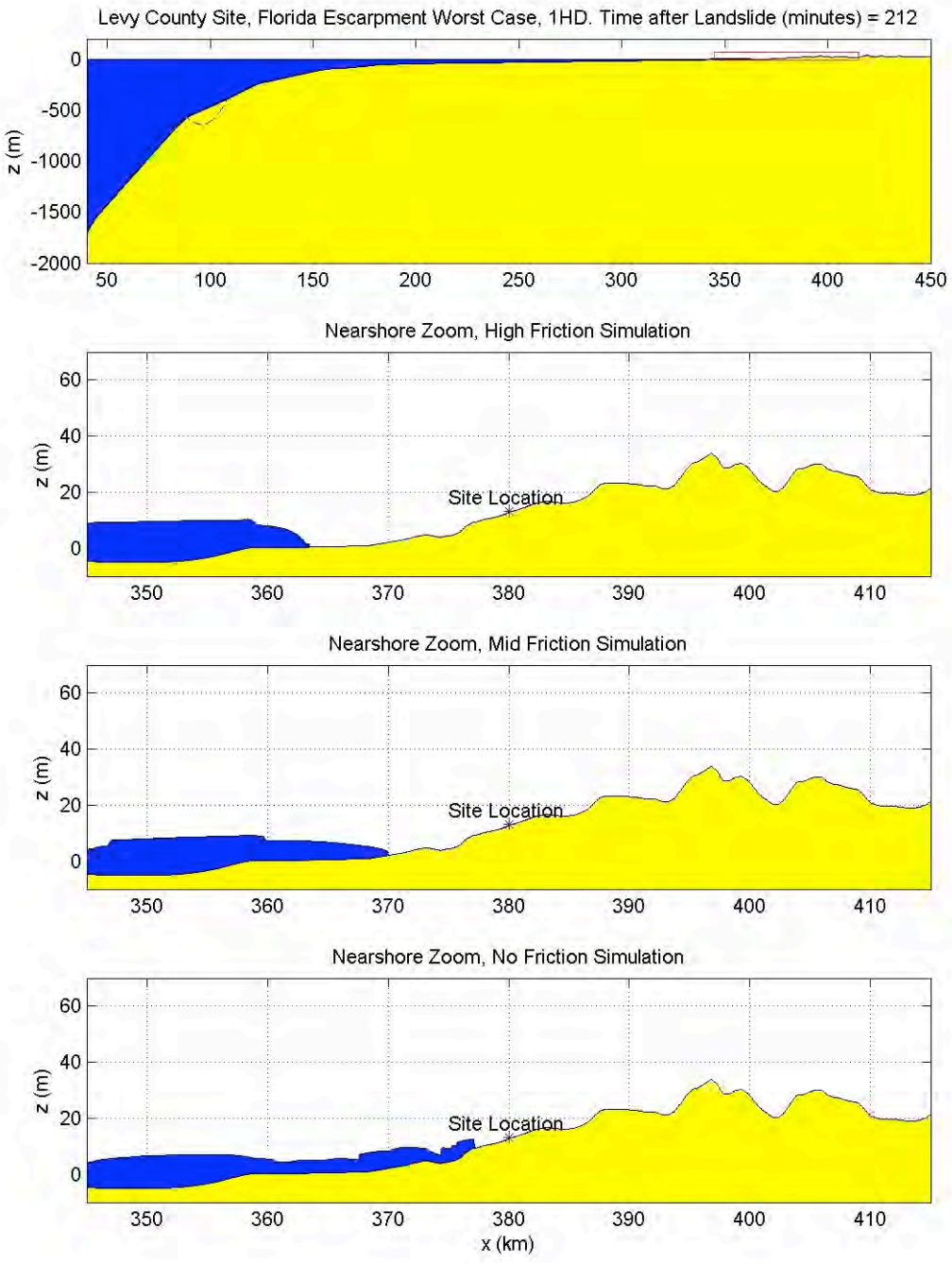

Figure 2.4.6.4.5-38. Same caption as Fig. 2.4.6.4.5-34. Time shown is t=212 min.

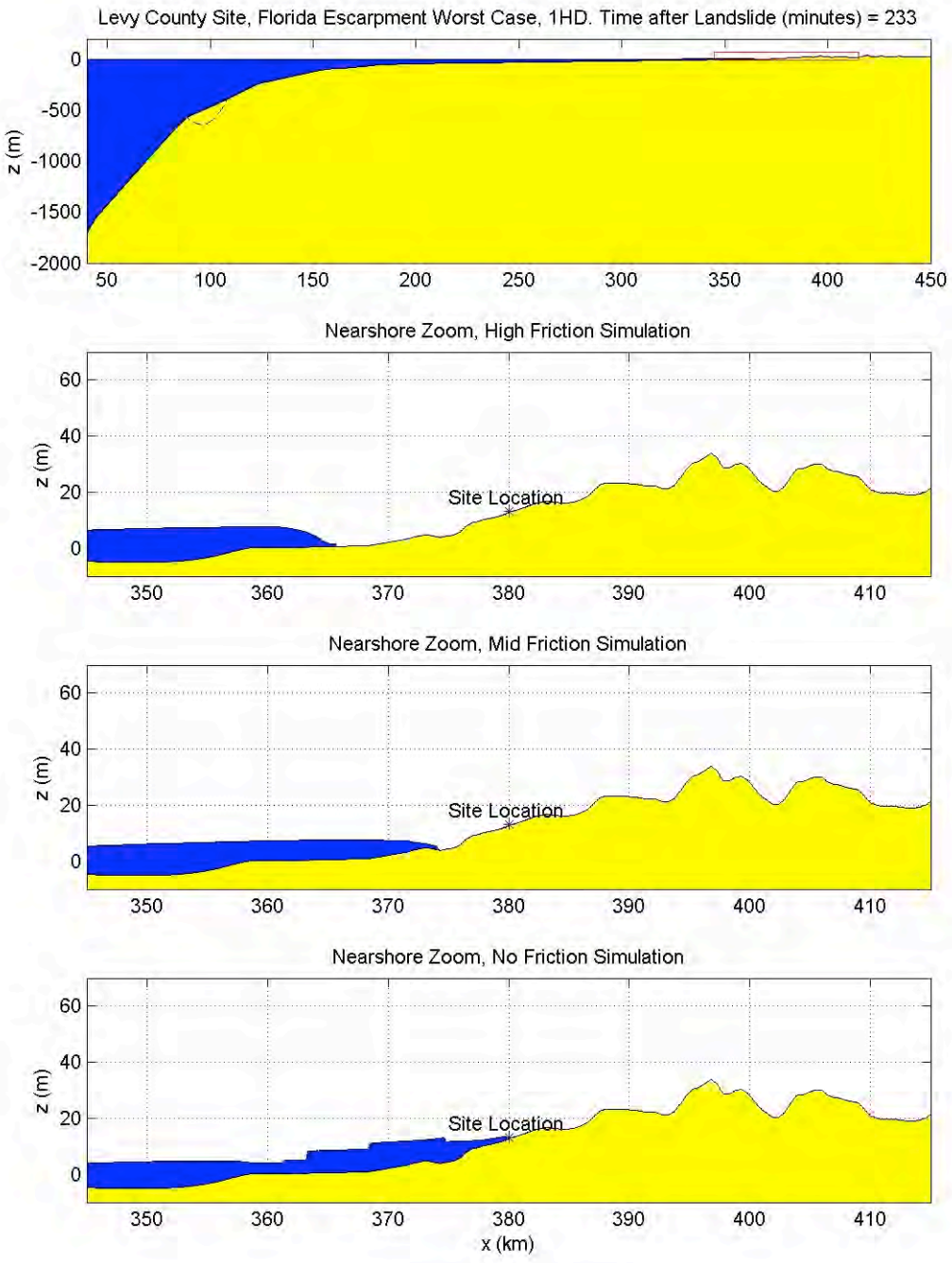

Figure 2.4.6.4.5-39. Same caption as Fig. 2.4.6.4.5-34. Time shown is t=233 min.

•Mississippi Canyon Landslide Source:

As provided in the landslide characterization section, the excavation depth of this slide is approximately 300 m. However, this excavation, in the upper canyon, occurs near the shelf break, where the water depths away from the scarp are ~150 m. This excavation depth will be used to set the initial depression surface. It is not reasonable to use the excavation depth of -300 m as the initial depression amplitude, as this wave cannot exist on the shelf. Thus, the initial depression is set to the water depth at the head of the scarp, 150 m. The horizontal dimensions of the slide source region are assumed to be ~30 km in width and 160 km in length, inferred from the multibeam bathymetric data. With this information, and knowledge of characteristic slide-generated waves taken from the literature (Lynett and Liu, 2002; Lynett and Liu, 2005), the hot-start initial condition is constructed as shown in Figure 2.4.6.4.5-40.

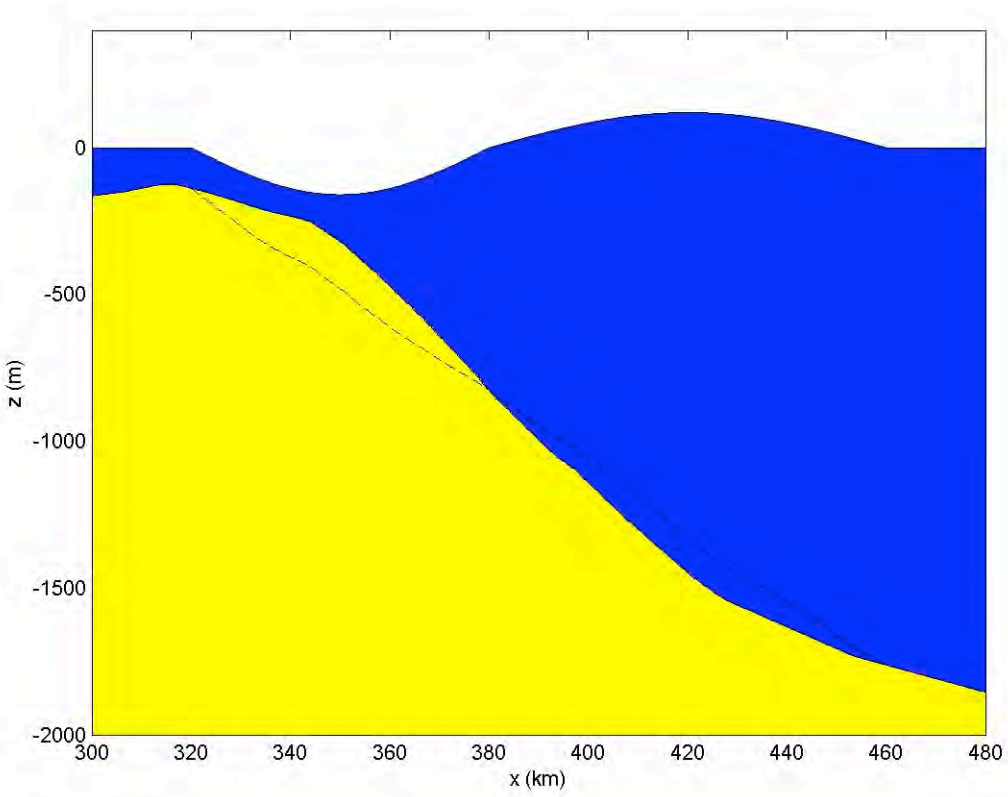

Figure 2.4.6.4.5-40. Centerline profile of the hot-start water surface condition used for the limiting Mississippi Canyon landslide tsunami simulations. Black dashed line shows the seafloor profile after mass failure.

The depth transect is taken from the source location directly to the Levy County site, as shown in Figure 2.4.6.4.5-41. A constant spatial grid size of 200 m is used across the transect for the 1HD cases. Predictions from three 1HD simulations are given for primarily **(A)** no bottom friction, **(B)** bottom friction due to moderate roughness characteristic of grass/turf ($f = 0.01$), and **(C)** bottom friction due to large roughness

characteristic of the trees and dense shrub-like vegetation currently existing seaward of the Levy County site ($f = 0.05$). Note that the three different bottom friction values are only applied over initially dry land; for all simulations, the initially submerged portions of the transect use no bottom friction.

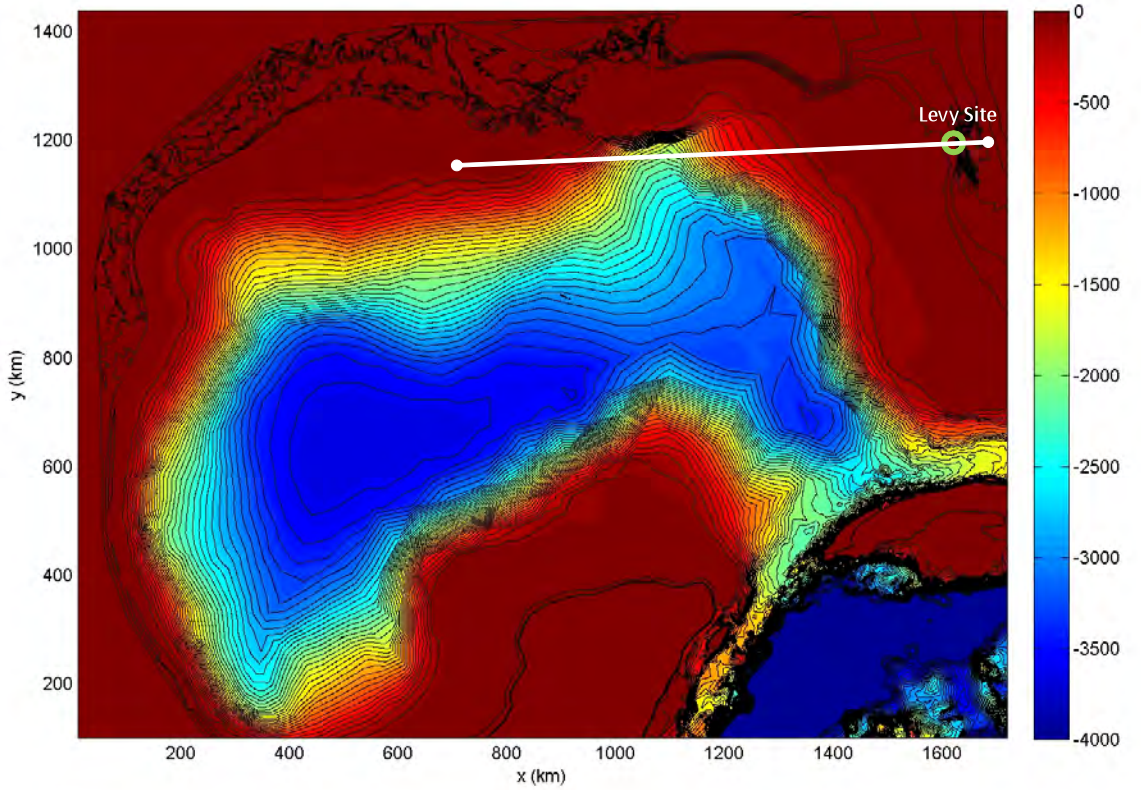

Figure 2.4.6.4.5-41. Bathymetry/topography contour surface in the GOM; the white line shows the transect used for the 1HD simulations. This transect passes through the Mississippi Canyon source location as well as the Levy County site.

A series of figures showing the evolution of this wave are provided in Figures 2.4.6.4.5-42 through 2.4.6.4.5-48. In the top subplot of all these figures, the entire transect is given, scaled vertically to show the limits of depth; due to this scaling the free surface wave appears small. The offshore evolution of the Mississippi Canyon wave can be seen in this top plot in Figures 2.4.6.4.5-42 and 2.4.6.4.5-43. The large, non-linear wave immediately steepens and forms a bore-front once on the shallow shelf. The wave in the nearshore zone is shown in the three lower subplots, which show a zoom-in of the transect near the site. For perspective, the red box in the top figure outlines the area shown in the lower three plots in these figures. All of the simulations provide identical results for the tsunami prior to reaching the shoreline, as all the simulations start with the same wave, use the same bathymetry, and are frictionless offshore. This is most evident in Figure 2.4.6.4.5-44, which shows the tsunami approaching the site.

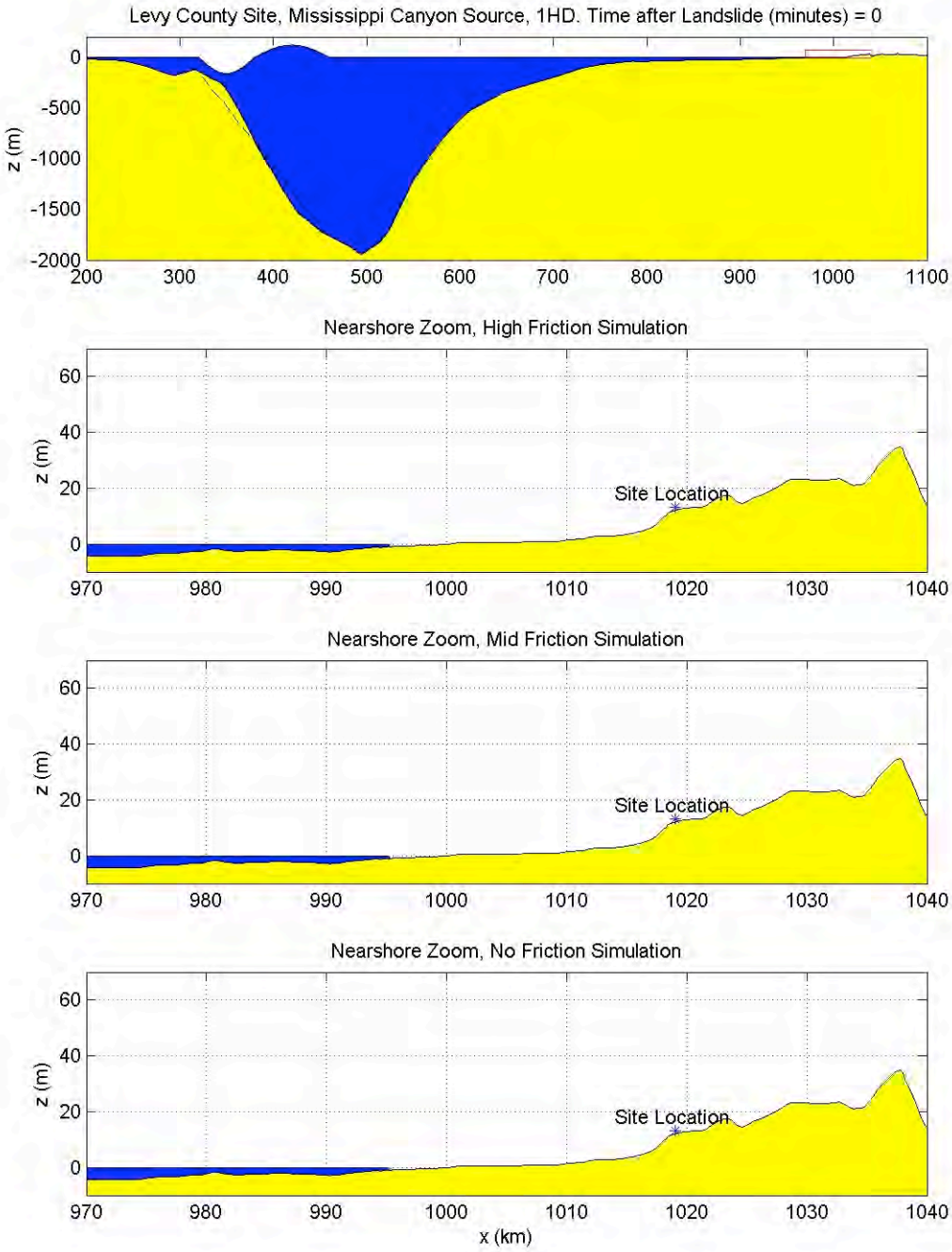

Figure 2.4.6.4.5-42. The offshore evolution of the hot-start tsunami condition for the Mississippi Canyon source. The top plot is the entire simulation transect, and the lower plots are zoom-in's of the nearshore areas, with each subplot showing the results using a different friction factor, as given in the title. Note that the vertical scale changes among the plots. Time shown is t=0 s.

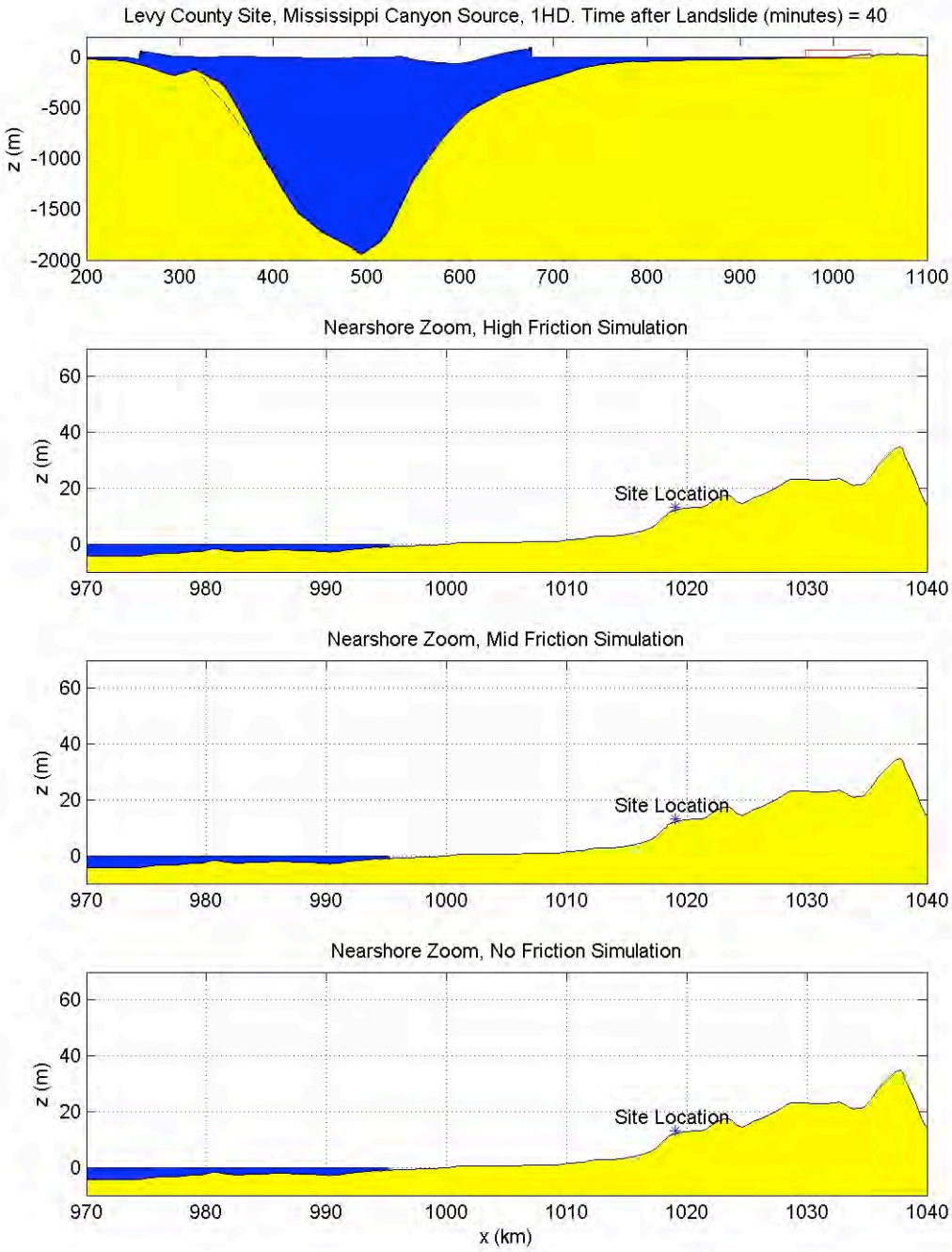

Figure 2.4.6.4.5-43. Same caption as Fig. 2.4.6.4.5-42. Time shown is t=36 min.

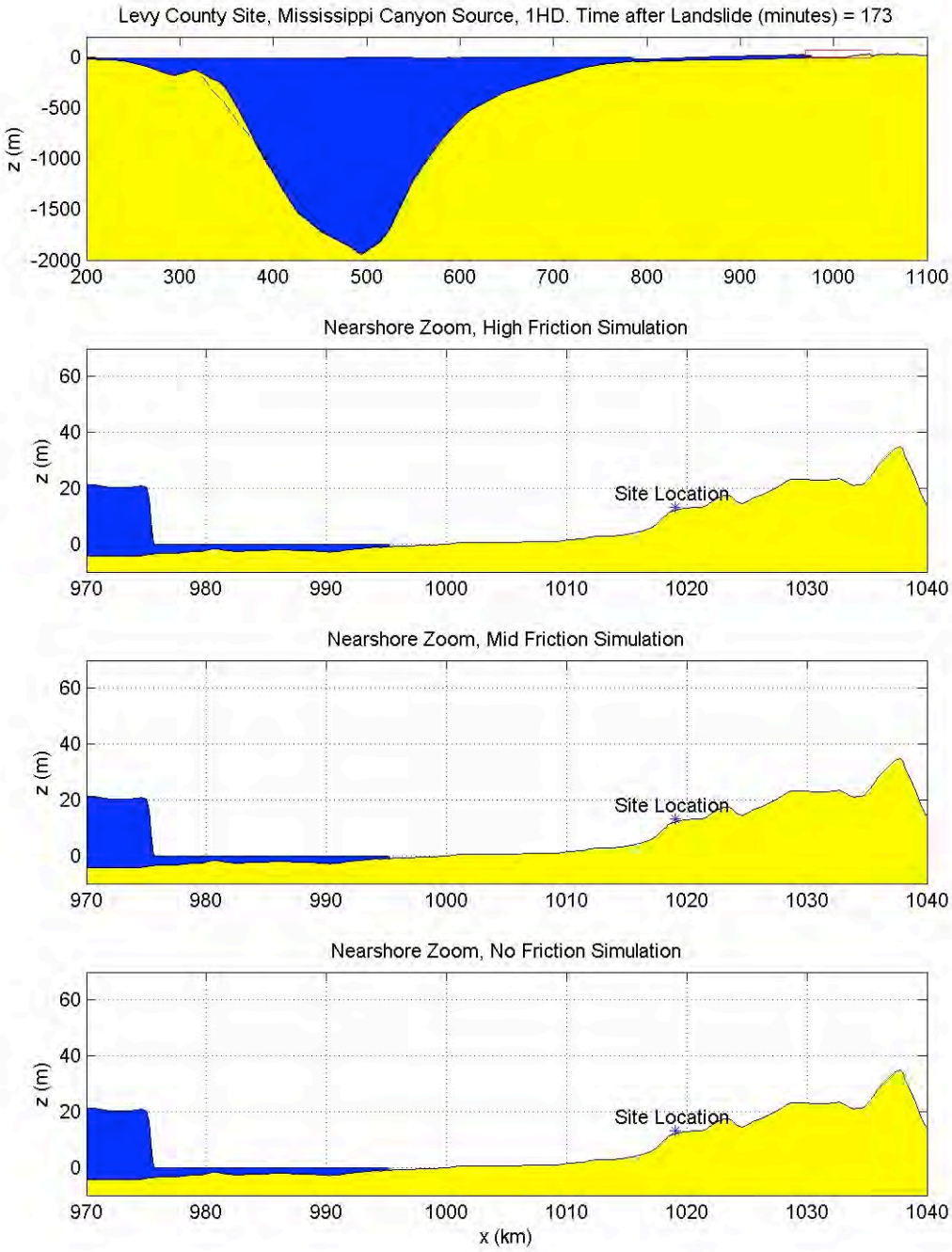

Figure 2.4.6.4.5-44. Same caption as Fig. 2.4.6.4.5-42. Time shown is t=173 min.

As the wave starts inundating dry land, friction becomes important and the results of the three simulations diverge (shown in Figures 2.4.6.4.6-45 through 2.4.6.4.6-48). The no-friction case (A) shows a fast moving bore front that easily reaches the Levy County site ground elevation, with maximum water surface elevations approaching +40 m at the site. Even with the modest friction value used in case (B), the tsunami wave front is not slowed significantly and easily reaches the site with water elevations of +33 m. Finally, for case (C), the large, realistic friction retards the flow considerably, but still, the tsunami reaches the site, although the site is near the inundation limit. A conclusion of this 1HD Mississippi Canyon study is that a tsunami approaching the site, with a bore height up to +20 m at the still water shoreline, may impact the site. A more detailed, 2HD analysis of this site is clearly needed.

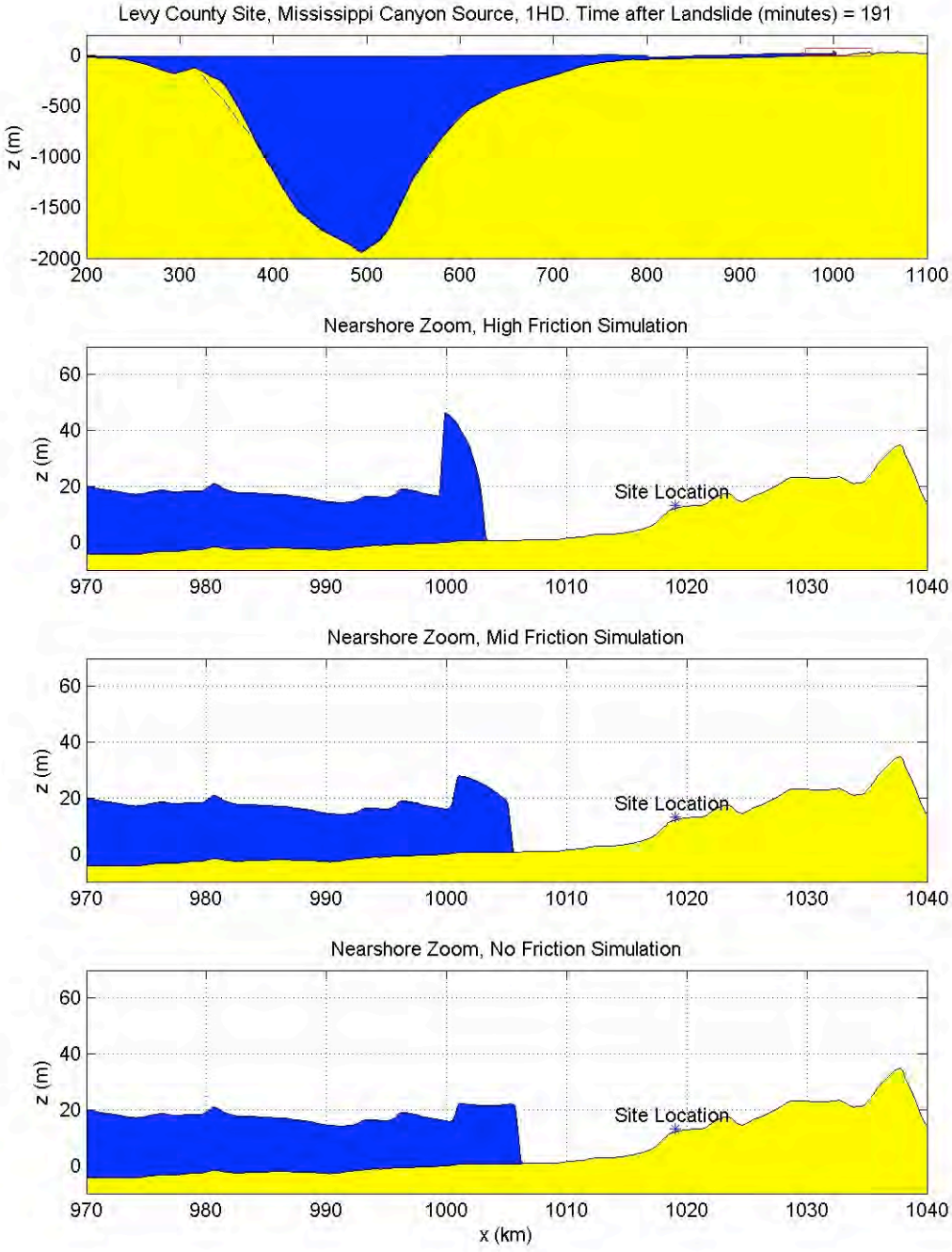

Figure 2.4.6.4.5-45. Same caption as Fig. 2.4.6.4.5-42. Time shown is t=191 min.

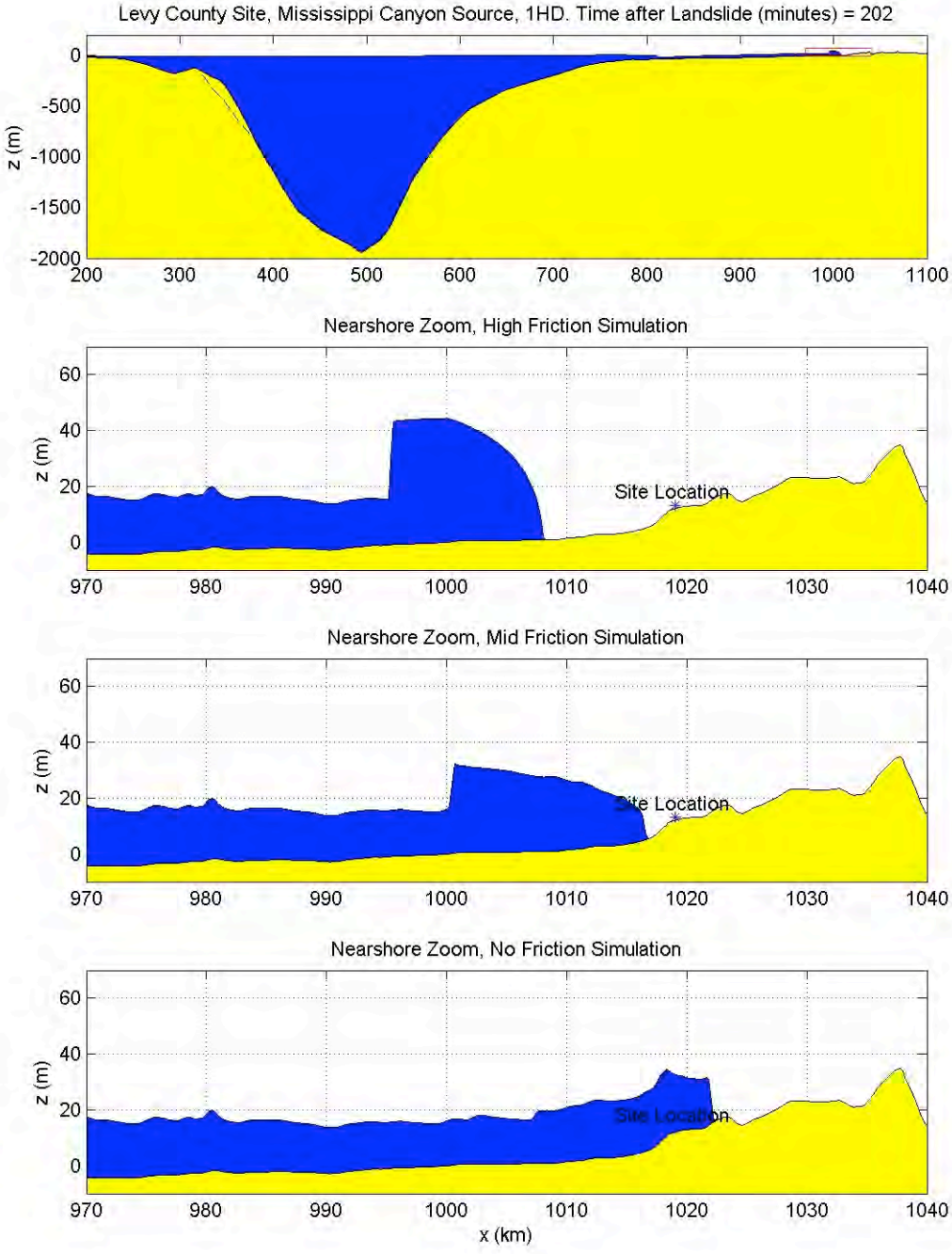

Figure 2.4.6.4.5-46. Same caption as Fig. 2.4.6.4.5-42. Time shown is t=202 min.

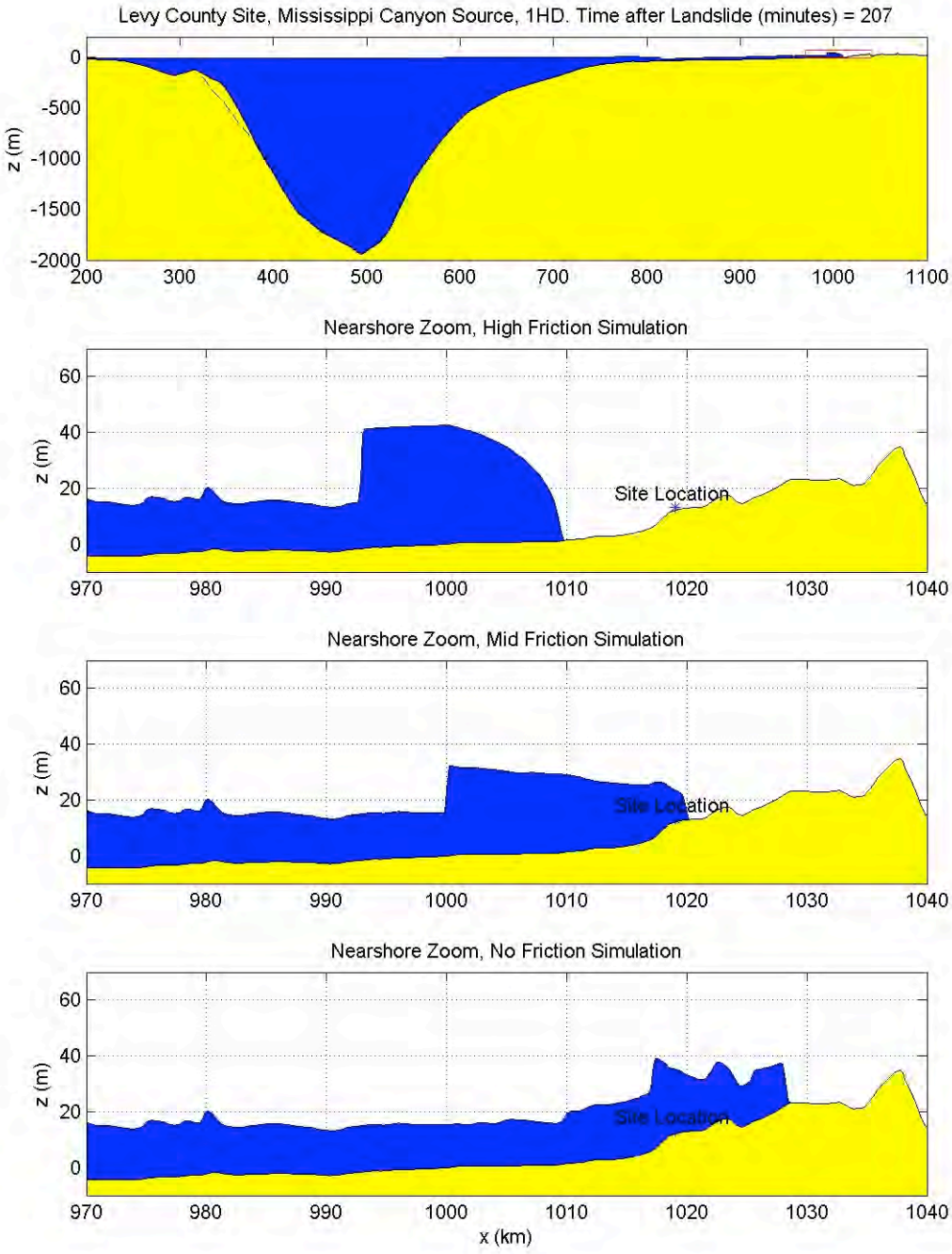

Figure 2.4.6.4.5-47. Same caption as Fig. 2.4.6.4.5-42. Time shown is t=207 min.

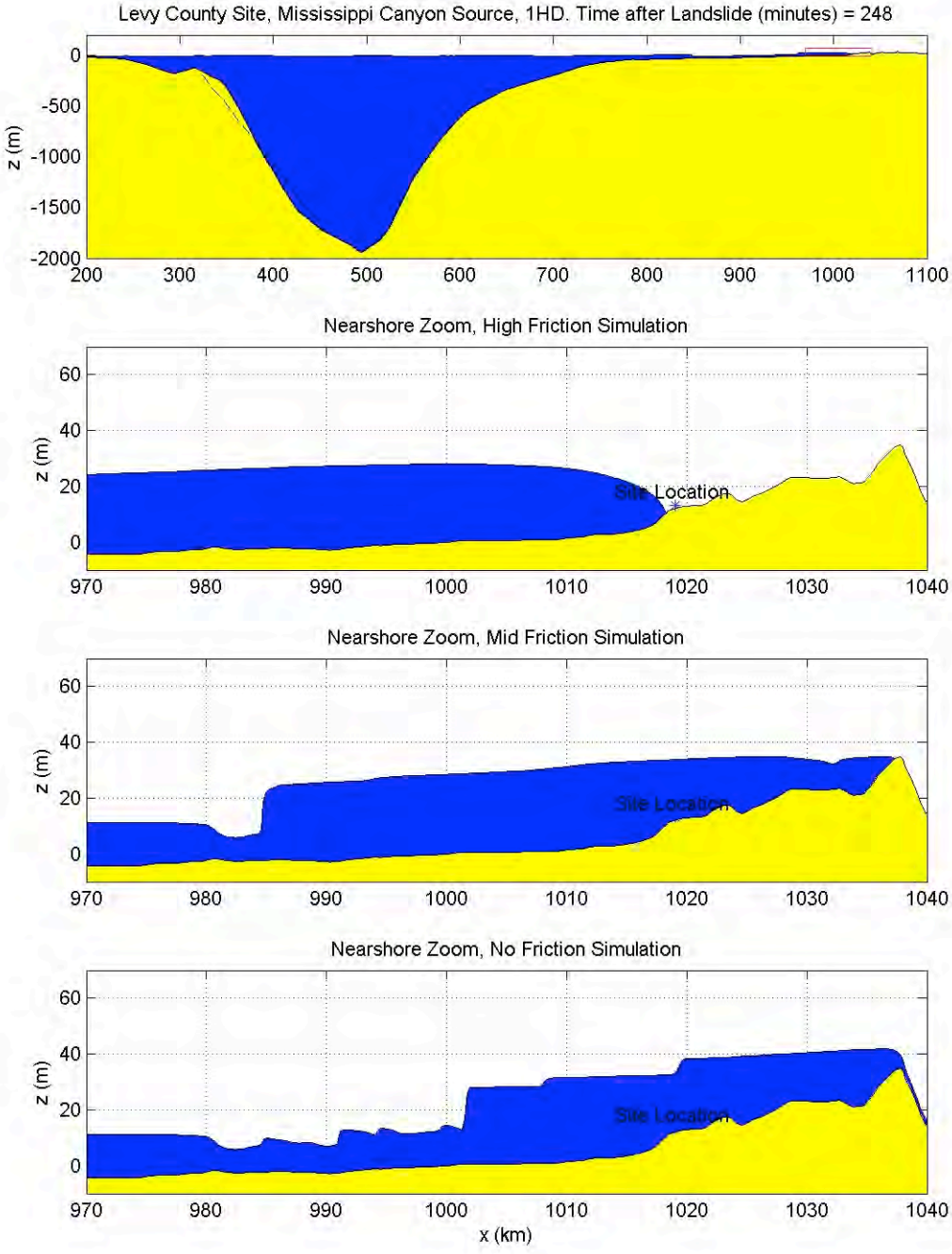

Figure 2.4.6.4.5-48. Same caption as Fig. 2.4.6.4.5-42. Time shown is t=248 min.

Two-Horizontal Dimension Simulations

From the 1HD simulations, it is possible to reduce the number of tsunami sources that need additional analysis. The Mississippi Canyon source clearly gives the largest wave near the site and must be further considered. Mississippi Canyon gives the largest heights at the shoreline, twice as large as the nearest source, and is also the closest non-Florida slope source to the site, so radial spreading effects should also be relatively minor for Mississippi Canyon. Thus, it can be reasonably expected that, if detailed 2HD simulations show that the Mississippi Canyon source has no impact at the site, then all other non-Florida slope sources (East Breaks, Campeche) can also be eliminated.

While it is also likely that elimination of the Mississippi Canyon source as impacting the Levy County site would eliminate the Florida Slope WORST CASE source, this should not be assumed. As the Florida Slope WORST CASE is on the immediate shelf, radial spreading effects may not act to decrease the incoming wave height significantly. 2HD wave heights may be quite similar to those predicted by the 1HD simulation, which showed the tsunami reaching the site for the no-friction case. Therefore, two sources, Mississippi Canyon and Florida Slope WORST CASE, will be further investigated here.

•Florida Slope WORST CASE Landslide Source:

The slide and initial water surface condition properties for this source are described above in the corresponding 1HD section, but are given again here for completeness. As provided in the landslide characterization section, the excavation depth of this slide is approximately 150 m. This length provides the trough elevation (i.e., -150 m) of the hot-start initial water surface condition. The horizontal dimensions of the slide source region are assumed to be ~20 km in width and 50 km in length, inferred from the various scarps visible in the multibeam bathymetric data. With this information, and knowledge of characteristic slide-generated waves taken from the literature (Lynett and Liu, 2002; Lynett and Liu, 2005), the hot-start initial condition is constructed as shown in Figure 2.4.6.4.5-49. A constant spatial grid size of 500 m is used in the numerical simulation.

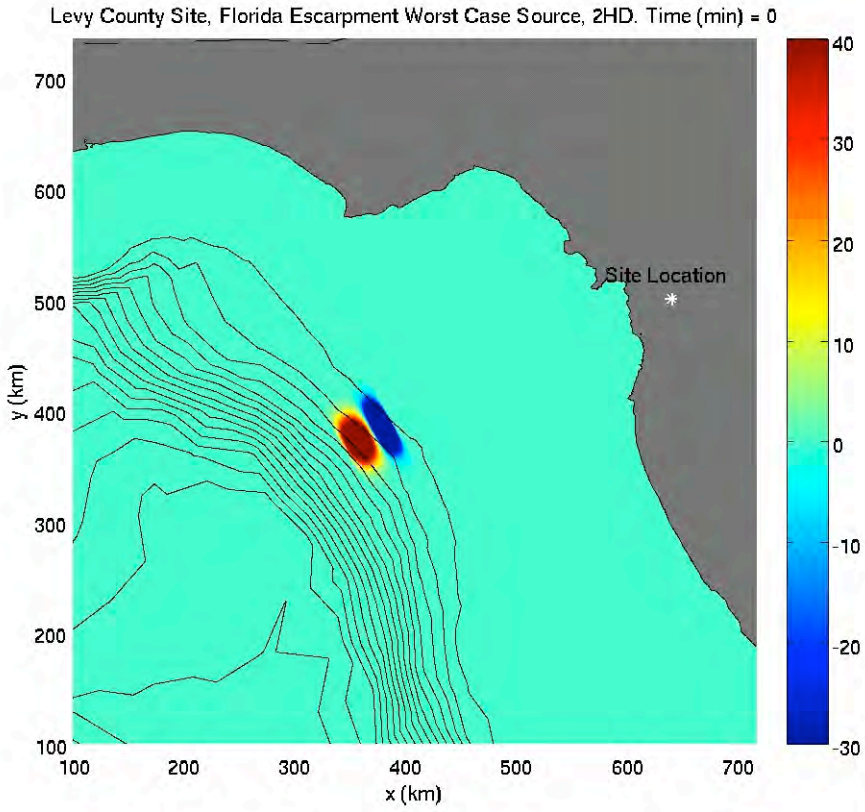

Figure 2.4.6.4.5-49. The offshore evolution of the 2HD hot-start tsunami condition for the Florida Slope WORST CASE source. The elevation of the ocean surface is given by the colors, with the scaling given by the color bar on the right. The contour lines indicate bathymetry (depths). Time shown is t=0 s.

The 2HD evolution of the slide is shown in Figures 2.4.6.4.5-50 through 2.4.6.4.5-54. Within 15 minutes of the landslide, given in Figures 2.4.6.4.5-50 and 2.4.6.4.5-51, it is clear that radial spreading effects are important offshore of the shelf. However, on the shelf, where the wave is approaching the Levy County site, spreading is minor, and the wave energy remains in a laterally compact front. The positive elevation component of the landward traveling wave forms into a bore about 30 minutes after the slide (Figure 2.4.6.4.5-52), and quickly overtakes the leading depression. The bore front height continues to diminish (Figure 2.4.6.4.5-53), and by the time the front reaches a depth of about 30 m (Figure 2.4.6.4.5-54), its elevation is approximately 7 m. Note that for the 1HD simulation without radial spreading, the wave height at this depth was 10 m. Results from this simulation will be analyzed further and compared with the 2HD Mississippi Canyon results in a later section.

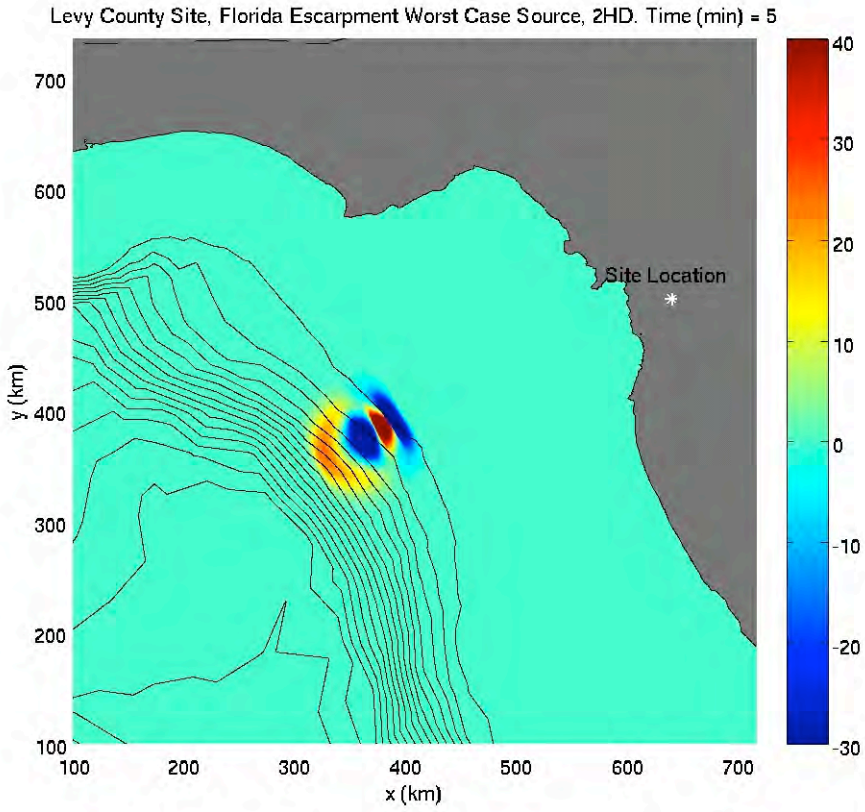

Figure 2.4.6.4.5-50. Same caption as Fig. 2.4.6.4.5-49. Time shown is t=5 min.

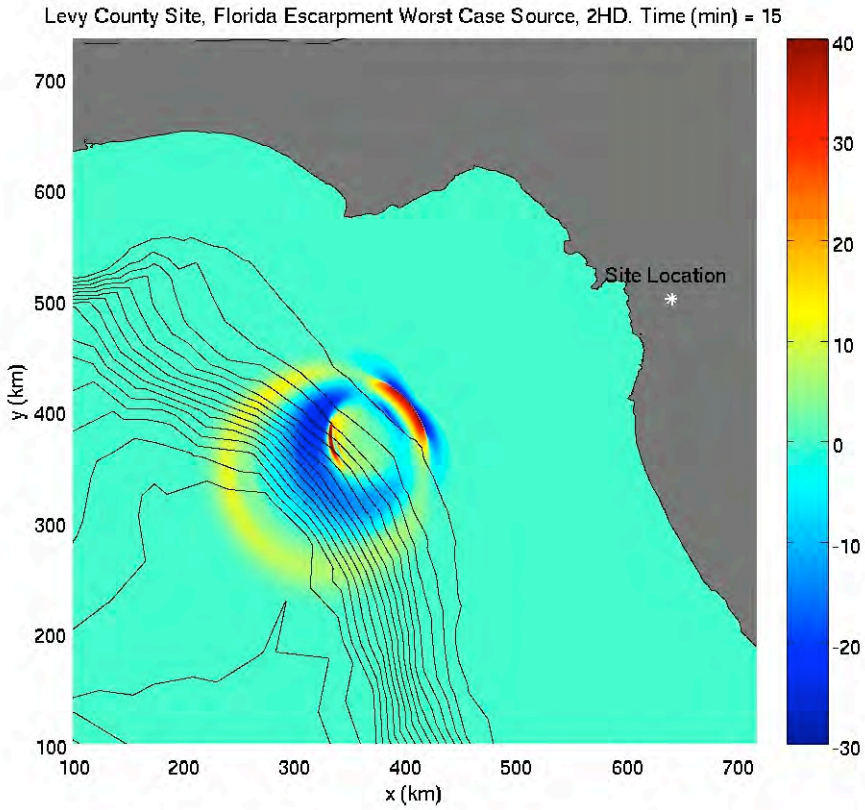

Figure 2.4.6.4.5-51. Same caption as Fig. 2.4.6.4.5-49. Time shown is t=15 min.

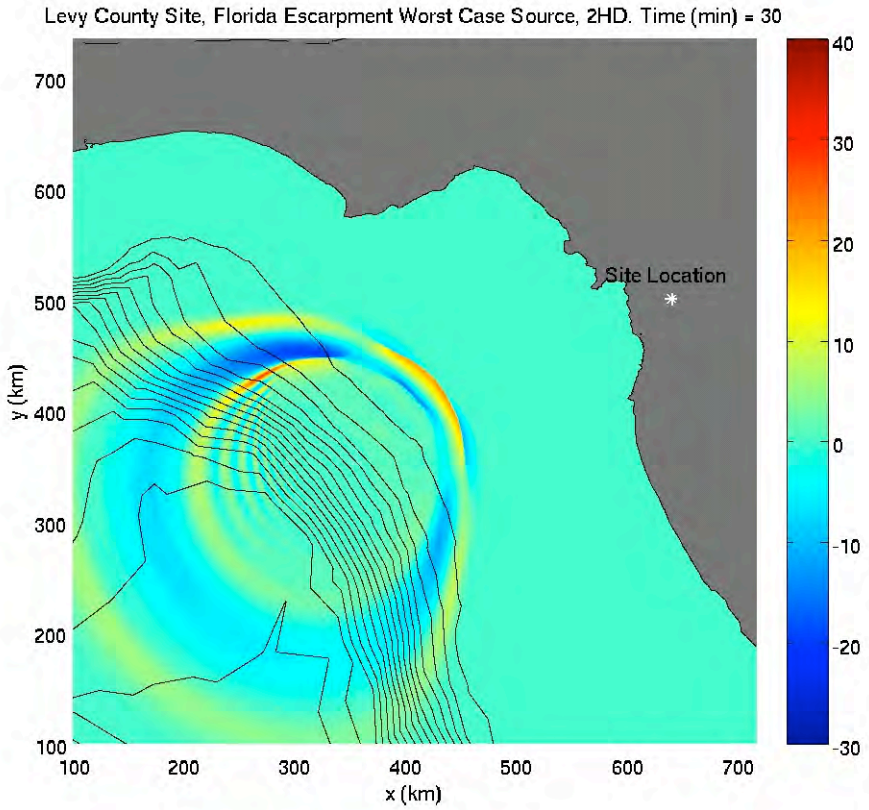

Figure 2.4.6.4.5-52. Same caption as Fig. 2.4.6.4.5-49. Time shown is t=30 min.

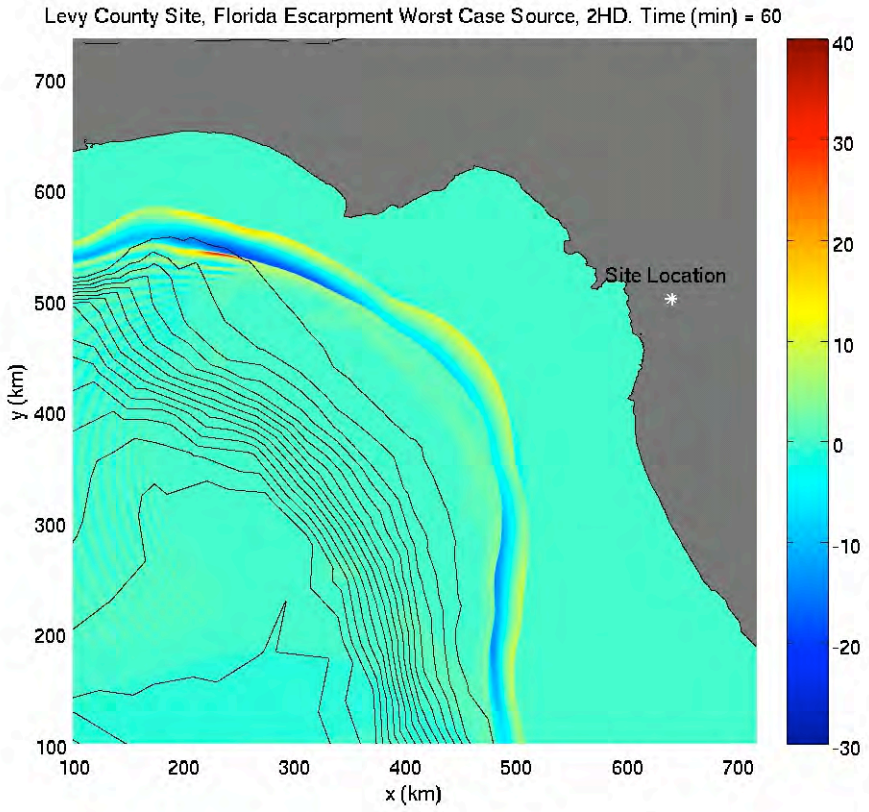

Figure 2.4.6.4.5-53. Same caption as Fig. 2.4.6.4.5-49. Time shown is t=60 min.

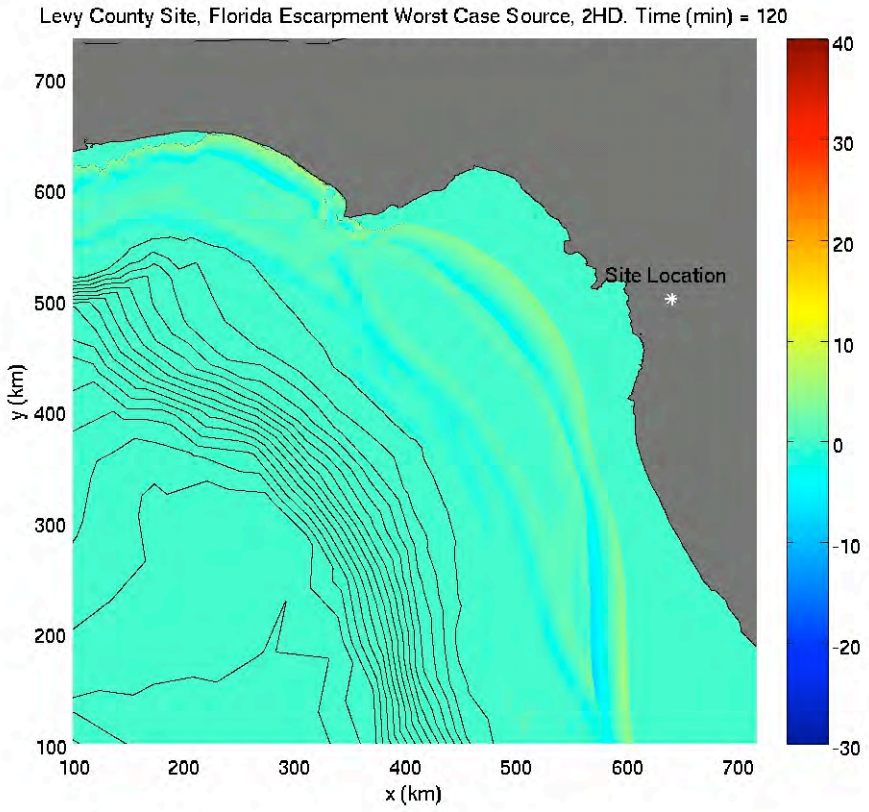

Figure 2.4.6.4.5-54. Same caption as Fig. 2.4.6.4.5-49. Time shown is t=120 min.

•Mississippi Canyon Landslide Source:

The slide and initial water surface condition properties for this source are described above in the corresponding 1HD section, but are given again here for completeness. The initial depression is set to the water depth at the head of the scarp, 150 m. The horizontal dimensions of the slide source region are assumed to be ~30 km in width and 160 km in length, inferred from the multibeam bathymetric data. With this information, and knowledge of characteristic slide-generated waves taken from the literature (Lynett and Liu, 2002; Lynett and Liu, 2005), the hot-start initial condition is constructed as shown in Figure 2.4.6.4.5-55. A constant spatial grid size of 500 m is used in the numerical simulation.

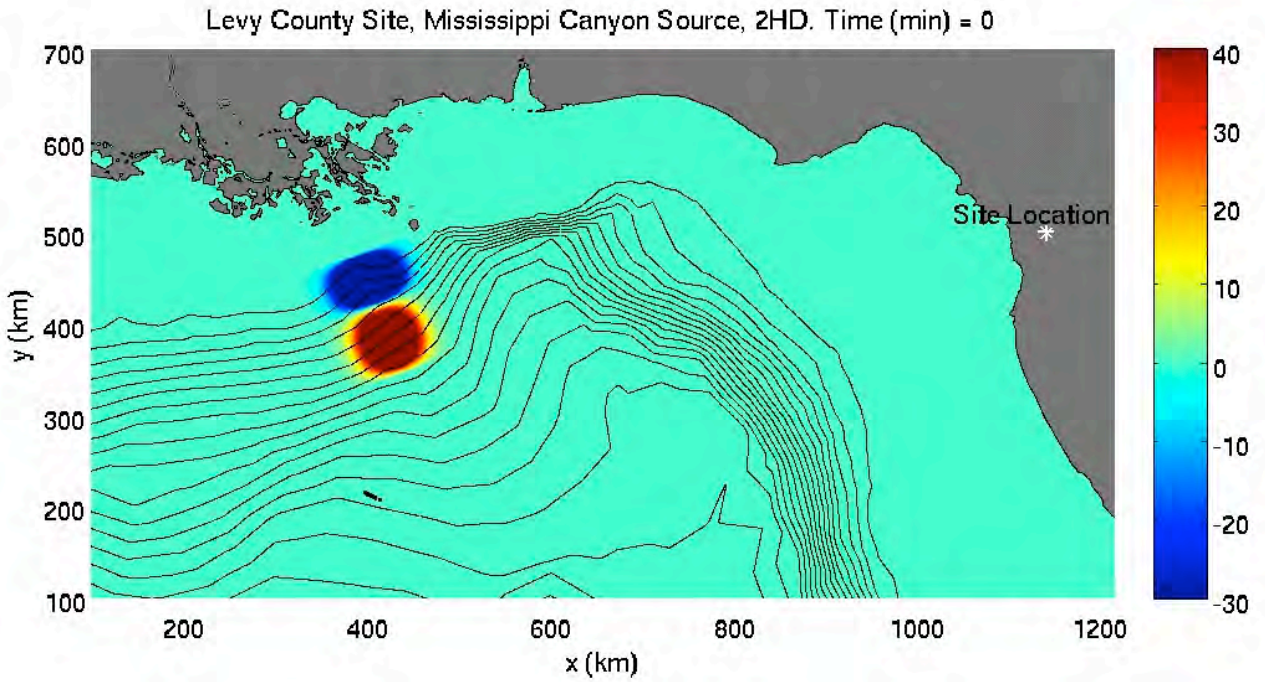

Figure 2.4.6.4.5-55. The offshore evolution of the 2HD hot-start tsunami condition for the Mississippi Canyon source. The elevation of the ocean surface is given by the colors, with the scaling given by the color bar on the right. The contour lines indicate bathymetry (depths). Time shown is t=0 s.

The 2HD evolution of the slide is shown in Figures 2.4.6.4.5-56 through 2.4.6.4.5-61. Within 20 minutes of the landslide, given in Figures 2.4.6.4.5-56 through 2.4.6.4.5-58, it is clear that radial spreading effects are important for the wave approaching the site. By the time the wave has reached the shelf break (Figure 2.4.6.4.5-59), the leading elevation wave height is ~15 m, a significant reduction from the hot start elevation of 120 m. The elevation component of the landward traveling wave forms into a bore once on the shelf (Figure 2.4.6.4.5-60). The bore front height continues to diminish, and by the time the front reaches a depth of about 30 m (Figure 2.4.6.4.5-61), its elevation is approximately 7 m. Note that for the 1HD simulation, the wave height at this depth was 25 m.

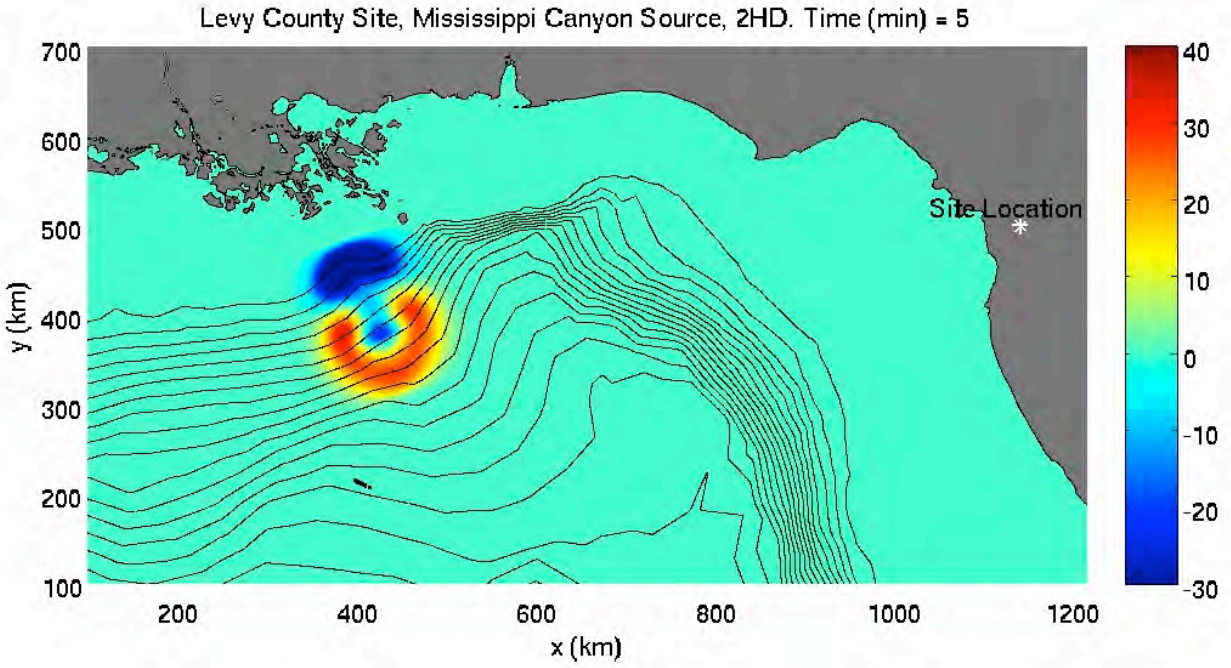

Figure 2.4.6.4.5-56. Same caption as Fig. 2.4.6.4.5-55. Time shown is t=5 min.

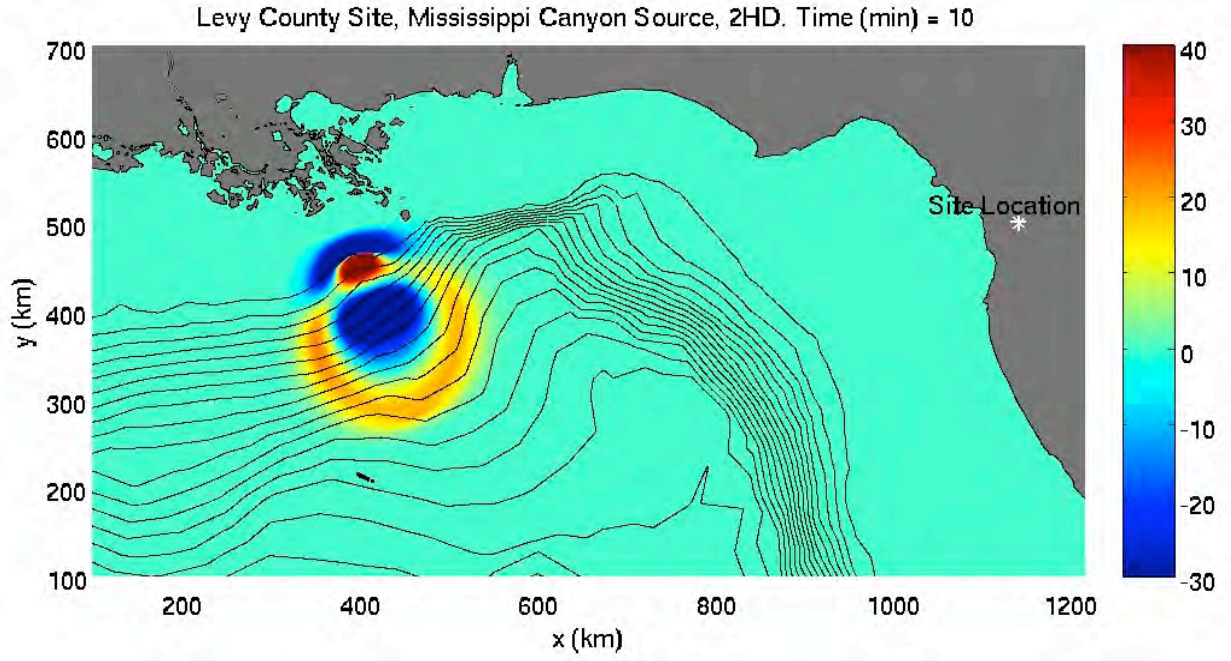

Figure 2.4.6.4.5-57. Same caption as Fig. 2.4.6.4.5-55. Time shown is t=10 min.

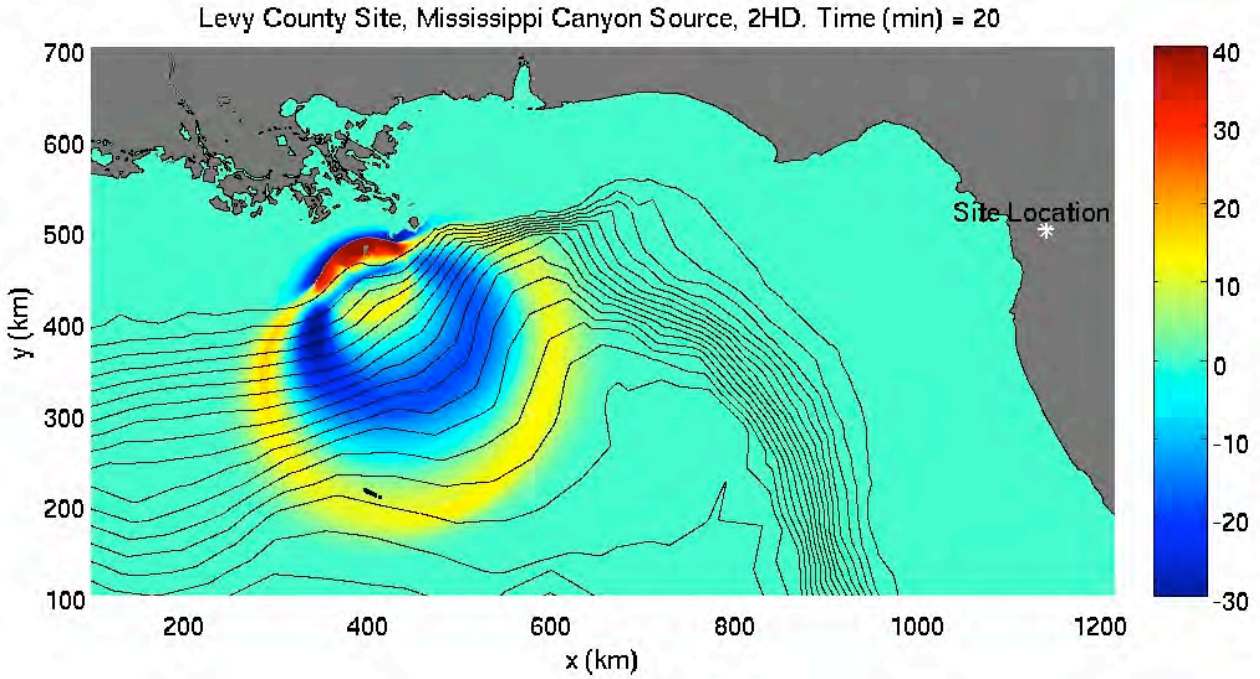

Figure 2.4.6.4.5-58. Same caption as Fig. 2.4.6.4.5-55. Time shown is t=20 min.

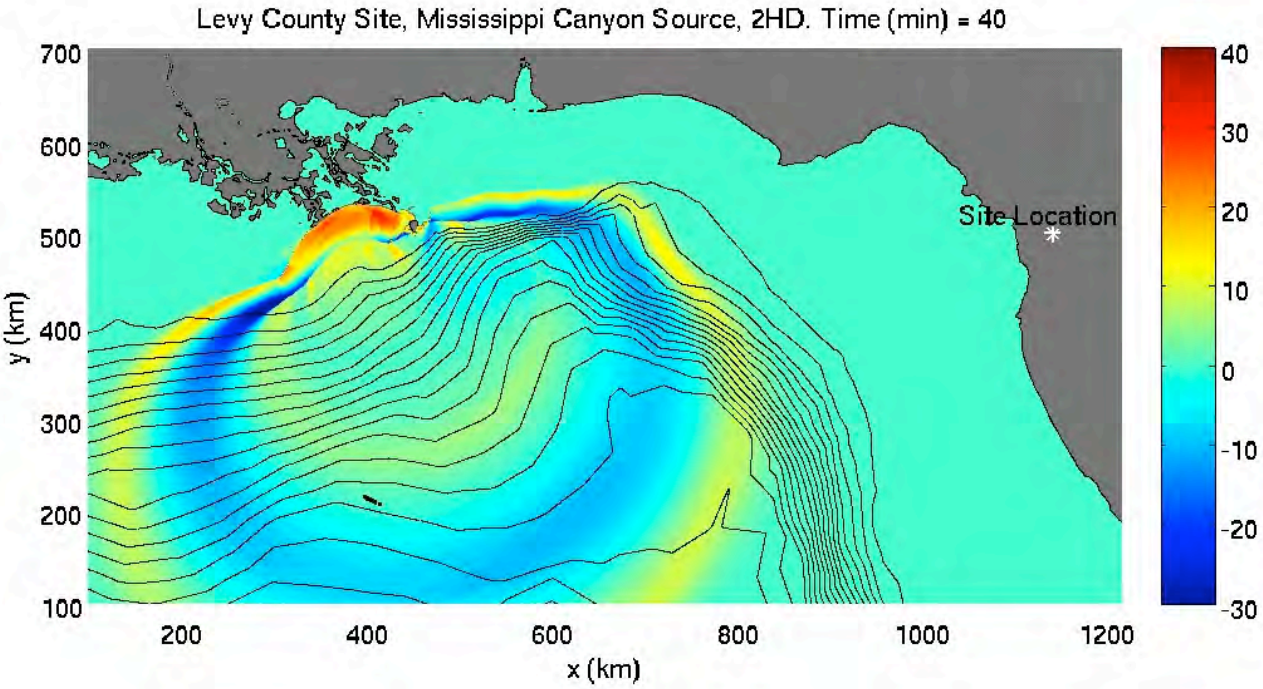

Figure 2.4.6.4.5-59. Same caption as Fig. 2.4.6.4.5-55. Time shown is t=40 min.

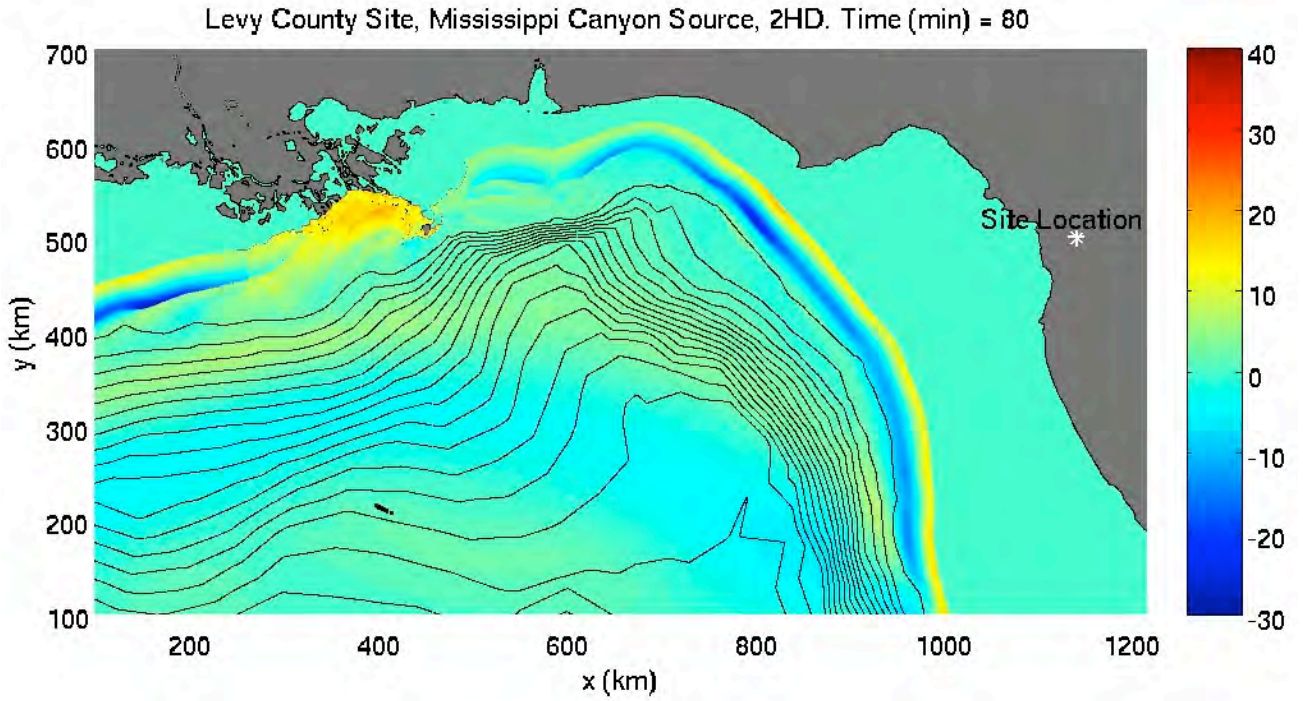

Figure 2.4.6.4.5-60. Same caption as Fig. 2.4.6.4.5-55. Time shown is t=80 min.

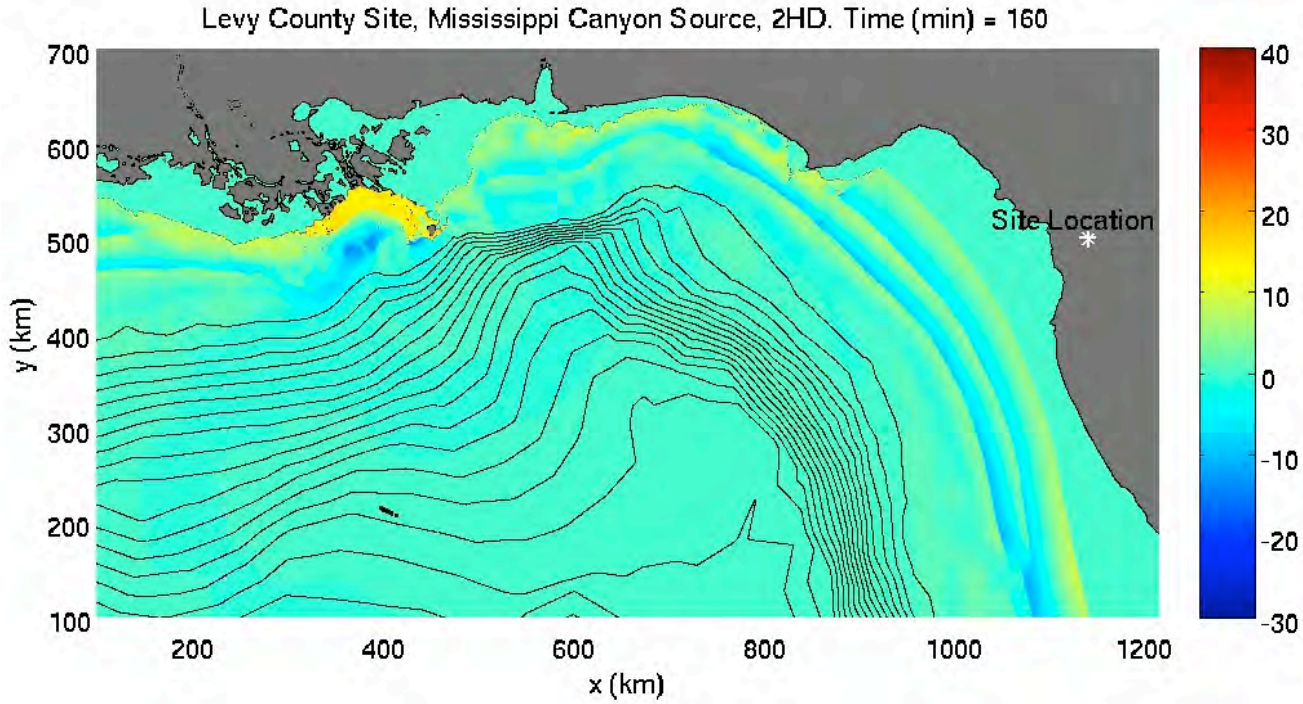

Figure 2.4.6.4.5-61. Same caption as Fig. 2.4.6.4.5-55. Time shown is t=160 min.

•Local Evolution of the Tsunami in the Nearshore Areas of the Site:

Finally, propagation over the shallow, nearshore bathymetry at the site is examined. The purpose of these simulations is to provide very refined 2HD inundation using the best available bathymetry and topography near the site. This subdomain is nested inside the large-scale 2HD domains discussed above for the Florida Slope WORST CASE and Mississippi Canyon sources. The offshore boundary, situated at a depth of 30 m, is forced with results from the large-scale 2HD simulations. Time series of sea surface elevation from these two simulations, at a depth of 30 m, are shown in Figure 2.4.6.4.5-62. Interestingly, the peak elevations of the wave trains are nearly identical, with the peak Mississippi Canyon crest elevation of 7.2 m, and the peak Florida Slope WORST CASE crest elevation of 6.9 m. The periods of the wave components in these two wave trains are slightly different, with the period from the Mississippi Canyon source at 45 minutes and that from the Florida Slope WORST CASE at 30 minutes. The most significant difference between the two trains is the number of large waves in the train. The Mississippi Canyon wave train has four distinct waves with crest elevation greater than 2 m, while the Florida Slope WORST CASE train has just one. With these comparisons in mind, is it evident that the Mississippi Canyon source produces the PMT for this site, and will be the only source used to simulate the refined, nearshore tsunami impact.

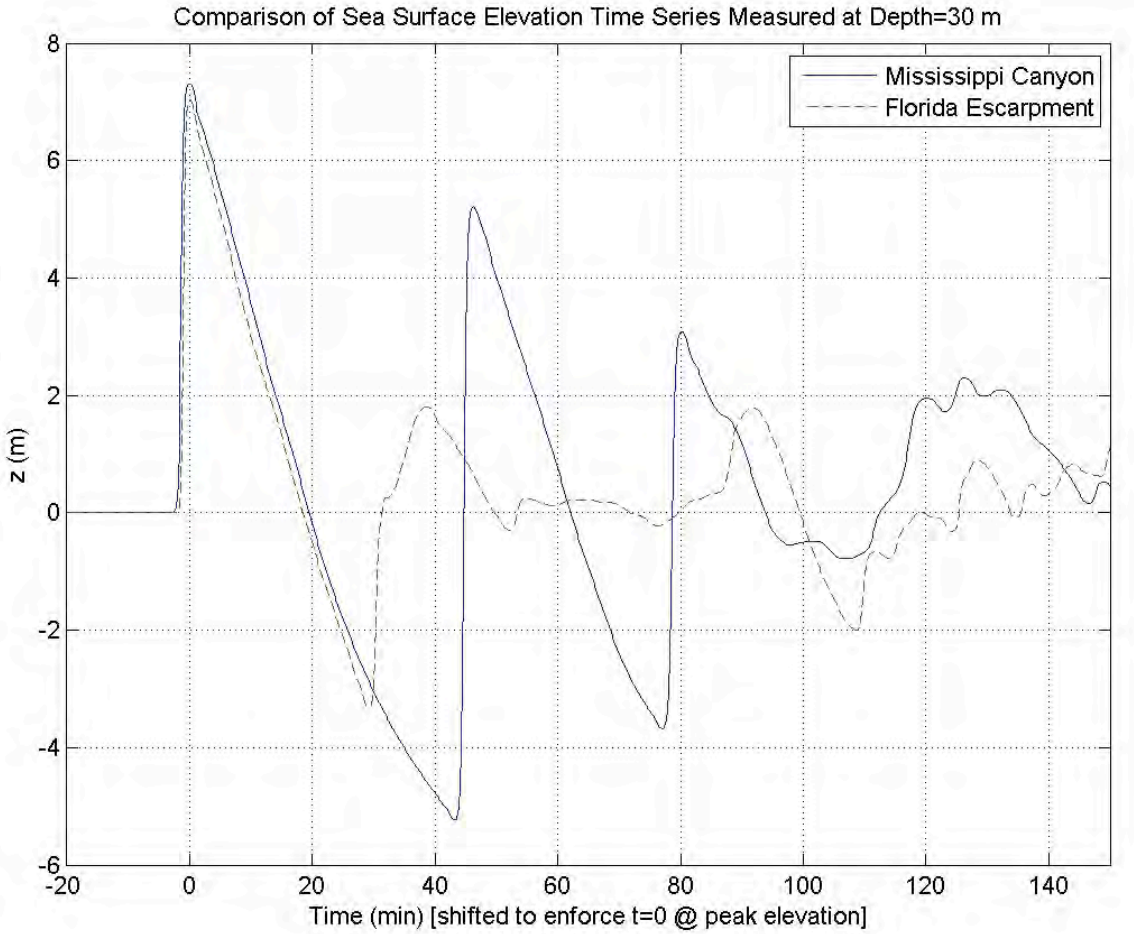

Figure 2.4.6.4.5-62. Comparison of free surface elevation time series at the same location, for two different landslide sources - the Mississippi Canyon source and the WORST CASE along the Florida Slope above the Florida Escarpment.

A subdomain, approximately 200 km by 150 km, centered 75 km offshore is used here, and is shown in Figure 2.4.6.4.5-63. A constant grid size of 100 m is used, and both the seafloor and initially dry land is assumed smooth, with no bottom friction dissipation. This is the most conservative assumption, and provides an upper physical limit for the inundation distance. As mentioned above, the offshore boundary is forced with the Mississippi Canyon sea surface time series given in Figure 2.4.6.4.5-62. Figures 2.4.6.4.5-63 through 2.4.6.4.5-67 are plan-view snapshots of the wave train attacking the coastline. The interaction with the coastline is complex, owing to the complex bathymetry and topography, and the runup elevation is highly variable across the shoreline. In the lower (southern) part of the domain, where relatively steep topography is located close to the shoreline, the maximum runup elevation is +8 m and the inundation distance is ~ 8 km. However, immediately seaward of the site, where a wide, coastal plan exists, the runup elevation is +3 m, but the inundation distance is ~13 km. Thus, the tsunami does not reach the ground elevation of the site.

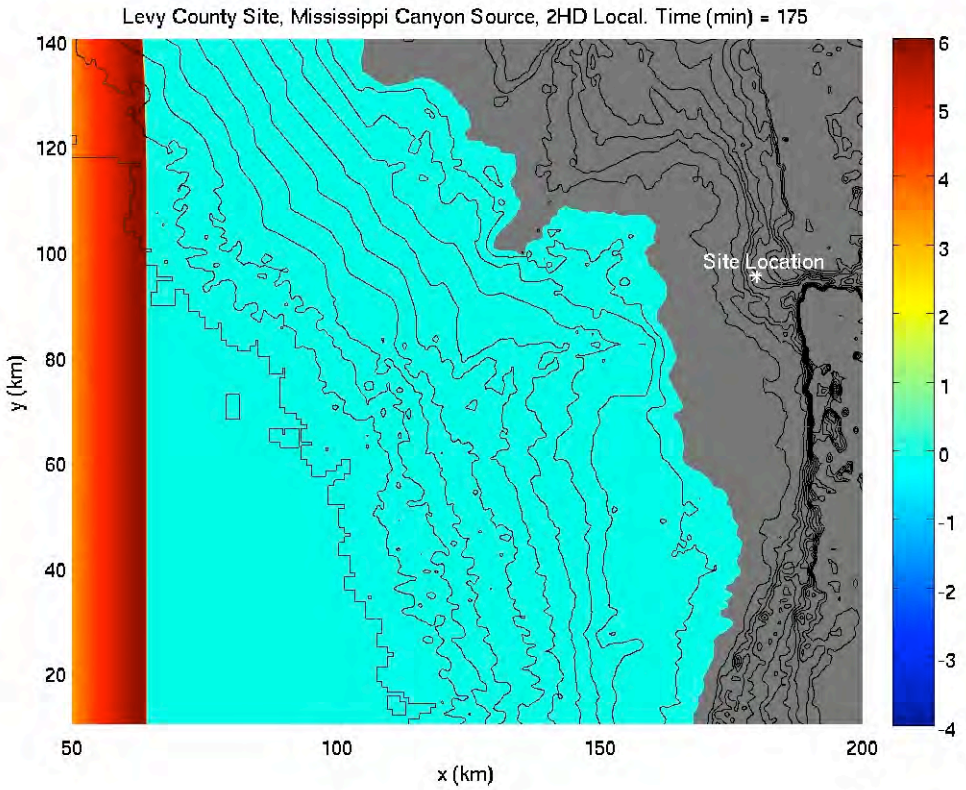

Figure 2.4.6.4.5-63. The nearshore evolution of the 2HD hot-start tsunami condition for the Mississippi Canyon source. The elevation of the ocean surface is given by the colors, with the scaling given by the color bar on the right. The contour lines indicate bathymetry/topography, and are drawn in 2m intervals. Time shown is t=175 minutes after the landslide.

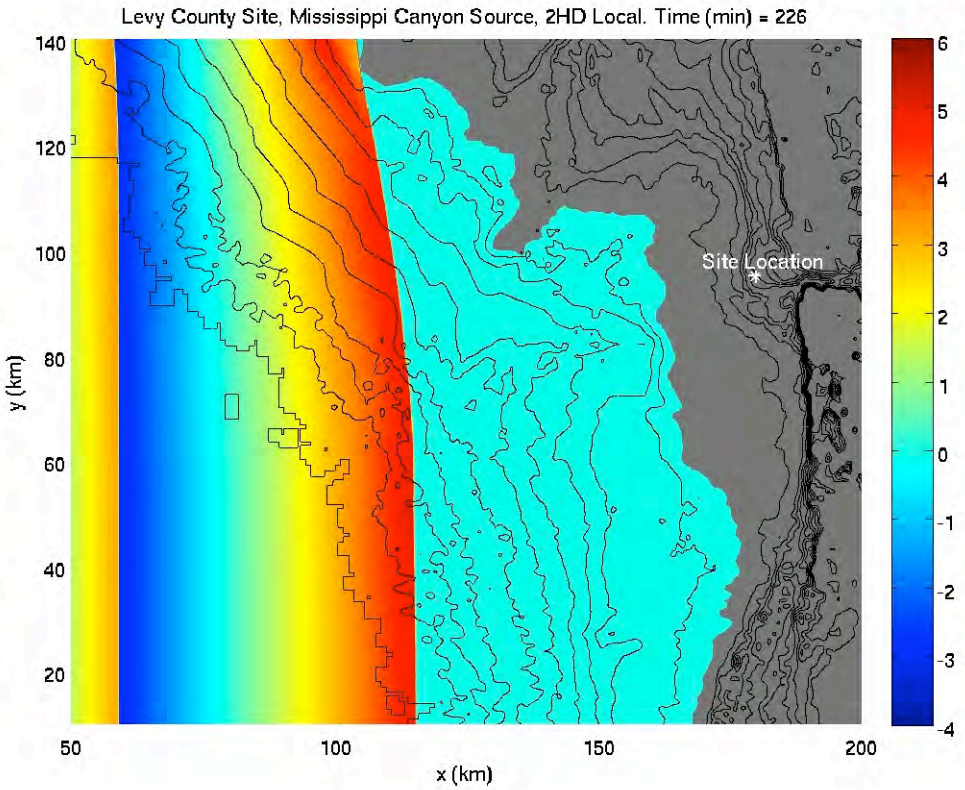

Figure 2.4.6.4.5-64. Caption is the same as Fig. 2.4.6.4.5-63. Time shown is t=226 minutes after the landslide.

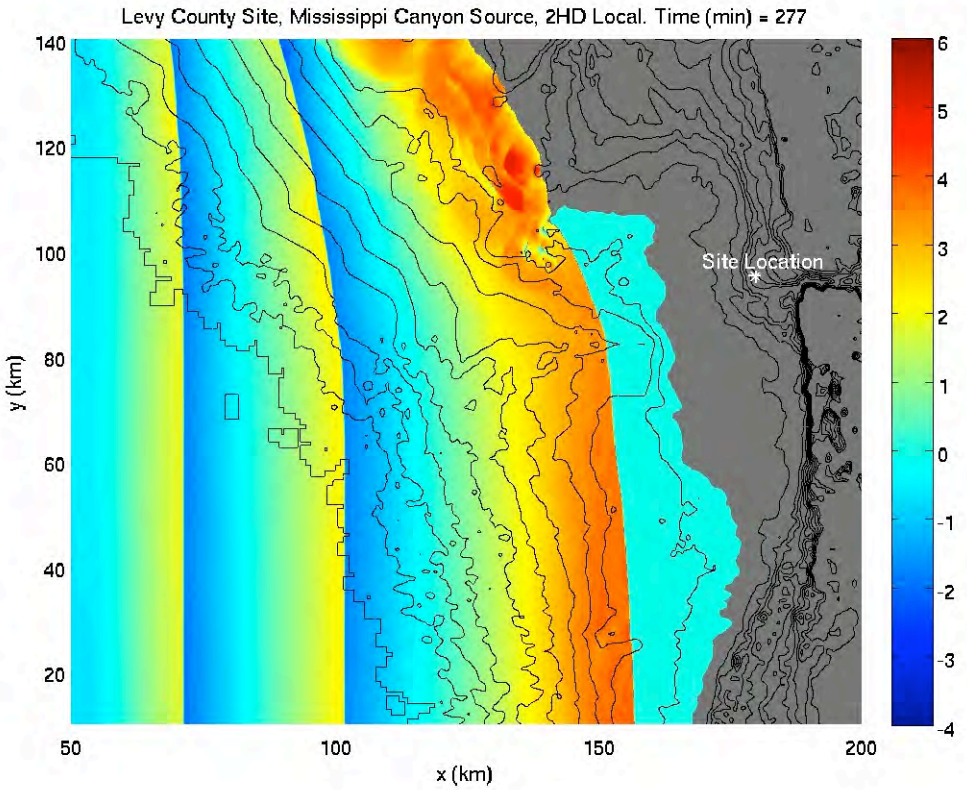

Figure 2.4.6.4.5-65. Caption is the same as Fig. 2.4.6.4.5-63. Time shown is t=277 minutes after the landslide.

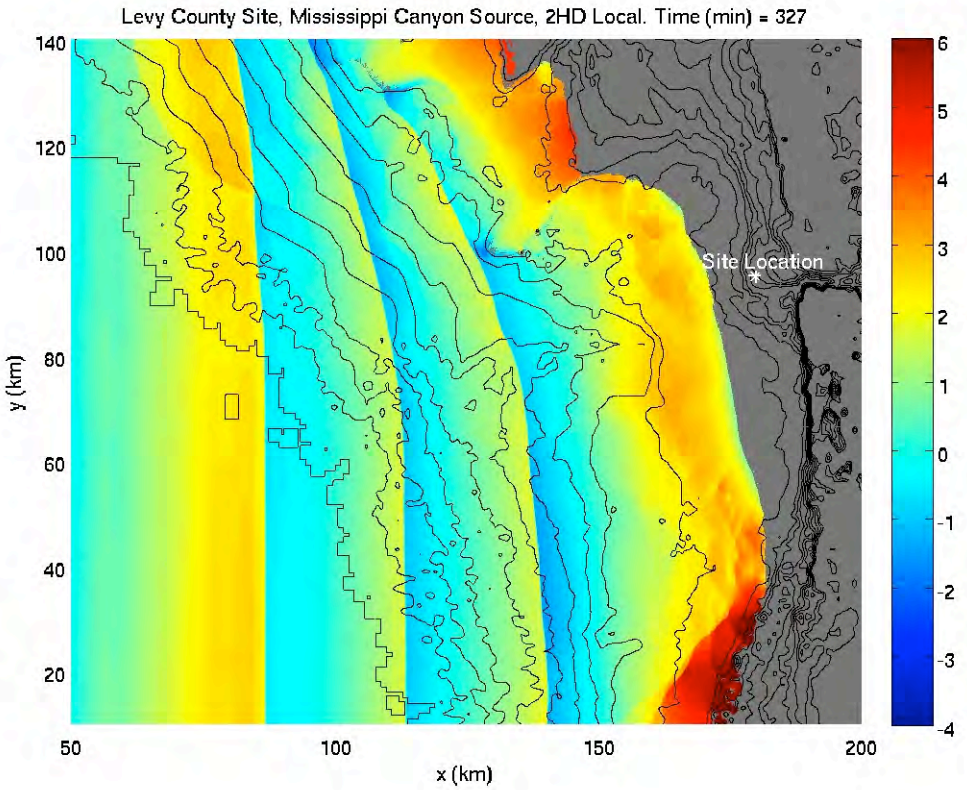

Figure 2.4.6.4.5-66. Caption is the same as Fig. 2.4.6.4.5-63. Time shown is t=327 minutes after the landslide.

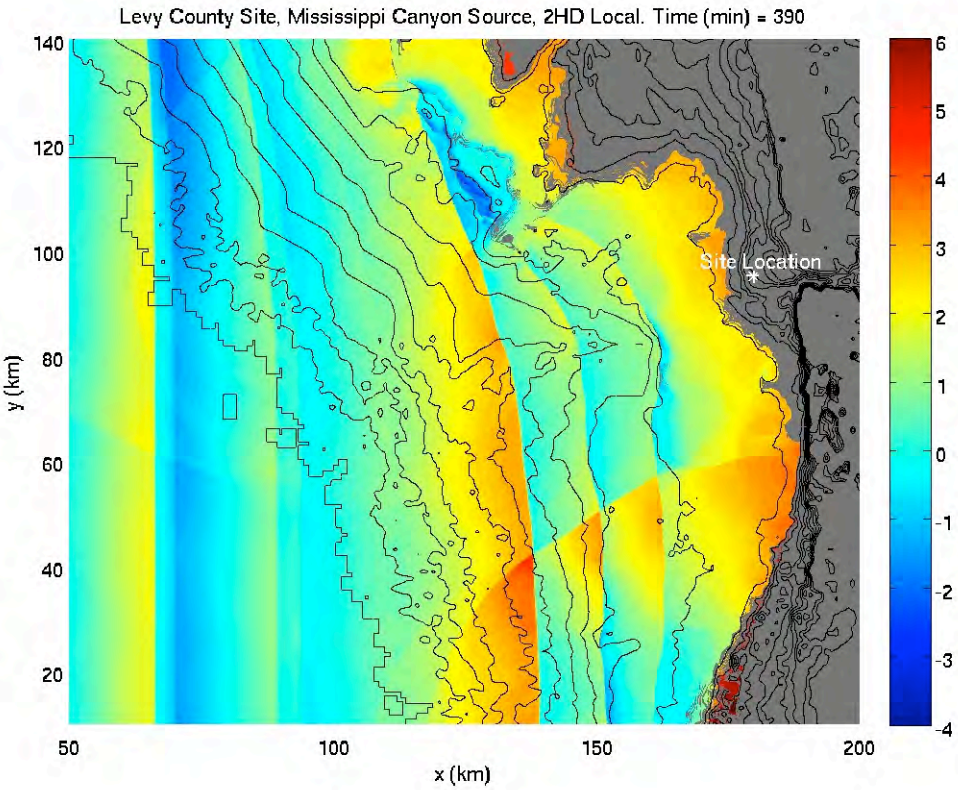

Figure 2.4.6.4.5-67. Caption is the same as Fig. 2.4.6.4.5-63. Time shown is t=390 minutes after the landslide.

The above simulation assumes that the tsunami event occurs at mid-tide with current sea levels. Independent analysis of the 10% exceedance high tide was conducted for 16 years of NOAA NOS CO-OPS data at the Clearwater Beach, Florida tide gauge station (years 1973-2006). The 10% exceedance high tide was determined to be 0.75 m (NAVD88) for these years, compared to 0.82 m indicated in the applicant's response to RAI 2.4.6-10. The long-term sea-level rise at the Clearwater Beach, Florida station is 2.43±0.80 mm/yr according to NOAA NOS-CO-OPS data. Therefore our estimated antecedent water level is 0.75 m (high tide) + 0.18 m (sea level anomaly) + 0.32 m (100-year sea level rise + 1s.d.) = 1.2 m (NAVD88). The applicant's estimated antecedent water level is 1.1 m (NAVD88) as indicated in their response to RAI 2.4.6-10.

A final simulation, using the identical numerical configuration described in the preceding paragraph was run using the higher water levels. The single plan-view snapshot from this simulation is provided, in Figure 2.4.6.4.5-68, given at the time of maximum runup offshore of the Levy County site. The maximum runup offshore of the site, using the water level increased by 1.2 m, is +6.1 m. Thus, by increasing the water depth by 1.2 m, the runup elevation was increased by 3.1 m. Clearly, the process of bore evolution is highly non-linear, and the increase in the water depth allows for a measurably larger wave to reach the shoreline and push farther inland than would be expected by a simple linear addition of the water depth increase (1.2 m) to the previous runup prediction (+3.0

m). However, even when considering this, the maximum tsunami runup in the vicinity of the site does not approach the Levy County site ground elevation.

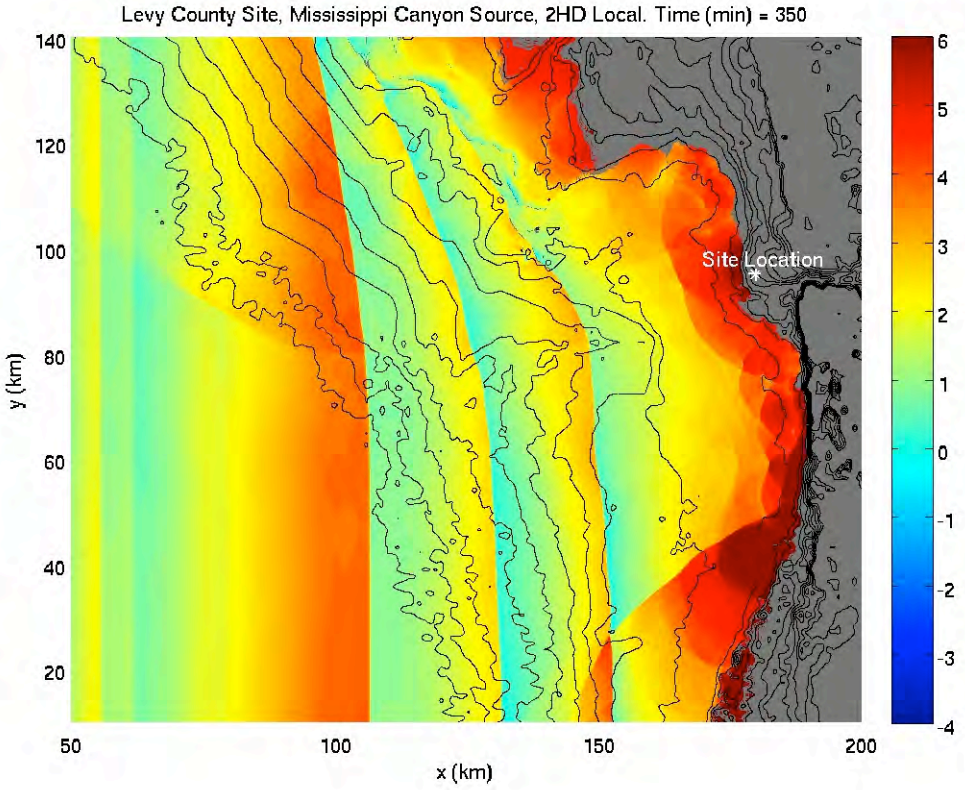

Figure 2.4.6.4.5-68. The nearshore evolution of the 2HD hot-start tsunami condition for the Mississippi Canyon source, assuming the tsunami occurs at an antecedent sea level of +1.2 m (NAVD88). The elevation of the ocean surface is indicated by the colors, with the scaling indicated by the color bar on the right. The contour lines indicate bathymetry/topography, and are drawn in 2m intervals. Time shown is t=350 minutes after the landslide, and is the time of maximum runup shoreward of the Levy County Site.

Conclusions

Numerical modeling of three different types of tsunami sources has been performed to determine their impact on the Levy County site. The three source types are (1) distant earthquake sources; (2) a regional earthquake source in the Gulf of Mexico; and (3) regional submarine landslide sources in the Gulf of Mexico. For the latter source type that defines the source for the PMT, water levels from five different submarine landslide scenarios were calculated using COULWAVE to determine the PMT.

Using conservative source parameters and neglecting the radial spreading of wave energy, the 1HD simulations indicate that the Mississippi Canyon source clearly has the greatest potential to bring a large wave to the Levy County site, with 1HD water

elevations near the site in excess of +30 m. 2HD simulations of this source and the WORST CASE Florida Slope landslide source that include radial spreading predict a maximum wave elevation of 7 m offshore of the site (30 m water depth). However, as the Mississippi Canyon wave is longer in period and has a longer train of large waves, it is designated as the PMT for the Levy County site. Highly refined nearshore simulations show that this source results in a maximum water level of +3 m. Because of non-linear effects during wave propagation, one cannot simply add an antecedent sea level that includes 10% exeedance high tide, sea level anomaly, and sea-level rise to the +3 m maximum water level. A separate 2HD simulation that includes the non-linear propagation effects and a +1.2 m (NAVD88) antecedent sea level (Figure 2.4.6.5.4-68) results in a maximum water level of +6.1 m. The PMT water level near the site estimated by the applicant is 12.94 feet (3.94 m). In both cases, the PMT does not reach the Levy County site plant grade elevation.

2.4.6.4.6 Hydrography and Harbor or Breakwater Influences on Tsunami

The applicant indicates that routing of the controlling tsunami, including breaking wave formation and resonance effects, is expected to be minor and limited to shorelines. In addition the applicant indicates that hydrography and harbor or breakwater influences are not expected to be severe enough to impact safety-related structures.

Results of Contractor's Independent Confirmatory Analysis:
Staff concurs that the hydrography and harbor or breakwater influences are not expected to be severe enough to impact safety-related structures. The offshore hydrodgraphy and harbor or breakwater influences are specifically accounted for in the numerical modeling performed during the independent confirmatory analysis.

2.4.6.4.7 Effects on Safety-related Facilities

The applicant indicates that the effects of the Probable Maximum Tsunami are not expected to be severe enough to impact the operation of safety-related structures. The applicant further indicates that measures to protect the site against the effects of tsunami are not included in the design criteria.

Results of Contractor's Independent Confirmatory Analysis:
Staff concurs that the effects of the Probable Maximum Tsunami are not expected to be severe enough to impact the operation of safety-related structures

2.4.6.4.8 Hydrostatic and Hydrodynamic Forces

The applicant did not include a section on Hydrostatic and Hydrodynamic Forces in the FSAR.

Results of Contractor's Independent Confirmatory Analysis:
Staff concurs that the PMT does not define the hydrostatic and hydrodynamic design basis.

2.4.6.4.9 Debris and Water-Borne Projectiles

The applicant did not include a section on Debris and Water-Borne Projectiles in the FSAR.

Results of Contractor's Independent Confirmatory Analysis:
Debris and water-borne projectiles associated with the PMT will likely not impact safety-related SSC.

2.4.6.4.10 Effects of Sediment Erosion and Deposition

The applicant did not include a section on the Effects of Sediment Erosion and Deposition in the FSAR.

Results of Contractor's Independent Confirmatory Analysis:
Effects related to sediment erosion and deposition associated with the PMT will likely not result in blockage or loss of function of safety-related SSC.

2.4.6.4.11 Consideration of Other Site-Related Evaluation Criteria

The applicant did not include a section on Consideration of Other Site-Related Evaluation Criteria in the FSAR.

Results of Contractor's Independent Confirmatory Analysis:
The PMT sources will not be combined with the design-basis earthquake when evaluating the design of safety-related SSC.

2.4.6.5 Conclusions

Model results by the applicant indicate that the tsunami from a Mississippi Canyon landslide yields the highest water levels near the site and is therefore the Probable Maximum Tsunami (PMT). The PMT water level near the site estimated by the applicant is 12.94 feet (3.94 m), compared to a PMT water level estimated by the independent confirmatory analysis of 20.0 feet (6.1 m). In both cases, the PMT water level does not reach the grade/floor elevation at the site.

2.4.6.6 References

Balzano, A., 1998, Evaluation of methods for numerical simulation of wetting and drying in shallow water flow models: Coastal Engineering, v. 34, p. 83-107.

Barkan, R., ten Brink, U.S., and Lin, J., 2009, Far field tsunami simulations of the 1755 Lisbon earthquake: Implications for tsunami hazard to the U.S. East Coast and the Caribbean: Marine Geology, v. 264, p. 109-122.

Bird, P., and Kagan, Y.Y., 2004, Plate-tectonic analysis of shallow seismicity: apparent boundary width, beta-value, corner magnitude, coupled lithosphere thickness, and coupling in 7 tectonic settings: Bulletin of the Seismological Society of America, v. 94, p. 2380-2399.

Blakey, R., 2005, Paleogeography and Geologic History of North America: Northern Arizona University, http://jan.ucc.nau.edu/~rcb7/nam.html.

Bourgeois, J., Hansen, T.A., Wiberg, P.L., and Kauffman, E.G., 1988, A tsunami deposit at the Cretaceous-Tertiary boundary in Texas: Science, v. 241, p. 567-241.

Capra, L., Macîas, J.L., Scott, K.M., Abrams, M., and Garduño-Monroy, V.H., 2002, Debris avalanches and debris flows transformed from collapses in the Trans-Mexican Volcanic Belt, Mexico--behavior, and implications for hazard assessment: Journal of Volcanology and Geothermal Research, v. 113, p. 81-110.

Chang, K.-A., Hsu, T.-J., and Liu, P.L.-F., 2001, Vortex generation and evolution in water waves propagating over a submerged rectangular obstacle. Part I. solitary waves: Coastal Engineering, v. 44, p. 13-36.

Chaytor, J.D., ten Brink, U.S., Solow, A.R., and Andrews, B.D., 2009, Size distribution of submarine landslides along the U.S. Atlantic Margin: Marine Geology, p. 16-27.

Chen, Q., Kirby, J.T., Dalrymple, R.A., Kennedy, A.B., and Chawla, A., 2000, Boussinesq modeling of wave transformation, breaking, and runup: Part I. 2D: Journal of Waterway, Port, Coastal, and Ocean Engineering, v. 126, p. 57-62.

Cheung, K.F., Phadke, A.C., Wei, Y., Rojas, R., Douyere, Y.J.-M., Martino, C.D., Houston, S.H., Liu, P.L.-F., Lynett, P.J., Dodd, N., Liao, S., and Nakazaki, E., 2003, Modeling of storm-induced coastal flooding for emergency management: Ocean Engineering, v. 30, p. 1353-1386.

Coleman, J.B., Prior, D.B., and Lindsay, J.F., 1983, Deltaic influences on shelf edge instability processes, *in* Stanley, D.J., and Moore, G.T., eds., The Shelfbreak:

Critical Interface on Continental Margins: Society of Economic Paleontologists and Mineralogists, Special Publication 33, p. 121-137.

Dellinger, J.A., and Blum, J.A., 2009, Insights into the mechanism of the Northern Gulf of Mexico Ms 5.3 "Green Canyon event" of 10 February 2006: Eos, Transactions American Geophysical Union, v. Fall Meeting Supplement, p. Abstract S53A-1484.

Dewey, J.W., and Dellinger, J.A., 2008, Location of the Green Canyon (offshore southern Louisiana) seismic event of February 10, 2006: U.S. Geological Survey, Open-File Report 2008-1184, 30 p.

Dodd, N., 1998, Numerical model of wave run-up, overtopping, and regeneration: Journal of Waterway, Port, Coastal, and Ocean Engineering, v. 124, p. 73-81.

Doyle, L.J., and Holmes, C.W., 1985, Shallow structure, stratigraphy, and carbonate sedimentary processes of West Florida Continental Slope: American Association of Petroleum Geologists Bulletin, v. 69, p. 1133-1144.

Fine, I.V., Rabinovich, A.B., Bornhold, B.D., Thomson, R., and Kulikov, E.A., 2005, The Grand Banks landslide-generated tsunami of November 18, 1929: preliminary analysis and numerical modeling: Marine Geology, v. 215, p. 45-57.

Gale, A.S., 2006, The Cretaceous-Palaeogene boundary on the Brazos River, Falls County, Texas: Is there evidence for impact-induced tsunami sedimentation: Proceedings of the Geologists; Association, v. 117, p. 173-185.

Geist, E.L., 2002, Complex earthquake rupture and local tsunamis: Journal of Geophysical Research, v. 107, p. doi:10.1029/2000JB000139.

Goodwin, R.H., and Prior, D.B., 1989, Geometry and depositional sequences of the Mississippi Canyon, Gulf of Mexico: Journal of Sedimentary Petrology, v. 59, p. 318-329.

Gopalakrishnan, T.C., 1989, A moving boundary circulation model for regions with large tidal flats: International Journal for Numerical Methods in Engineering, v. 28, p. 245-260.

Hansen, J.B., and Svendsen, I.A., 1979, Regular waves in shoaling water: Experimental data: Univ. of Denmark [Tech. Rep., ISVA Ser., 21].

Harbitz, C.B., Løvholt, F., Pedersen, G., and Masson, D.G., 2006, Mechanisms of tsunami generation by submarine landslides: a short review: Norwegian Journal of Geology, v. 86, p. 255-264.

Hibberd, S., and Peregrine, D.H., 1979, Surf and run-up on a beach: Journal of Fluid Mechanics, v. 95, p. 323-345.

Hildebrand, A.R., Penfield, G.T., Kring, D.A., Pilkington, M., Camargo Z., A., Jacobsen, S.B., and Boynton, W.V., 1991, Chicxulub Crater: A possible Cretaceous/Tertiary boundary impact crater on the Yucatán Peninsula, Mexico: Geology, v. 19, p. 867-871.

Hsu, T.-J., Sakakiyama, T., and Liu, P.L.-F., 2002, A numerical model for wave motions and turbulence flows in front of a composite breakwater: Coastal Engineering, v. 46, p. 25-50.

Hu, K., Mingham, C.G., and Causon, D.M., 2000, Numerical simulation of wave overtopping of coastal structures using the non-linear shallow water equations: Coastal Engineering, v. 41, p. 433-465.

Imamura, F., 1996, Simulation of wave-packet propagation along sloping beach by TUNAMI-code, *in* Yeh, H., Liu, P.L.F., and Synolakis, C.E., eds., Long-Wave Runup Models: World Scientific, p. 25-42.

Johnson, D.B., Raad, P.E., and Chen, S., 1994, Simulations of impacts of fluid free surface with solid boundary: International Journal for Numerical Methods in Fluids, v. 19, p. 153-174.

Keller, G., Adatte, T., Berner, Z., Harting, M., Baum, G., Prauss, M., Tantawy, A., and Stueben, D., 2007, Chicxulub impact predates K-T boundary: New evidence from Brazos, Texas: Earth and Planetary Science Letters, v. 255, p. 339-356.

Keller, G., and Stinnesbeck, W., 1996, Near-K/T age of clastic deposits from Texas to Brazil: impact, volcanism and/or sea-level lowstand?: Terra Nova, v. 8, p. 277-285.

Kennedy, A.B., Chen, Q., Kirby, J.T., and Dalrymple, R.A., 2000, Boussinesq modeling of wave transformation, breaking and runup: I. one dimension: Journal of Waterway, Port, Coastal, and Ocean Engineering, v. 126, p. 39-47.

Knight, B, 2006, West Coast and Alaska Tsunami Warning Center, Model Predictions of Gulf and Southern Atlantic Coast Tsunami Impacts From a Distribution of Sources, Science of Tsunami Hazards, V. 24, Number 5, pp. 304-312.

Kobayashi, N., and Wurjanto, A., 1989, Wave overtopping on coastal structures: Journal of Waterway, Port, Coastal, and Ocean Engineering, v. 115, p. 235-251.

Korycansky, D.G., and Lynett, P.J., 2005, Offshore breaking of impact tsunami: The Van Dorn effect revisited: Geophysical Research Letters, v. 32, p. doi:10.1029/2004GL021918.

Korycansky, D.G., and Lynett, P.J., 2007, Run-up from impact tsunami: Geophysical Journal International, v. 170, p. 1076-1088.

Kowalik, Z., and Murty, T.S., 1993, Numerical simulation of two-dimensional tsunami runup: Marine Geodesy, v. 16, p. 87-100.

Lander, J. F., Whiteside, L.S., and Lockridge, P.A., 2002, A Brief History of Tsunamis in the Caribbean Sea, The International Journal of the Tsunami Society, v. 20, Number 2.

Leendertse, J.J., 1987, Aspects of SIMSYS2D: A System for Two-Dimensional Flow Computation: The RAND Corporation R-3572-USGS, 80 p.

Lin, P., Chang, K.-A., and Liu, P.L.-F., 1999, Runup and run-down of solitary waves on sloping beaches: Journal of Waterway, Port, Coastal, and Ocean Engineering, v. 125, p. 247-255.

Lin, P., and Liu, P.L.-F., 1998a, A numerical study of breaking waves in the surf zone: Journal of Fluid Mechanics, v. 359, p. 239-264.

Lin, P., and Liu, P.L.-F., 1998b, Turbulence transport, vorticity dynamics, and solute mixing under plunging breaking waves in surf zone: Journal of Geophysical Research, v. 103, p. 15677-15694.

Liu, C., and Olsson, R.K., 1992, Evolutionary radiation of microperforate planktonic foraminifera following the K/T mass extinction event: Journal of Foraminiferal Research, v. 22, p. 328-346.

Liu, P.L.F., Cho, Y.S., Yoon, S.B., and Seo, S.N., 1995, Numerical simulations of the 1960 Chilean tsunami propagation and inundation at Hilo, Hawaii, *in* Tsuchiya, Y., and Shuto, N., eds., Tsunami: Progress in Prediction, Disaster Prevention and Warning: Kluwer Academic Publishers, p. 99-115.

Lynett, P., 2007, The effect of a shallow water obstruction on long wve runup and overland flow velocity: Journal of Waterway, Port, Coastal, and Ocean Engineering, v. 133, p. 455-462.

Lynett, P., Borrero, J.C., Liu, P.L.F., and Synolakis, C.E., 2003, Field survey and numerical simulations: A review of the 1998 Papua New Guinea tsunami: Pure and Applied Geophysics, v. 160, p. 2119-2146.

Lynett, P., and Liu, P.L.F., 2002, A numerical study of submarine-landslide-generated waves and run-up: Proceedings of the Royal Society of London, A, v. 458, p. 2885-2910.

Lynett, P., and Liu, P.L.F., 2006, Three-dimensional runup due to submerged and subaerial landslides, *in* Mercado, A., and Liu, P.L.F., eds., Caribbean Tsunami Hazard: Singapore, World Scientific Publishing Co., p. 289-307.

Lynett, P.J., 2006, Nearshore wave modeling with high-order Boussinesq-type equations: Journal of the Waterways and Harbors Division, A.S.C.E., v. 132, p. 348-357.

Lynett, P.J., and Liu, P.L.-F., 2005, A numerical study of run-up generated by three-dimensional landslides: Journal of Geophysical Research, v. 10, p. doi:10.1029/2004JC002443.

Lynett, P.J., Wu, T.-R., and Liu, P.L.-F., 2002, Modeling wave runup with depth-integrated equations: Coastal Engineering, v. 46, p. 89-107.

Mader, C.L., 2001, Modeling the 1755 Lisbon tsunami: Science of Tsunami Hazards, v. 19, p. 93-98.

Madsen, P.A., Sorensen, O.E., and Schaffer, H.A., 1997, Surf zone dynamics simulated by a Boussinesq-type model: Part 1. Model description and cross-shore motion of regular waves: Coastal Engineering, v. 32, p. 255-287.

Mancini, E.A., Tew, B.H., and Smith, C.C., 1989, Cretaceous-Tertiary contact, Mississippi and Alabama: Journal of Foraminiferal Research, v. 19, p. 93-104.

McGarr, A., 1965, Excitation of seiches in channels by seismic waves: Journal of Geophysical Research, v. 70, p. 847-854.

Mueller, C.S., 2010, The influence of maximum magnitude on seismic-hazard estimates in the Central and Eastern United States: Bulletin of the Seismological Society of America, v. 100, p. 699-711.

Myers, E.P., and Baptista, A.M., 1995, Finite element modeling of the July 12, 1993 Hokkaido Nansei-Oki tsunami: Pure and Applied Geophysics, v. 144, p. 769-801.

Nettles, M., 2007, Analysis of the 10 February 2006: Gulf of Mexico earthquake from global and regional seismic data, in 2007 Offshore Technology Conference, Houston, Texas, p. 2.

Owen, M., 1980, Design of seawalls allowing for wave overtopping: Hydraulics Research Rep. EX924.

Pedrozo-Acuña, A., Simmonds, D.J., Otta, A.K., and Chadwick, A.J., 2006, On the cross-shore profile change of gravel beaches: Coastal Engineering, v. 53, p. 335-347.

Pelinovsky, E., Zahibo, N., Dunkley, P., Edmonds, M., Herd, R., Talipova, T., Kozelkov, A., and Nikolkina, I., 2004, Tsunami generated by the volcano eruption on July

12-13, 2003 at Montserrat, Lesser Antilles: Science of Tsunami Hazards, v. 22, p. 44-57.

Petera, J., and Nassehi, V., 1996, A new two-dimensional finite element model for the shallow water equations using a Lagrangian framework constructed along fluid particle trajectories: International Journal for Numerical Methods in Engineering, v. 39, p. 4159-4182.

Petersen, M.D., Frankel, A.D., Harmsen, S.C., Mueller, C.S., Haller, K.M., Wheeler, R.L., Wesson, R.L., Zeng, Y., Boyd, O.S., Perkins, D.M., Luco, N., Field, E.H., Wills, C.J., and Rukstales, K.S., 2008, Documentation for the 2008 update of the United States National Seismic Hazard Maps U.S. Geological Survey Open-File Report 2008-1128, 128 p.

Piper, J.N., 1997, Downslope sediment transport processes and sediment distributions at the East Breaks, northwest Gulf of Mexico: Austin, University of Texas, Thesis.

Piper, J.N., and Behrens, W.E., 2003, Downslope sediment transport processes and sediment distributions at the East Breaks, northwest Gulf of Mexico, in Proceedings of the 23rd Annual Gulf Coast Section SEPM Research Conference, Houston, TX, p. 359-385.

Raubenheimer, B., 2002, Observations and predictions of fluid velocities in the surf and swash zones: Journal of Geophysical Research, v. 107, p. 3190.

Rothwell, R.G., Kenyon, N.H., and McGregor, B.A., 1991, Sedimentary features of the south Texas continental slope as revealed by side-scan sonar and high-resolution seismic data: American Association of Petroleum Geologists Bulletin, v. 75, p. 298-312.

Saville, T., 1955, Laboratory data on wave runup and overtopping on shore structures: U.S. Army, Beach Erosion Board, Document Service Center Technical Memo. No. 64 [Technical Report].

Savrda, C.E., 1993, Ichnosedimentologic evidence for a noncatastrophic origin of Cretaceous-Tertiary boundary sands in Alabama: Geology, v. 21, p. 1075-1078.

Schulte, P., Speijer, R., Mai, H., and Kontny, A., 2006, The Cretaceous-Paleogene (K-P) boundary at Brazos, Texas: Sequence stratigraphy, depositional events and the Chicxulub impact: Sedimentary Geology, v. 184, p. 77-109.

Sielecki, A., and Wurtele, M.G., 1970, The numerical integration of the nonlinear shallow-water equations with sloping boundaries: Journal of Computational Physics, v. 6, p. 219-236.

Silver, E., Day, S., Ward, S., Hoffmann, G., Llanes, P., Driscoll, N., Appelgate, B., and Saunders, S., 2009, Volcano collapse and tsunami generation in the Bismarck Volcanic Arc, Papua New Guinea, Journal of Volcanology and Geothermal Research, doi: 10.1016/j.jvolgeores.2009.06.013

Smit, J., Roep, T.B., Alvarez, W., Montanari, A., Claeys, P., Grajales-Nishimura, J.M., and Bermudez, J., 1996, Coarse-grained, clastic sandstone complex at the K/T boundary around the Gulf of Mexico: Deposition by tsunami waves induced by the Chicxulub impact?, *in* Ryder, G., Fastovsky, D., and Gartner, S., eds., The Cretaceous-Tertiary Event and Other Catastrophes in Earth History: Boulder, Colorado, Geological Society of America, Special Paper 307, p. 151-182.

Smith, M.S., and Shepherd, J.B., 1995, Potential Cauchy-Poisson wave generated by submarine eruptions of Kick 'em Jenny Volcano: Natural Hazards, v. 11, p. 75-94.

Tao, J., 1983, Computation of wave runup and wave breaking: Danish Hydraulics Institute [Internal Report].

Tao, J., 1984, Numerical modeling of wave runup and breaking on the beach: Acta Oceanologica Sinica, v. 6, p. 692-700.

ten Brink, U.S., Geist, E.L., and Andrews, B.D., 2006, Size distribution of submarine landslides and its implication to tsunami hazard in Puerto Rico: Geophysical Research Letters, v. 33, p. doi:10.1029/2006GL026125.

ten Brink, U., Twichell, D.K., Geist, E., Chaytor, J., Locat, J., Lee, H., Buczkowski, and Sansoucy, M., 2007, The Current State of Knowledge Regarding Potential Tsunami Sources Affecting U.S. Atlantic and Gulf Coasts, USGS Adminstrative Reports.

ten Brink, U.S., Twichell, D., Geist, E.L., Chaytor, J., Locat, J., Lee, H., Buczkowski, B., Barkan, R., Solow, A.R., Andrews, B.D., Parsons, T., Lynett, P., Lin, J., and Sansoucy, M., 2008, Evaluation of Tsunami Sources with the Potential to Impact the U.S. Atlantic and Gulf Coasts: An Updated Report to the Nuclear Regulatory Commission, 302 p. [U.S. Geological Survey Administrative Report].

Ting, F.C.-K., and Kirby, J.T., 1995, Dynamics of surf-zone turbulence in a strong plunging breaker: Coastal Engineering, v. 24, p. 177-204.

Titov, V.V., and Synolakis, C.E., 1995, Modeling of breaking and nonbreaking long wave evolution and runup using VTSC-2: Journal of Waterway, Port, Coastal, and Ocean Engineering, v. 121, p. 308-316.

Titov, V.V., and Synolakis, C.E., 1998, Numerical modeling of tidal wave runup: Journal of Waterway, Port, Coastal, and Ocean Engineering, v. 124, p. 157-171.

Trabant, P., Watts, P., Lettieri, F.L., and Jamieson, A., 2001, East Breaks slump, northwest Gulf of Mexico, OTC 12960, in 2001 Offshore Technology Conference, Houston, TX, p. 231-238.

Twichell, D., Chaytor, J.D., ten Brink, U.S., and Buczkowski, B., 2009, Morphology of late Quaternary submarine landslides along the U.S. Atlantic continental margin: Marine Geology, v. 264, p. 4-15.

Twichell, D.C., Kenyon, N.H., Parson, L.M., and McGregor, B.A., 1991, Depositional patterns of the Mississippi Fan surface: Evidence from GLORIA II and high-resolution seismic profiles, *in* Weimer, P., and Link, M.H., eds., Seismic Facies and Sedimentary Processes of Subarine Fans and Turbidite Systems: New York, Springer-Verlag, p. 349-363.

Twichell, D.C., Valentine, P.C., and Parson, L.M., 1993, Slope failure of carbonate sediment on the West Florida Slope, *in* Schwab, W.C., Lee, H.J., and Twichell, D.C., eds., Submarine Landslides: Selected Studies in the U.S. Exclusive Economic Zone: U.S. Geological Survey Bulletin 2002, p. 69-78.

Van de Meer, J.W., and Janssen, J.P.F.M., 1995, Wave run-up and wave overtopping at dikes, *in* Kobayashi, N., and Demirbilek, Z., eds., Wave Forces on inclined and Vertical Wall Structures: ASCE, p. 1-27.

Ward, S.N., 2001, Landslide tsunami: Journal of Geophysical Research, v. 106, p. 11,201-211,215.

Wei, G., Kirby, J.T., Grilli, S.T., and Subramanya, R., 1995, A fully nonlinear Boussinesq model for surface waves. Part 1. Highly nonlinear unsteady waves: Journal of Fluid Mechanics, v. 294, p. 71-92.

Wei, G., Kirby, J.T., and Sinha, A., 1999, Generation of waves in Boussinesq models using a source function method: Coastal Engineering, v. 36, p. 271-299.

Wells, D.L., and Coppersmith, K.J., 1994, New empirical relationships among magnitude, rupture length, rupture width, rupture area, and surface displacement: Bulletin of the Seismological Society of America, v. 84, p. 974-1002.

Wheeler, R.L., 2009, Sizes of the largest possible earthquakes in the Central and Eastern United States--Summary of a workshop, September 8-9, 2008, Golden, Colorado: U.S. Geological Survey, 314 p. [Open-File Report 2009-1263].

Woo, S.-B., and Liu, P.L.-F., 2004, A finite element model for modified Boussinesq equations. Part I: Model development: Journal of Waterway, Port, Coastal, and Ocean Engineering, v. 130, p. 1-16.

Zaibo, N., Pelinovsky, E., Kurkin, A., and Kozelkov, A., 2003, Estimation of Far-Field Tsunami Potential for the Caribbean Coast Based on Numerical Simulation, Science of Tsunami Hazards, V. 21, Number 4, pp. 202 – 222.

Zelt, J.A., 1991, The runup of nonbreaking and breaking solitary waves: Coastal Engineering, v. 15, p. 205-246.